UNIVERSITÉ PARIS-EST

Thèse de doctorat

École doctorale : Science, Ingénierie et Environnement

Spécialité : Structures et Matériaux

Présentée par

Lionel du Peloux de Saint Romain

Modeling of bending-torsion couplings in active-bending structures

Application to the design of elastic gridshells

Soutenue à l'Ecole Nationale des Ponts et Chaussées,
le 20 décembre 2017, devant le jury composé de :

Président	Bernard MAURIN	Université Montpellier 2
Rapporteurs	Sébastien NEUKIRCH	Université Pierre et Marie Curie
	Carlos LÁZARO	Universitat Politècnica de València
Examinateurs	Alberto PUGNALE	University of Melbourne
	Jean-François CARON	École des Ponts ParisTech
	Cyril DOUTHE	École des Ponts ParisTech
Invité	Bernard VAUDEVILLE	T/E/S/S atelier d'ingénierie
Directeur de thèse	Olivier BAVEREL	École des Ponts ParisTech

“Quia nominor leo.”

A Jacques & Christiane, mes grands-parents bien-aimés.

Préface

Tu ne peux vivre que de cela que tu transformes,
et dont un peu chaque jour, puisque tu t'échanges
contre, tu meurs.

Antoine de Saint-Exupéry
Citadelle

Si pour une raison quelconque il ne devait subsister qu'une unique page de ce manuscrit, j'aimerais autant que ce soit celle-là. Et qu'alors, seuls vivent les quelques mots de gratitude qui suivent pour les personnes qui m'ont accompagné sur ce chemin de fortune ; chemin initié en 2010 au sortir de l'Ecole Centrale et qui m'a conduit à présenter cette thèse.

Plus que la perspective d'une éventuelle contribution scientifique, c'est avant tout un certain goût pour la liberté *d'aller et venir* qui m'a animé : liberté des pieds qui vont ; liberté des mains qui font ; liberté de penser ; cette même liberté que je quête à travers mes sorties en montagne.

L'une de mes plus grandes chances aura été de faire participer mon corps tout entier à cette entreprise, de pouvoir d'un même mouvement concevoir et bâtir des gridshells, objets de cette étude, sans quoi ma compréhension du sujet serait restée beaucoup plus superficielle. Par ailleurs, les joies simples glanées sur les chantiers de ces projets atypiques – je pense en particulier aux séminaires *Construire le Courbe* avec des étudiants, à la construction du pavillon Solidays en 2011 avec des bénévoles et plus encore à la réalisation de la cathédrale éphémère de Créteil en 2013 avec des paroissiens – furent pour moi sans égales avec celles, plus rares, reçues dans mon quotidien quelque peu taciturne de chercheur.

Chers Jean-François et Olivier, merci de m'avoir accueilli au sein de l'équipe MSA et d'avoir su me trouver une place sur mesure au fil de ces années. Merci pour la liberté que vous m'avez procurée et pour la confiance que vous m'avez accordée dans la conduite de mon travail de recherche, mais aussi dans certains projets annexes (e.g. solidays, thinkshell, booby). L'équipe s'est étoffée de nouveaux talents et la construction de cette dynamique

vous doit beaucoup : vous savez catalyser notre enthousiasme.

Cher Cyril, merci de ce compagnonnage de quelques années. Je me souviens de t'avoir (un peu) connu avant même de te rencontrer, par l'étude de ta thèse ! J'ai pris beaucoup de plaisir à travailler avec toi au cours de ces années et il en est sorti de beaux projets. Merci plus particulièrement pour les responsabilités que tu m'as confiées dans le séminaire Construire le Courbe et d'avoir accepté d'en chambouler le programme pédagogique d'année en année. Merci également pour ton écoute, tes conseils et ton précieux travail de relecture tout au long de l'élaboration de ce manuscrit. Sa qualité s'en est trouvée grandement améliorée.

Cher Bernard, nous avons partagé sans doute quelques angoisses sans nous le dire, mais cette cathédrale de Créteil restera pour moi un projet mémorable et intense. Merci de m'avoir fait confiance pour développer ce projet et d'avoir été présent dans les moments critiques de cette aventure. Plus qu'un bagage technique, j'ai appris durant ces trois années chez T/E/S/S une certaine façon de résoudre des problèmes, de chercher des solutions sans me décourager. Et cela m'a beaucoup profité dans mon travail de thèse et me restera acquis pour les années à venir. Merci donc à toi ainsi qu'à Tom et à Matt pour ce qui m'a été transmis au bureau.

Cher Frédéric, avec toi j'ai manié la clef dynamométrique comme jamais ! Ton travail a grandement contribué à la réussite des projets Solidays et Créteil. Tu es toujours disponible pour trouver une solution, bricoler un montage, faire fonctionner un four ou une fraise, imprimer une pièce en 3D, réparer des gouttières, partager ton analyse, donner un conseil, etc. J'ai beaucoup appris du travail que tu as initié au cours de ta thèse avec l'aide de Baptiste et dans la continuité duquel je m'inscris. Merci pour tout cela.

Je tiens à remercier Sébastien Neukirch et Carlos Lázaro, rapporteurs, qui par leurs remarques et conseils avisés ont contribué à améliorer la qualité de ce mémoire de thèse. Je remercie également les autres membres du jury – Bernard Maurin son président, Alberto Pugnale, Jean-François Caron, Cyril Douthe et Bernard Vaudeville – pour leur écoute et leurs remarques de qualité. C'est toujours une grande chance de bénéficier d'une relecture rigoureuse de son propre travail par des personnes d'expérience ; et cela permet d'en regarder avec plus de lucidité les solidités comme les faiblesses.

Merci chers Marine, Romain(s), Robert, Gilles, Arthur, Ioanis, Marie, Tristan, Pierre(s), Victor, Philippe, Vianney ... co-bureaux ou collègues de travail plus ponctuels, notamment lors des semaines *Construire le Courbe*, pour les petits mots échangés ça et là lors d'un café ou d'un repas et pour votre enthousiasme quotidien. Merci Marie-Françoise, Christophe, Anne, Gilles, Géraldine, Alain, Hocine, pour l'aide constante apportée au cours de ces années passées au laboratoire.

Enfin, je ne serais pas allé au bout de ce travail sans le soutien des nombreux parents et amis qui m'entourent quotidiennement. A vous tous, merci de votre soutien et de votre patience lors de ces derniers mois, avec une mention toute spéciale pour Blandine qui m'a gratifié de son affection indéfectible et a supporté mes horaires incongrus.

Lyon, le 4 novembre 2017
Lionel du Peloux

Abstract

An *elastic gridshell* is a freeform structure, generally doubly curved, but formed out through the reversible deformation of a regular and initially flat structural grid. Building curved shapes that may seems to offer the best of both worlds : shell structures are amongst the most performant mechanically speaking while planar and orthogonal constructions are much more efficient and economic to produce than curved ones. This ability to “form a form” efficiently is of peculiar importance in the current context where morphology is a predominant component of modern architecture, and envelopes appear to be the neuralgic point for building performances.

The concept was invented by Frei Otto, a German architect and structural engineer who devoted many years of research to gridshells. In 1975 he designed the Multihalle of Mannheim, a $7500\,\mathrm{m}^2$ wooden shell which demonstrated the feasibility of this technology and made it famous to a wide audience. However, despite their potential, very few projects of this kind were built after this major realization. And for good reason, the resources committed at that time cannot guarantee the replicability of this experiment for more standard projects, especially on the economic level. Moreover, the technics and methods developed by Otto’s team in the 1960s have mostly fall into disuse or are based on disciplines that have considerably evolved. New materials, such as composite materials, have recently emerged. They go beyond the limitations of conventional materials such as timber and offer at all levels much better technical performances for this kind of application. Finally, it should be noted that the regulatory framework has also deeply changed, bringing a certain rigidity to the penetration of innovations in the building industry. Therefore, the design of gridshells arises in new terms for current architects and engineers and comes up against the inadequacy of existing tools and methods.

In this thesis, which marks an important step in a personal research adventure initiated in 2010, we try to embrace the issue of the design of elastic gridshells in all its complexity, addressing both theoretical, technical and constructive aspects. In a first part, we deliver a thorough review of this topic and we present in detail one of our main achievements, the ephemeral cathedral of Créteil, built in 2013 and still in service. In a second part, we develop an original discrete beam element with a minimal number of degrees of freedom adapted to the modeling of bending and torsion inside gridshell members with anisotropic cross-section. Enriched with a ghost node, it allows to model more accurately physical phenomena that occur at connections or at supports. Its numerical implementation is presented and validated through several test cases. Although this element has been developed specifically for the study of elastic gridshells, it can advantageously be used in any type of problem where the need for an interactive computation with elastic rods taking into account flexion-torsion couplings is required.

Keywords : gridshell, form-finding, active-bending, free-form, torsion, elastic rod, coupling, fibreglass, composite material.

Résumé

Les structures de type *gridshell élastique* permettent de réaliser des enveloppes courbes par la déformation réversible d'une grille structurelle régulière initialement plane. Cette capacité à "former la forme" de façon efficiente prend tout son sens dans le contexte actuel où, d'une part la forme s'impose comme une composante prédominante de l'architecture moderne, et d'autre part l'enveloppe s'affirme comme le lieu névralgique de la performance des bâtiments.

Fruit des recherches de l'architecte et ingénieur allemand Frei Otto dans les années 1960, elles ont été rendues populaires par la construction de la Multihalle de Mannheim en 1975. Cependant, en dépit de leur potentiel, très peu de projets de ce type ont vu le jour suite à cette réalisation emblématique qui en a pourtant démontré la faisabilité à grande échelle. Et pour cause, les moyens engagés à l'époque ne sauraient assurer la reproductibilité de cette expérience dans un contexte plus classique de projet, notamment sur le plan économique. Par ailleurs, les techniques et les méthodes développées alors sont pour la plus part tombées en désuétude ou reposent sur des disciplines scientifiques qui ont considérablement évoluées. Des matériaux nouveaux, composites, ont vu le jour. Ils repoussent les limitations intrinsèques des matériaux usuels tel que le bois et offrent des performances techniques bien plus intéressantes pour ce type d'application. Enfin, notons que le cadre réglementaire a lui aussi profondément muté, apportant une certaine rigidité vis-à-vis de la pénétration des innovations. Ainsi la conception des gridshells se pose-t-elle en des termes nouveaux aux architectes et ingénieurs actuels et se heurte à l'inadéquation des outils et méthodes existant.

Dans cette thèse, qui marque une étape importante dans une aventure de recherche personnelle initiée en 2010, nous tentons d'embrasser la question de la conception des gridshells élastiques dans toute sa complexité, en abordant aussi bien les aspects théoriques que techniques et constructifs. Dans une première partie, nous livrons une revue approfondie de cette thématique et nous présentons de façon détaillée l'une de nos principales réalisation, la cathédrale éphémère de Créteil, construite en 2013 et toujours en service. Dans une seconde partie, nous développons un élément de poutre discret original avec un nombre minimal de degrés de liberté adapté à la modélisation de la flexion et de la torsion dans les gridshells constitués de poutres de section anisotrope. Enrichi d'un noeud fantôme, il permet de modéliser plus finement les phénomènes physiques au niveau des connexions et des appuis. Son implémentation numérique est présentée et validée sur quelques cas tests. Bien que cet élément ait été développé spécifiquement pour l'étude des gridshells élastiques, il pourra avantageusement être utilisé dans tout type de problème où la nécessité d'un calcul interactif avec des tiges élastiques prenant en compte les couplages flexion-torsion s'avère nécessaire.

Keywords : gridshell, form-finding, active-bending, free-form, torsion, elastic rod, coupling, fibreglass, composite material.

Contents

Préface v
Abstract (English/Français) vii

Contents xi
List of Figures xv
List of Tables xvii

Introduction 1

I Elastic gridshells 5

II Rich Kirchhoff beam model 7

1 Geometry of smooth and discrete space curves 9
1.1 Introduction . . . 9
1.1.1 Overview . . . 9
1.1.2 Contributions . . . 10
1.1.3 Related work . . . 11
1.2 Parametric curves . . . 11
1.2.1 Definition . . . 12
1.2.2 Regularity . . . 12
1.2.3 Reparametrization . . . 12
1.2.4 Natural parametrization . . . 13
1.2.5 Curve length . . . 13
1.2.6 Arc length parametrization . . . 13
1.3 Frenet trihedron . . . 13
1.3.1 Tangent vector . . . 14
1.3.2 Normal vector . . . 15
1.3.3 Binormal vector . . . 16

1.3.4 Osculating plane . . . 16
1.4 Curves of double curvature . . . 16
1.4.1 First invariant : the curvature . . . 17
1.4.2 Second invariant : the torsion . . . 19
1.4.3 Fundamental theorem of space curves . . . 20
1.4.4 Serret-Frenet formulas . . . 20
1.5 Curve framing . . . 21
1.5.1 Moving frame . . . 22
1.5.2 Adapted moving frame . . . 25
1.5.3 Rotation-minimizing frame . . . 25
1.5.4 Parallel transport . . . 25
1.5.5 Frenet frame . . . 26
1.5.6 Bishop frame . . . 28
1.5.7 Comparison between Frenet and Bishop frames . . . 30
1.6 Discrete curves . . . 32
1.6.1 Definition . . . 32
1.6.2 Regularity . . . 33
1.6.3 Parametrization . . . 34
1.7 Discrete curvature . . . 34
1.7.1 Definition from osculating circles . . . 35
1.7.2 Benchmarking : sensitivity to non uniform discretization . . . 38
1.7.3 Benchmarking : accuracy in bending energy representation . . . 40
1.8 Discrete tangent vector . . . 43
1.8.1 Circumscribed case . . . 43
1.8.2 Inscribed case . . . 46
1.9 Discrete parallel transport . . . 49
1.9.1 The rotation method . . . 49
1.9.2 The double reflexion method . . . 49
1.10 Conclusion . . . 51
1.11 References . . . 53

III Appendix 57

A Review of built elastic gridshells 59
A.1 References . . . 62

B Parabolic interpolation 63
B.1 Introduction . . . 63
B.2 Lagrange interpolating polynomial . . . 63
B.3 Reparametrization . . . 64
B.4 Characteristic values . . . 64
B.5 Extremum value . . . 65

Bibliography 67

Publications from the author 71

List of Figures

1.1 Definition of the tangent vector and the osculating circle of a curve 14
1.2 Osculating circles for a spiral curve at different parameters 17
1.3 Discontinuity of the Frenet trihedron at an inflexion point 21
1.4 Geometric interpretation of the angular velocity vector of a moving frame 23
1.5 Adapted moving frame on a circular helix 24
1.6 Angular velocities of Frenet and Bishop frames for a circular helix 31
1.7 Discrete curve representation and parametrization 33
1.9 Comparison of circumscribed and inscribed osculating circles 39
1.10 Sensitivity of discrete curvatures to non uniform discretization 39
1.11 Discretization of a semicircle and evaluation of its bending energy 41
1.12 Relative error in the estimation of the bending energy of a semicircle 41
1.13 Discretization of an elastica curve and evaluation of its bending energy 42
1.14 Relative error in the estimation of the bending energy of an elastica 42
1.15 Definition of the tangent vector associated to the circumscribed curvature 45
1.16 Definition of the tangent vector associated to the inscribed curvature 47
1.17 Two methods to parallel transport a vector 50

List of Tables

1.1 Review of several discrete curvature definitions 36

A.1 Project review - general informations. 60
A.2 Project review - key numbers 61

Introduction

La paternité des structures de type *gridshell élastique* est couramment attribuée à l'architecte et ingénieur allemand Frei Otto, qui les a intensivement étudiées au XX$^{\text{ème}}$ siècle. Fruit de son travail de recherche, il réalise en 1975, en collaboration avec l'ingénieur Edmund Happold du bureau Arup, un projet expérimental de grande ampleur : la Multihalle de Mannheim [1, 2]. Cette réalisation emblématique ancrera durablement les gridshells dans le paysage des typologies structurelles candidates à l'avènement de géométries non-standard, caractérisées par l'absence d'orthogonalité. Cette capacité à *former la forme* de façon efficiente prend tout son sens dans le contexte actuel où, d'une part la forme s'impose comme une composante prédominante de l'architecture moderne (F. Gehry, Z. Hadid, ...) et d'autre part l'enveloppe s'affirme comme le lieu névralgique de la performance des bâtiments, notamment environnementale.

Littéralement, le terme *grid-shell* désigne une résille à double courbure dont le comportement mécanique s'apparente à celui d'une coque ; c'est à dire que les efforts y transitent principalement de manière membranaire. Ces ouvrages peuvent franchir de grandes portées en utilisant un minimum de matière. Cependant, il semble plus rigoureux et plus fidèle à l'histoire de désigner par *gridshell élastique* la combinaison indissociable d'un principe structurel – le gridshell, une résille qui fonctionne telle une coque – et d'une méthode constructive astucieuse – la déformation réversible d'une grille de poutre initialement plane pour former une surface tridimensionnelle à double courbure. Le projet de Mannheim – dans lequel une grille en bois de trame régulière, initialement plane et sans rigidité de cisaillement est déformée élastiquement jusqu'à la forme désirée via un dispositif d'étaiement, puis contreventée pour mobiliser la raideur d'une coque et finalement couverte d'une toile – pose les bases de ce nouveau concept et le rend populaire auprès d'un large public d'architectes et d'ingénieurs de par le monde.

Cependant, en dépit du potentiel de cette typologie, très peu de projets ont vu le jour suite à la construction de la Multihalle. Il faut en effet attendre 25 ans et le développement des méthodes de calcul numérique pour voir de nouveau éclore quelques réalisations iconiques : Shigeru Ban innove en passant du bois au carton pour la construction du Pavillon de Hanovre en 2000 [3] ; puis viennent les gridshells en bois de Downland en 2002 [4] et de Savill en 2006 [5] qui reprennent fidèlement les principes développés à Mannheim mais emploient des méthodes constructives différentes. Depuis une dizaine d'années le laboratoire Navier a investi ce champ de recherche sous le double aspect de la structure et du matériau, donnant lieu à la réalisation de quelques prototypes (en 2006 et 2007 [6, 7]) et des deux premiers bâtiments de type gridshell élastique en matériau composite construits à ce jour (Solidays 2011 [8] et Créteil 2013 [9]).[1] Plus récemment, on a pu observer un

[1] Ici, le matériau employé, un composite à base de fibres de verre imprégnées dans une matrice polyester et obtenu par pultrusion, apporte

certain engouement pour la construction de pavillons en bois de petite taille, non couverts, réalisés selon des principes similaires à ceux de la Multihalle, essentiellement dans le cadre de workshops pédagogiques ou bien de projets de recherche [10, 11, 12, 13].

Il est naturel de se demander pourquoi cette innovation prometteuse peine ainsi à essaimer ? S'il est vrai que la construction de la Multihalle de Mannheim a permis de prouver la faisabilité économique et technique du concept de gridshell élastique à grande échelle, il faut bien reconnaître que cette prouesse n'a été rendue possible qu'au terme d'un long processus de maturation pour développer et acquérir l'ensemble des compétences scientifiques, techniques, méthodologiques et humaines nécessaires à sa conception et à sa construction.[2]

En vérité, une telle dépense de moyens pour développer et rassembler ces compétences ne saurait assurer la reproductibilité de cette experience sauf en de très rares occasions et pour des projets d'exception. Par ailleurs, les techniques développées à l'époque sont pour partie tombées en désuétude (e.g. la recherche de forme par maquette physique) ou bien ont fortement évoluées voir même mutées (e.g. le calcul numérique). Des matériaux nouveaux, composites, ont vu le jour. Ils repoussent les limitations intrinsèques des matériaux usuels tel que le bois et offrent des performances techniques bien plus intéressantes pour ce type d'application (durabilité, allongement à la rupture, légèreté, résistance mécanique, fiabilité de niveau industrielle, . . .). Enfin, notons que le cadre réglementaire s'est considérablement étoffé apportant aussi son lot de rigidités vis-à-vis de la pénétration des innovations dans le secteur de la construction.

Ainsi la conception des gridshells se pose-t-elle en des termes nouveaux aux architectes et ingénieurs actuels. Elle se heurte aux deux difficultés majeures suivantes :

- La première difficulté est d'ordre technique et concerne la fonctionnalisation de la structure. En effet, bien que le principe du gridshell permette de réaliser des ossatures courbes de manière optimisée, il n'en reste pas moins complexe de constituer à partir de cette résille porteuse une véritable enveloppe de bâtiment capable de répondre à un large panel de critères performantiels (tels que l'étanchéité, l'isolation thermique, l'isolation acoustique, . . .) sur un support qui ne présente aucune rationalité géométrique.[3]
- La seconde difficulté est d'ordre théorique et concerne la mise au point d'outils et de processus de conception adaptés à l'étude de ces structures d'un genre nouveau où Architecture et Ingénierie collaborent de manière indissociable à l'identité formelle de l'ouvrage. L'inadéquation des méthodes et des outils de design actuels, orientés davantage vers la justification des ouvrages que vers leur conception, constitue un des principaux freins à la diffusion de cette innovation.

La présent manuscrit s'articule autour de deux grandes parties qui tentent chacune de construire des éléments de réponse aux défis identifiés précédemment. La première partie, composée des chapitres 1 et 2, est destinée à présenter en profondeur le concept de gridshell élastique, son potentiel et les difficultés techniques sous-jacentes (voir part I). La seconde partie, composée des chapitres 3 à 6, est consacrée au développement d'un élément de poutre discret original prenant en compte les sollicitations de flexion et de torsion et applicable à tout type de

un gain de performance très significatif par rapport au bois et permet de rester sur une conception à simple nape là où le bois aurait nécessité une grille à double nape beaucoup plus complexe à réaliser.

[2] "This is not a case of a building creatively designed, but based on a support system of additive known elements. This design is the result of a symposium of creative thought in the formation, the invention of building elements with the simultaneous integration of the theoretical, scientific contributions from mathematics, geodesy, model measuring, statics as well as control loading and calculation. We are dealing with more than pure 'teamwork', we are dealing with team creation." [Georg Lewenton 1, p. 201]

[3] Pour contourner cette difficulté, une approche prometteuse consiste à identifier des classes de surfaces courbes (comme les maillages isoradiaux) dont certaines propriétés géométriques (e.g. facettes planes, noeuds sans torsion) s'avèrent avantageuses sur le plan constructif [14].

section dont le centre de torsion est confondu avec le centre de masse, ainsi que certains types de discontinuités liées à la présence de connexions dans les résilles de type gridshell (voir part II). Cette seconde partie constitue le coeur *académique* de ce travail de thèse.

Dans **??** nous rappelons la genèse de cette invention et nous en donnons une définition précise et actualisée. Puis nous dressons un état des lieux critique des projets réalisés sur ce principe depuis le début des années 1960 à nos jours. Cette brève histoire des gridshells dessine à elle seule le potentiel de ces structures, notamment en terme d'expression formelle et de performance structurelle. Loin de les enfermer dans un style d'architecture particulier, elle en souligne au contraire la formidable variété. Cette revue de projet est complétée par une revue approfondie de la littérature existante sur l'ensemble des domaines connexes à cette thématique (géométrie, structure, matériaux, logiciel).

Dans **??** nous présentons de manière détaillée la conception et la réalisation de la cathédrale éphémère de Créteil, un gridshell élastique en matériau composite construit en 2013 et toujours en service. Cette expérience peu commune a été une source inépuisable pour alimenter ce travail de thèse. Cette relecture expose les méthodes et les outils de conceptions développés pour faire aboutir le projet, les difficultés rencontrées, les pistes d'amélioration. Elle fournit également une analyse économique pour cerner les axes de progrès prioritaires dans l'optique d'une commercialisation future.

Dans chapter 1 nous rappelons les notions fondamentales déjà connues, indispensables à notre étude, pour la caractérisation géométrique de courbes de l'espace et de repères mobiles attachés à des courbes. Ces notions sont présentées pour le cas continu puis pour le cas discret ; ce dernier étant essentiel pour la résolution numérique de notre modèle. Cependant, nous observons que la notion clef de courbure géométrique perd son univocité dans le cas discret. Nous identifions alors plusieurs définitions de la courbure discrète. Puis nous les comparons selon des critères propres à notre application (convergence géométrique, représentativité énergétique, forme d'interpolation). A l'issu de cette analyse, la définition la plus pertinente est retenue pour le développement du nouveau modèle numérique au cours des chapitres suivants.

Dans **??** nous élaborons un premier modèle de poutre à 4-DOFs par une approche variationnelle. Ici nous reprenons et enrichissons un travail initié lors d'une précédente thèse [15] inspirée par des travaux récents sur la simulation des tiges élastiques dans le domaine des *computer graphics* [16], et à laquelle j'ai collaboré [17, 18]. En particulier, notre développement permet d'aboutir à des expressions purement locales des efforts internes et prouve l'équivalence avec le membre statique des équations de Kirchhoff. Sur le plan mathématique, le modèle est développé en continu et son implémentation numérique n'est pas traité.

Dans **??** nous développons une nouvelle approche, plus directe et plus complète, pour construire à partir des équations de Kirchhoff un élément de poutre enrichi par un noeud fantôme et possédant lui aussi un nombre de degré de liberté minimal. L'originalité de cet élément est de pouvoir localiser proprement dans l'espace certains types de discontinuités, notamment des discontinuités de courbures provoquées par des efforts ponctuels ou des sauts de propriétés matérielles. Cela permet une modélisation plus fine des phénomènes physiques au sein de la grille, aussi bien au niveau des connexions que des conditions aux appuis, ce qui était le principal objectif de ce travail de thèse.

Dans **??** nous combinons les résultats des chapitres précédents pour construire un élément de poutre discret tout à fait adapté à la modélisation numérique des gridshells élastiques. Nous présentons la construction de cet élément et la méthode de résolution numérique employée pour trouver l'état d'équilibre statique du système, à savoir le relaxation dynamique. Enfin, nous donnons quelques éléments sur *Marsupilami*, le programme informa-

tique que nous avons mis au point et qui implémente l'élément de poutre discret élaboré au cours de cette thèse. Nous exposons aussi quelques résultats de comparaison avec des logiciels du commerce qui ont permi de valider notre travail. Plus généralement, l'élément développé convient bien pour modéliser des problèmes de couplage flexion-torsion dans des poutres élancées, comme par exemple les phénomènes de repositionnement des câbles et des gaînes accrochées aux bras robots, un matériel industriel qui se démocratise à grande vitesse.

Elastic gridshells Part I

Rich Kirchhoff beam model

Part II

1 Geometry of smooth and discrete space cur

1.1 Introduction

In this chapter, our goal is to develop a comprehensive view of the geometry of space curves and how to frame such curves. Indeed, framed curve representations are of central importance when dealing with slender beam models, as they are often modeled using curvilinear coordinate systems. This is the kind of representation on which our beam model will be based on.

Although the theoretical beam model takes place in the smooth world, our model will be implemented in a numerical solver, hence the necessity of a discrete representation. However, the two worlds are intimately related to each other and this is why we chose to present them both in this chapter.[1]

A comprehensive understanding of the geometry of discrete curves will enable to build a beam model with reduced degrees of freedom and capable of representing discontinuities in curvature. This last point is of particular interest when modeling real structures with complex boundary conditions and connexions where concentrated moments are transferred (this is where jumps in curvature occur).

1.1.1 Overview

We start this chapter by recalling the fundamentals of smooth parametric curves (see section 1.2). We introduce the *Frenet frame*, a crucial tool for the local characterization of space curves (see section 1.3), and we identify two geometric invariants, the curvature and the torsion of Frenet, that fully describe the geometry of a given space curve (see section 1.4).[2] We then introduce the notion of moving frame which allow to define a local orientation to each material point on a curve (see section 1.5). This description will later be essential when

[1] L'Hospital 1696 [19, preface] : "Car les courbes n'étant que des polygones d'une infinité de côtés, & ne différant entr' elles que par la différence des angles que ces côtés infiniment petits font entr'eux ; il n'appartient qu'à l'Analyse des infiniment petits de déterminer la position de ces cotés pour avoir la courbure qu'ils forment [. . .]."

[2] Here, invariant means invariant under affine isometries.

modeling cross-section of beams. Among all the possible ways to frame a curve we look at rotation-minimizing frames. These frames are constructed thanks to the parallel transport operator, defined in the same section, which leads to the introduction of the *Bishop frame* : a torsion-free moving frame that will be at the heart of the beam model developed in the following chapters.

We then move on the discrete case and we first draw up a representation of a discrete curve as an ordered sequence of vertices linked by edges (see section 1.6). We gather several definitions of the curvature for a discrete curve and we interpret them in terms of their osculating circle (see section 1.7). Among these definitions, we focus on the curvatures defined respectively by the circumscribed and the inscribed osculating circles. We extend their definition to the curve endings as this is a matter of concern when dealing with mechanical boundary conditions – such as pinned or fixed endings. We study their behavior with respect to the turning angle – that is the angle between two consecutive edges – and we analyze their sensitivity to non uniform discretizations as this is a matter of concern when modeling real structures (see section 1.7.2). We then compare to what extent these curvatures can represent accurately the bending energy of typical curves, namely a circular curve and an elastica curve (see section 1.7.3). For these two curvatures we demonstrate that a natural definition for the tangent vector emerges and we show how to construct it all along the discrete curve. This vector will later be associated to the cross-section normal vector in our Kirchhoff beam model (see section 1.8). Finally, we recall two methods to parallel transport vectors or frames along a discrete curve (see section 1.9). These methods will be used later to construct a twist-free reference frame from our beam model.

1.1.2 Contributions

- We gather several definitions of the curvature for a discrete curve and we interpret them in terms of their osculating circle.
- We focus on the discrete curvatures defined respectively by the circumscribed and the inscribed osculating circles. We extend their definition to curve endings, which is crucial when modeling mechanical boundary conditions where nodes are positioned at points of interest.
- We study their behavior with respect to the turning angle and we analyze their sensitivity to non uniform discretization, which is likely to arise when modeling real structures.
- We compare to what extent these curvatures can represent accurately the bending energy of typical bended shapes (circle and elastica) regarding the sharpness of the discretization. This help us to choose which curvature representation to implement in our beam model.
- We demonstrate that a natural definition for the tangent vector at vertices emerges for these curvatures. This will lead to a model with reduced number of degrees of freedom.
- We show how the local curvature and the tangent vector are related one to each other. This will lead to a straightforward modeling of boundary conditions and connections. This will also allow to model discontinuities in curvature at vertices, thus enabling the modeling of applied concentrated moments and jumps in beam properties (ES, EI, GJ).

1.1.3 Related work

Delcourt 2011 [20] gives a thorough historical review of the study of space curves from Clairaut to Darboux. This history is paved with the nouns of illustre mathematicians such as Euler, Bernoulli, Monge, Fourier, Lagrange, Cauchy, Serret, Frenet, ... It reveals that the study of curves was often related to the study of physical problems (e.g. the elastica for Bernoulli & Euler, the helix for Pito).

In his lecture notes on discrete differential geometry of curves and curfaces, Hoffmann 2009 [21] presents three definitions for the discrete curvature. In his lecture notes on discrete differential geometry of plane curves, Vouga 2014 [22] constructs new discrete curvatures that mimic some of the interesting properties of the curvature in the smooth case. He remarks that none of the established discrete curvatures can reproduce all the properties of the curvature in the smooth case.

Bishop 1975 [23] remarks that the usual Frenet frame is not the only way to frame a curve. He gives the skew-symmetric system of differential equations that any moving frame satisfies. He remarks that this system is governed by only three coefficient entries, which represent the components of the angular velocity vector of the frame expressed on the frame axes. He argues that the Frenet frame gains part of its significance because it is adapted to the curve and because one component of its angular velocity is null. Hence, he looks for other kind of moving frames that are both adapted and with one of the components of the angular velocity vector that is null. In particular, he looks at adapted frames that does not turn around the curve : what will be called a Bishop frame hereafter.

Klok 1986 [24] makes use of the Bishop frame to produce rotation-minimizing sweeps for visualizing 3D ribbons and cylinders. He remarks that for closed trajectories the start and end frames might not align properly. Guggenheimer 1989 [25] proposes a faster method to compute Klok's frame in relation to the Frenet frame. For that, he remarks that any frame is obtained from the Frenet frame by a rotation around the tangent vector. Bloomenthal 1990 [26] introduces the rotation method to propagate reference frames along a curve. Hanson and Ma 1995 [27] propose an algorithm to parallel transport frames along a curve using the rotation method. Poston *et al.* 1995 [28] propose a quadratically convergent algorithm, also based on the rotation method, to find untwisted sweeping NURBS surfaces within a given error bound.

Wang *et al.* 2008 [29] introduce the double reflexion method to propagate rotation minimizing frames. This method is supposed to be more stable than the rotation method. Farouki *et al.* 2014 [30] investigate the use of rotation-minimizing frames that minimize the rotation around the binormal vector of the curve (compared to Bishop frame that minimizes the rotation around the tangent vector of the curve).

1.2 Parametric curves

In this section we recall some fundamental results on (smooth) parametric curves.[3] In particular, we recall that there is more than one way to parametrize a curve. Amongst all the possible ways to parametrize a given curve, the arc length parametrization is of special interest. With this parametrization, the way a curve is described

[3] Definition form mathworld : "A smooth curve is a curve which is a smooth function, where the word 'curve' is interpreted in the analytic geometry context. In particular, a smooth curve is a continuous map from a one-dimensional space to an n-dimensional space which on its domain has continuous derivatives up to a desired order.".

by a single parameter becomes unequivocal.[4] This parametrization is naturally related to what is commonly understood as the "length of a curve".

1.2.1 Definition

Let I be an interval of $\mathbb{R}$ and $F\colon t \mapsto F(t)$ be a map of $\mathcal{C}^0(I, \mathbb{R}^3)$. Then $\gamma = (I, F)$ is called a *parametric curve* and :

- The 2-uplet (I, F) is called a *parametrization* of γ.
- $\gamma = F(I) = \{F(t), t \in I\}$ is called the *graph* or *trace* of γ.
- γ is said to be $\mathcal{C}^k$ if $F \in \mathcal{C}^k(I, \mathbb{R}^3)$.[5]

Note that for a given graph in $\mathbb{R}^3$ there are different possible parameterizations. Thereafter γ will simply refers to its graph $F(I)$.

1.2.2 Regularity

Let $\gamma = (I, F)$ be a parametric curve, and $t_0 \in I$ be a parameter.

- A point of parameter t_0 is called *regular* if $F'(t_0) \neq 0$.
  The curve γ is called *regular* if γ is $\mathcal{C}^1$ and $F'(t) \neq 0, \forall t \in I$.
- A point of parameter t_0 is called *biregular* if $F'(t_0)$ and $F''(t_0)$ are not collinear.
  The curve γ is called *biregular* if γ is $\mathcal{C}^2$ and $F'(t) \times F''(t) \neq 0, \forall t \in I$.

Here and thereafter, the prime symbol denotes the derivation with respect to the parameter and the product symbol denotes the cross product.

1.2.3 Reparametrization

Let $\gamma = (I, F)$ be a parametric curve of class $\mathcal{C}^k$, $J \in \mathbb{R}^3$ an interval, and $\varphi\colon I \mapsto J$ be a $\mathcal{C}^k$ diffeomorphisme. Let us define $G = F \circ \varphi$. Then :

- $G \in \mathcal{C}^k(J, \mathbb{R}^3)$
- $G(J) = F(I)$
- φ is said to be an admissible *change of parameter* for γ.
- (J, G) is said to be another *admissible parametrization* for γ.

[4] This is not rigorously exact but that is the idea. Indeed, this is true only for a given choice of orientation and to within a constant.
[5] A function f is said to be of class $\mathcal{C}^k$ if $f, f', f'', \ldots, f^{(k)}$ exist and are continuous.

1.2.4 Natural parametrization

Let γ be a space curve of class $\mathcal{C}^1$. A parametrization (I, F) of γ is called *natural* if $\|F'(t)\| = 1, \forall t \in I$. Thus :

- The curve is necessarily regular.
- F is strictly monotonic.

1.2.5 Curve length

Let $\gamma = (I, F)$ be a parametric curve of class $\mathcal{C}^1$. The length of γ is defined as :

$$L = \int_I \|F'(t)\| dt \tag{1.1}$$

Note that as expected, the length of γ is invariant under reparametrization.

1.2.6 Arc length parametrization

Let $\gamma = (I, F)$ be a regular parametric curve. Let $t_0 \in I$ be a given parameter. The following map is said to be the *arc length of origin* t_0 of γ :

$$s \colon t \mapsto \int_{t_0}^{t} \|F'(u)\| du \quad , \quad s \in I \times \mathbb{R} \tag{1.2}$$

The arc length $s \colon I \mapsto s(I)$ is an admissible change of parameter for γ. Indeed, s is a $\mathcal{C}^1$ diffeomorphisme because it is bijective ($s' > 0$).

Let us define $G = F \circ s^{-1}$ and $J = s(I)$. Thus (J, G) is a natural reparametrization of γ and $\forall s \in J,\ \|G'(s)\| = 1$. This parametrization is preferred because the natural parameter s traverses the image of γ at unit speed ($\|G'\| = 1$).[6]

Thereafter, for a regular curve γ, $\gamma(t)$ will denote the point $F(t)$ of parameter $t \in I$ while $\gamma(s)$ will denote the point $G(s)$ of arc length $s \in J = [0, L]$.

1.3 Frenet trihedron

The Frenet trihedron is a fundamental mathematical tool from the field of differential geometry to study the local characterization of planar and non-planar space curves. It is a direct orthonormal basis attached to any point P of parameter $t \in I$ on a parametric curve γ. This basis is composed of three unit vectors $\{\boldsymbol{t}(t), \boldsymbol{n}(t), \boldsymbol{b}(t)\}$ called respectively the *tangent*, the *normal*, and the *binormal* unit vectors.[7]

[6] Regular curves are also known as *unit speed* curves.

[7] Strictly speaking the map $\boldsymbol{t} : t \longmapsto \boldsymbol{t}(t)$ is a *vector field* while $\boldsymbol{t}(t)$ is a *vector* of $\mathbb{R}^3$. For the sake of simplicity, and if there is no ambiguity, these two notions will not be explicitly distinguished hereinafter.

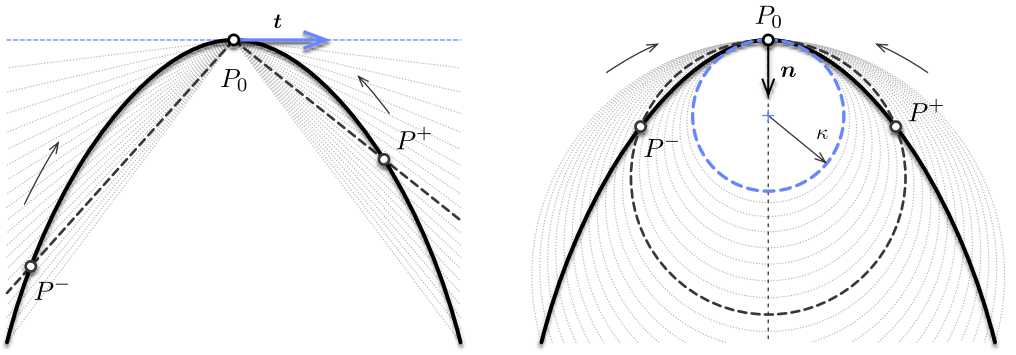

(a) Curve's tangent

(b) Curve's normal and osculating circle

Figure 1.1 – Definition of the tangent vector and the osculating circle of a curve.

Introduced by Frenet in 1847 in his thesis "Courbes à Double Courbure" [31], it brings out intrinsic local properties of space curves : the curvature (κ) which evaluates the deviance of γ from being a straight line (see section 1.4.1) ; and the torsion (τ_f) which evaluates the deviance of γ from being a planar curve (see section 1.4.2).

These quantities, also known as "generalized curvatures" in modern differential geometry, are essential to understand the geometry of space curves. As stated by the *Fundamental Theorem of Space Curves*,[8] a curve is fully determined by its curvature and torsion up to a solid movement in space (see section 1.4.3).

1.3.1 Tangent vector

The first component of the Frenet trihedron is called the *unit tangent vector*. Let $\gamma = (I, F)$ be a regular parametric curve. Let $t \in I$ be a parameter. The *unit tangent vector* is defined as :

$$\boldsymbol{t}(t) = \frac{\gamma'(t)}{\|\gamma'(t)\|} \quad , \quad \|\boldsymbol{t}(t)\| = 1 \tag{1.3}$$

For a curve parametrized by arc length, this expression simply becomes :

$$\boldsymbol{t}(s) = \gamma'(s) \quad , \quad s \in [0, L] \tag{1.4}$$

In differential geometry, the unit tangent to the curve γ at point P_0 is obtained as the limit of the (normalized) vector $\overrightarrow{P_0P}$, when P approaches P_0 on the path γ (see figure 1.1). For a regular curve, the left-sided and right-sided limits coïncide as P^- and P^+ approach P_0 respectively from its left and right sides :

$$\boldsymbol{t}(P_0) = \lim_{P \to P_0} \frac{\overrightarrow{P_0P}}{\|\overrightarrow{P_0P}\|} = \lim_{P^- \to P_0} \frac{\overrightarrow{P_0P^-}}{\|\overrightarrow{P_0P^-}\|} = \lim_{P^+ \to P_0} \frac{\overrightarrow{P_0P^+}}{\|\overrightarrow{P_0P^+}\|} \tag{1.5}$$

[8] The full demonstration of this theorem is attributed to Darboux in [32, p.11].

1.3.2 Normal vector

The second component of the Frenet trihedron is called the *unit normal vector*. It is constructed from $\boldsymbol{t}'$ which is necessarily orthogonal to $\boldsymbol{t}$. Indeed :

$$\|\boldsymbol{t}\| = 1 \Rightarrow \boldsymbol{t}' \cdot \boldsymbol{t} = 0 \Leftrightarrow \boldsymbol{t}' \perp \boldsymbol{t} \tag{1.6}$$

Remark that for a curve parametrized by arc length equation (1.6) implies that $\gamma'(s) \cdot \gamma''(s) = 0$.

Let $\gamma = (I, F)$ be a biregular parametric curve. Let $t \in I$ be a parameter. The *unit normal vector* is defined as : [9]

$$\boldsymbol{n}(t) = \frac{\boldsymbol{t}'(t)}{\|\boldsymbol{t}'(t)\|} \quad , \quad \|\boldsymbol{n}(t)\| = 1 \tag{1.7}$$

Using equation (1.3) in equation (1.7) plus the usual derivation rules leads to : [10]

$$\boldsymbol{t}'(t) = \frac{\gamma'(t) \times (\gamma''(t) \times \gamma'(t))}{\|\gamma'(t)\|^3} \tag{1.8}$$

Because $\gamma'(t)$ and $\gamma''(t) \times \gamma'(t)$ are perpendicular the following identity holds :

$$\|\gamma'(t) \times (\gamma''(t) \times \gamma'(t))\| = \|\gamma'(t)\| \|\gamma''(t) \times \gamma'(t)\| \tag{1.9}$$

Thus, combining equations (1.8) and (1.9) gives :

$$\boldsymbol{n}(t) = \frac{\gamma'(t) \times (\gamma''(t) \times \gamma'(t))}{\|\gamma'(t)\| \|\gamma''(t) \times \gamma'(t)\|} \tag{1.10}$$

For a curve parametrized by arc length this expression becomes :

$$\boldsymbol{n}(s) = \frac{\gamma''(s)}{\|\gamma''(s)\|} \quad , \quad s \in [0, L] \tag{1.11}$$

In differential geometry, the unit normal to the curve γ at point P_0 is obtained as the limit of the (normalized) vector $\overrightarrow{P_0P^+} - \overrightarrow{P_0P^-}$, as P^- and P^+ approach P_0 respectively from its left and right side (figure 1.1) :

$$\boldsymbol{n}(P_0) = \lim \frac{\overrightarrow{P_0P^+} - \overrightarrow{P_0P^-}}{\|\overrightarrow{P_0P^+} - \overrightarrow{P_0P^-}\|} \tag{1.12}$$

Remark that the notion of *normal vector* is ambiguous for non-planar curves as there is an infinite number of possible normal vectors lying in the plane orthogonal to the curve's tangent. In practice, the tangent derivative is a convenient choice as it allows to extend the notion of curvature from planar to non-planar space curves. However, we will see in section 1.5.6 that other kinds of trihedron can be constructed regarding this choice and that one of them is especially suitable for the study of slender beams.

[9] Note that $\boldsymbol{n}$ exists if only γ is biregular, that is $\boldsymbol{t}'$ never vanishes, or equivalently γ is never locally a straight line. In that case the Frenet trihedron is undefined.

[10] Recall that $\gamma'(t) \times (\gamma''(t) \times \gamma'(t)) = \gamma''(t)(\gamma'(t) \cdot \gamma'(t)) - \gamma'(t)(\gamma''(t) \cdot \gamma'(t))$ and that $\|\gamma'(t)\| = \sqrt{\gamma'(t) \cdot \gamma'(t)}$.

1.3.3 Binormal vector

The third vector of Frenet's trihedron is called the *unit binormal vector*. It is constructed from $\boldsymbol{t}$ and $\boldsymbol{n}$ to form an orthonormal direct basis of $\mathbb{R}^3$. Let $\gamma = (I, F)$ be a biregular parametric curve. Let $t \in I$ be a parameter. The *unit binormal vector* is defined as :

$$\boldsymbol{b}(t) = \boldsymbol{t}(t) \times \boldsymbol{n}(t) \quad , \quad \|\boldsymbol{b}(t)\| = 1 \tag{1.13}$$

Combining equation (1.3) and equation (1.10) with equation (1.13) leads to :

$$\boldsymbol{b}(t) = \frac{\gamma'(t) \times \gamma''(t)}{\|\gamma'(t) \times \gamma''(t)\|} \tag{1.14}$$

For a curve parametrized by arc length, this expression becomes : [11]

$$\boldsymbol{b}(s) = \boldsymbol{t}(s) \times \boldsymbol{n}(s) = \frac{\gamma'(s) \times \gamma''(s)}{\|\gamma''(s)\|} \quad , \quad s \in [0, L] \tag{1.15}$$

1.3.4 Osculating plane

The tangent and normal unit vectors $\{\boldsymbol{t}, \boldsymbol{n}\}$ form an orthonormal basis of the so-called *osculating plane*, whereas the binormal vector $(\boldsymbol{b})$ is orthogonal to it. This plane is of prime importance because it is the plane in which the curve takes its curvature (see section 1.4.1).

As reported in [32, p.45], the osculating plane seems to have been first introduced by Bernoulli as the plane passing through three infinitely near points on a curve.[12] Likewise, in modern differential geometry, the osculating plane is defined as the limit of the plane passing through the points P^-, P_0 and P^+ while P^- and P^+ approach P_0 respectively from its left and right side (figure 1.1).

Note that the normal unit vector and the binormal unit vector $\{\boldsymbol{n}, \boldsymbol{b}\}$ define the so-called *normal plane*, while the normal tangent vector and the binormal unit vector $\{\boldsymbol{t}, \boldsymbol{b}\}$ define the so-called *rectifying plane*. These planes are secondary for the present study.

1.4 Curves of double curvature

The study of space curves belongs to the field of differential geometry. According to [32, p.28], the terminology *curve of double curvature* is attributed to Pitot around 1724.[13] However, as stated in [35, p.321] curvature and torsion where probably first thought by Monge around 1771.[14] It is also interesting to note that, at that time,

[11] For an arc length parametrized curve the following identity holds : $\|\gamma'(s) \times \gamma''(s)\| = \|\gamma'(s)\|\|\gamma''(s)\|$.

[12] "Voco autem planum osculans, quod transit per tria curvae quaesitae puncta infinite sibi invicem propinqua" [33, p.113].

[13] "Les Anciens ont nommé cette courbe Spirale ou Hélice ; parce que la formation sur le cylindre suit la même analogie que la formation d'une spirale ordinaire sur un plan; mais elle est bien différente de la spirale ordinaire, étant une des courbes à double courbure, ou une des lignes qu'on conçoit tracée sur la surface des Solides. Peut-être que ces sortes de courbes à double courbure, ou prises sur la surface des Solides, feront un jour l'objet des recherches des géomètres. Celle que nous venons d'examiner est, je crois, la plus simple de toutes. " [34, p.28]

[14] "On appelle point d'inflexion, dans une courbe plane, le point où cette ligne, après avoir été concave dans un sens, cesse de l'être pour devenir concave dans l'autre sens. Il est évident que dans ce point, la courbe perd sa courbure, et que les deux élémens consécutifs sont

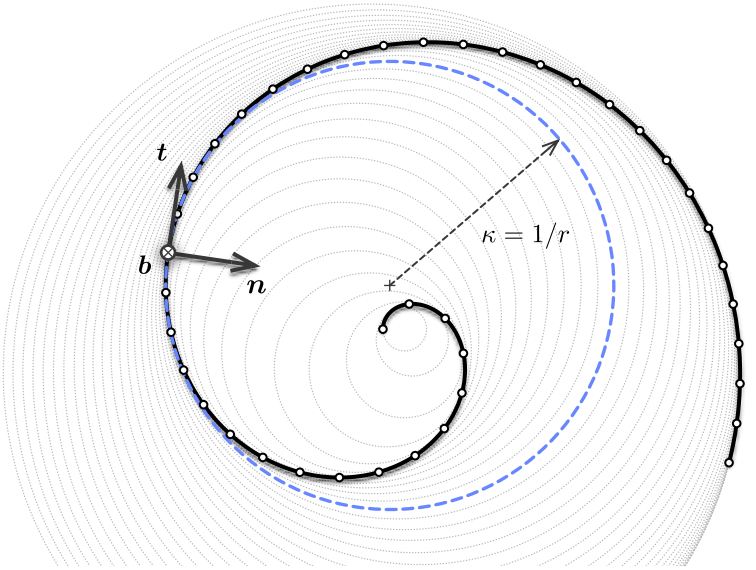

Figure 1.2 – Osculating circles for a spiral curve at different parameters.

curvature was also referred to as *flexure*, reflecting that the study of physical problems (e.g. *the elastica*) and the study of curves of double curvature were intimately related to each other.

Space curves were historically understood as *curves of double curvature* by extension to the case of planar curves, where the curvature measures the deviance of a curve from being a straight line. The second curvature, nowadays known as the *torsion* or *second generalized curvature*, measures the deviance of a curve from being planar.

1.4.1 First invariant : the curvature

In differential geometry, the *osculating circle* is defined as the limit of the circle passing through the points P^-, P_0 and P^+ while P^- and P^+ approach P_0 (figure 1.1). This circle lies on the osculating plane and its radius is nothing but the inverse of the local curvature of a curve.[15] While the tangent gives the best local approximation of the curve as a straight line, the osculating circle gives the best local approximation of that curve as an arc.

The curvature is also known to be the *gradient of arc length* (see [22, p.4]) and calculated as : $\nabla L = \kappa \boldsymbol{n}$. Thus,

en ligne droite. Mais une courbe à double courbure peut perdre chacune de ses courbures en particulier, ou les perdre toutes deux dans le même point ; c'est-à-dire, qu'il peut arriver ou que trois élémens consécutifs d'une même courbe à double courbure se trouvent dans un même plan, ou que deux de ces élémens soient en ligne droite. Il suit de là que les courbes à double courbure peuvent avoir deux espèces d'inflexions ; la première a lieu lorsque la courbe devient plane, et nous l'appellerons simple inflexion ; la seconde, que nous appellerons double inflexion, a lieu lorsque la courbe devient droite dans un de ses points." [36, p.363].

[15] As explained by Euler himself, at a given arc length parameter (s), the osculating plane is the plane in which a curve takes its curvature : "in quo bina fili elementa proxima in curvantur" [37, p.364].

the curvature gives the first-order variation in arc length when deforming a curve γ into the curve $\gamma + \epsilon\delta\gamma$:

$$L(\gamma + \epsilon\delta\gamma) = L(\gamma) + \epsilon(\nabla L \cdot \delta\gamma) + o(\epsilon) \tag{1.16a}$$

$$\nabla L \cdot \delta\gamma = \frac{d}{d\epsilon} L(\gamma + \epsilon\delta\gamma)\Big|_{\epsilon=0} = \int_0^L \kappa(\delta\gamma \cdot \boldsymbol{n}) \tag{1.16b}$$

This is easily understood in the case of a circle of radius r extended to a circle of radius $r + dr$, where the total arc length variation is given by : $L(r + dr) - L(r) = \kappa dr L(r)$.

Note that due to the inner product with the normal vector, only the normal component of the deformation results in an effective extension of the curve. This point is worth to note as it will be related to the *inextensibility assumption* made later in our beam model (see **??**).

Curvature

Let γ be a regular arc length parametrized curve. Let $s \in [0, L]$ be an arc length parameter. The *curvature* is a positive scalar quantity defined as :

$$\kappa(s) = \|\boldsymbol{t}'(s)\| \geq 0 \quad , \quad \boldsymbol{t}'(s) = \kappa(s)\boldsymbol{n}(s) \tag{1.17}$$

The curvature is *independent* regarding the choice of parametrization. This makes the curvature an *intrinsic property* of a given curve and that is why it is also referred to as a *geometric invariant*. Following [38, pp.203-204] it can be computed for any parametrization (I, F) of γ as :

$$\kappa(t) = \frac{\|\gamma'(t) \times \gamma''(t)\|}{\|\gamma'(t)\|^3} \quad , \quad \boldsymbol{t}'(t) = \|\gamma'(t)\|\kappa(t)\boldsymbol{n}(t) \tag{1.18}$$

Note that in equation (1.17) the prime symbol denotes the derivative with respect to the natural parameter (s) while in equation (1.18) it denotes the derivative with respect to any parameter (t). Consequently, the *speed* of the curve's parametrization appears in the latter equation :

$$v(t) = \frac{ds}{dt} = \|\gamma'(t)\| = s'(t) \tag{1.19}$$

The curvature measures how much a curve bends instantaneously in its osculating plane, that is how fast the tangent vector is rotating in the osculating plane around the binormal vector. In differential geometry this is expressed for a planar curve as :

$$\kappa(s) = \lim_{ds \to 0} \frac{\angle(\boldsymbol{t}(s), \boldsymbol{t}(s + ds))}{ds} = \lim_{ds \to 0} \frac{(\boldsymbol{t}(s + ds) - \boldsymbol{t}(s)) \cdot \boldsymbol{n}(s)}{ds} \tag{1.20}$$

where $\angle(\boldsymbol{t}(s), \boldsymbol{t}(s + ds))$ denotes the angle between $\boldsymbol{t}(s)$ and $\boldsymbol{t}(s + ds)$. This is equivalent as measuring how fast the osculating plane itself is rotating around the binormal vector. Consequently a curve is locally a *straight line* when its curvature vanishes $(\kappa(s) = 0)$.

Radius of curvature

The *radius of curvature* is defined as the inverse of the curvature ($r = 1/\kappa$). From a geometric point of view, one can demonstrate that it is the radius of the osculating circle (see figure 1.2). Remark that where the curvature vanishes the radius of curvature goes to infinity ; that is the osculating circle becomes a line, a circle of infinite radius.

Center of curvature

The *center of curvature* is defined as the center of the osculating circle (see figure 1.2). The locus of all the centers of curvature of a curve is called the *evolute*.

Curvature binormal vector

Finally, following [16] we define the *curvature binormal vector*. Let γ be a biregular arc length parametrized curve. Let $s \in [0, L]$ be an arc length parameter. The *curvature binormal vector* is defined as :

$$\boldsymbol{\kappa b}(s) = \kappa(s)\,\boldsymbol{b}(s) = \boldsymbol{t}(s) \times \boldsymbol{t}'(s) \quad , \quad \|\boldsymbol{\kappa b}(s)\| = \kappa(s) \tag{1.21}$$

This vector will be useful as it embeds all the necessary information on the curvature of the curve. We will see in section 1.5.6 that this vector is associated to the angular velocity of a specific adapted moving frame attached to the curve and called the *Bishop frame*.

1.4.2 Second invariant : the torsion

Let γ be a biregular arc length parametrized curve. Let $s \in [0, L]$ be an arc length parameter. The *torsion* is a scalar quantity defined as :

$$\tau_f(s) = \boldsymbol{n}'(s) \cdot \boldsymbol{b}(s) = -\boldsymbol{b}'(s) \cdot \boldsymbol{n}(s) \tag{1.22}$$

The torsion is *independent* regarding the choice of parametrization. This makes the torsion an *intrinsic property* of a given curve and that is why it is also referred to as a *geometric invariant*. Following [38, p.204] it can be computed for any parametrization (I, F) of γ as :

$$\tau_f(t) = \frac{\gamma'(t) \cdot (\gamma''(t)) \times \gamma'''(t))}{\|\gamma'(t) \times \gamma''(t)\|^2} \quad when \quad \kappa(t) > 0 \tag{1.23}$$

The torsion measures how much a curve goes *instantaneously out of its plane*, that is to say how fast the normal or binormal vectors are rotating in the normal plane around the tangent vector. In differential geometry this is expressed as :

$$\tau_f(s) = \lim_{ds \to 0} \frac{\angle(\boldsymbol{n}(s), \boldsymbol{n}(s+ds))}{ds} = \lim_{ds \to 0} \frac{(\boldsymbol{n}(s+ds) - \boldsymbol{n}(s)) \cdot \boldsymbol{b}(s)}{ds} \tag{1.24}$$

This is equivalent as measuring how fast the osculating plane is rotating around the tangent vector. Consequently a curve is locally *plane* when its torsion vanishes ($\tau_f(s) = 0$).

Remark that the *torsion* is denoted "τ_f" and not simply "τ" as the latter will be reserved to denote any angular velocity of a moving adapted frame around its tangent vector. Thus, τ_f refers to the particular angular velocity of the Frenet trihedron around its tangent vector. This torsion, which is a geometric property of the curve, will be indifferently referred to as the *Frenet torsion* or the *geometric torsion*.

1.4.3 Fundamental theorem of space curves

These two *generalized curvatures*, respectively the curvature (κ) and the torsion (τ_f), are *invariant* regarding the choice of parametrization and under *euclidean motions*.[16] The *fundamental theorem of space curves* states that a curve is fully described, up to a Euclidean motion of $\mathbb{R}^3$, by its positive curvature ($\kappa > 0$) and torsion (τ_f) [38, p.229].

1.4.4 Serret-Frenet formulas

The *fundamental theorem of space curves* is somehow a consequence of the *Serret-Frenet formulas*, which is the first-order system of differential equations satisfied by the Frenet trihedron. Let γ be a biregular arc length parametrized curve. Let $s \in [0, L]$ be an arc length parameter. Then, the Frenet trihedron satisfies the following formulas :

$$\boldsymbol{t}'(s) = \kappa(s)\boldsymbol{n}(s) \tag{1.25a}$$
$$\boldsymbol{n}'(s) = -\kappa(s)\boldsymbol{t}(s) + \tau_f(s)\boldsymbol{b}(s) \tag{1.25b}$$
$$\boldsymbol{b}'(s) = -\tau_f(s)\boldsymbol{n}(s) \tag{1.25c}$$

This system can be seen as the *equations of motion* of the Frenet trihedron moving along the curve γ at unit speed ($\|\gamma'\| = 1$). Indeed, introducing its *angular velocity vector* also known as the *Darboux vector* ($\boldsymbol{\Omega_f}$), the previous system is expressed as :

$$\begin{bmatrix} \boldsymbol{t}'(s) \\ \boldsymbol{n}'(s) \\ \boldsymbol{b}'(s) \end{bmatrix} = \boldsymbol{\Omega_f}(s) \times \begin{bmatrix} \boldsymbol{t}(s) \\ \boldsymbol{n}(s) \\ \boldsymbol{b}(s) \end{bmatrix} \quad \text{where} \quad \boldsymbol{\Omega_f}(s) = \begin{bmatrix} \tau_f(s) \\ 0 \\ \kappa(s) \end{bmatrix} \tag{1.26}$$

Because the Frenet trihedron satisfies a first-order system of differential equations of parameters κ and τ_f it is possible, by integration, to reconstruct the trace of the moving frame and thus the curve, up to a constant of integration (a trihedron in this case).

Finally, these formulas can be generalized to any non unit-speed parametrization of a curve.[17] Let $\gamma = (I, F)$ be a biregular parametric curve. Let $t \in I$ be a parameter. Then the following *generalized Serret-Frenet formulas*

[16] Or equivalently under affine isometries.
[17] See [38, p.203] for a complete proof.

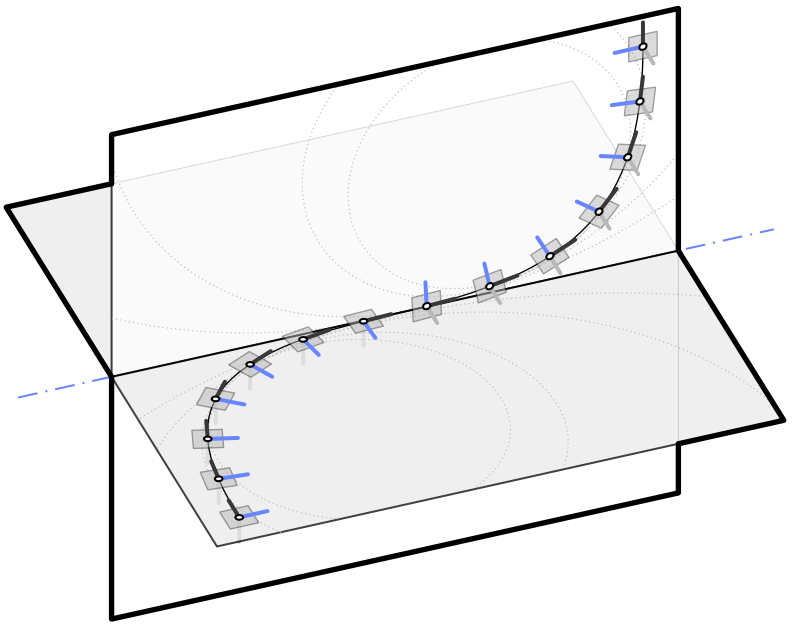

Figure 1.3 – Discontinuity of the Frenet trihedron at an inflexion point where the curvature vanishes and the orientation of the osculating plane is subject to a jump of angle $\pi/2$.

hold :

$$\boldsymbol{t}'(t) = v(t)\kappa(t)\boldsymbol{n}(t) \tag{1.27a}$$
$$\boldsymbol{n}'(t) = -v(t)\kappa(t)\boldsymbol{t}(t) + v(t)\tau_f(t)\boldsymbol{b}(t) \tag{1.27b}$$
$$\boldsymbol{b}'(t) = -v(t)\tau_f(t)\boldsymbol{n}(t) \tag{1.27c}$$

Again, this system can be seen as the *equations of motion* of the Frenet trihedron moving along the curve γ at non unit-speed ($v(t) = \|\gamma'(t)\|$). This time the *angular velocity vector* ($\boldsymbol{\Omega}$) is distinct from the *Darboux vector* ($\boldsymbol{\Omega_f}$) and the previous system is expressed as :

$$\begin{bmatrix}\boldsymbol{t}'(t)\\ \boldsymbol{n}'(t)\\ \boldsymbol{b}'(t)\end{bmatrix} = \boldsymbol{\Omega}(t) \times \begin{bmatrix}\boldsymbol{t}(t)\\ \boldsymbol{n}(t)\\ \boldsymbol{b}(t)\end{bmatrix} \quad \text{where} \quad \boldsymbol{\Omega}(t) = v(t)\begin{bmatrix}\tau_f(t)\\ 0\\ \kappa(t)\end{bmatrix} \tag{1.28}$$

1.5 Curve framing

While the Frenet trihedron "has long been the standard vehicle for analysing properties of the curve invariant[18] under euclidean motions" [23, p.1], a curve can be potentially framed with any arbitrary *moving frame*, under-

[18] Namely the curvature (κ) and the Frenet torsion (τ_f).

stood as an *orthonormal basis field*. Thus, the Frenet frame is not the only way to frame a curve and other frames may also exhibit some interesting properties.[19]

In his paper [23] Bishop establishes the differential equation that a moving frame must satisfy and remarks that, because of the orthonormality condition, the first derivatives of the frame components can be expressed in terms of themselves through a skew-symmetric coefficient matrix. For such a frame, the understanding of its motion along the curve is thus reduced to the knowledge of only three scalar coefficient functions. He remarks that most of the interesting properties that the Frenet frame exhibits are due to the fact that one of these coefficient functions is vanishing everywhere on the curve (that is the frame is *rotation-minimizing* regarding one of its components) ; and that the Frenet frame is *adapted* to the curve (that is one of its components is nothing but the unit tangent vector).

In this section we introduce the notion of *moving frame* and two properties of interest that such a frame can exhibit in addition, namely : to be *adapted* to the curve ; and to be *rotation-minimizing* regrading a given direction. We then reconsider the case of the Frenet frame regrading this mathematical framework. Finally, we introduce the *zero-twisting* frame also known as the *Bishop* frame.[20] This tool will be fundamental for our futur study of slender beams.

1.5.1 Moving frame

Let γ be a curve parametrized by arc length. A map F which associates to each point of arc length parameter s a direct orthonormal trihedron is said to be a *moving frame* :

$$\begin{array}{rccl} F: & [0,L] & \longrightarrow & \mathcal{SO}_3(\mathbb{R}) \\ & s & \longmapsto & F(s) = \{\boldsymbol{e}_3(s), \boldsymbol{e}_1(s), \boldsymbol{e}_2(s)\} \end{array} \tag{1.29}$$

Note that a direct orthonormal trihedron (or basis) is an element of the *rotation group* denoted $\mathcal{SO}_3$. Consequently, a moving frame F attached to γ satisfies for all $s \in [0,L]$:

$$\|\boldsymbol{e}_i(s)\| = 1 \tag{1.30a}$$

$$\boldsymbol{e}_i(s) \cdot \boldsymbol{e}_j(s) = 0 \quad , \quad i \neq j \tag{1.30b}$$

The term “moving frame” will refer indifferently to the map itself (denoted $F = \{\boldsymbol{e}_3, \boldsymbol{e}_1, \boldsymbol{e}_2\}$), or to a specific evaluation of the map (denoted $F(s) = \{\boldsymbol{e}_3(s), \boldsymbol{e}_1(s), \boldsymbol{e}_2(s)\}$).

At first sight this indexing could seem strange but it will be convenient later in our mechanical model where $\boldsymbol{e}_3$ will be associated to the centerline’s tangent and $\boldsymbol{e}_1$ and $\boldsymbol{e}_2$ to the two cross-section principal axes of inertia. These axes will also be called *material axes*. We chose to introduce this indexing right now to maintain consistency between notations through out the chapters of this manuscript.

[19] Recall the title of Bishop’s paper : “There is more than one way to frame a curve” [23].
[20] Named after Bishop who introduced it.

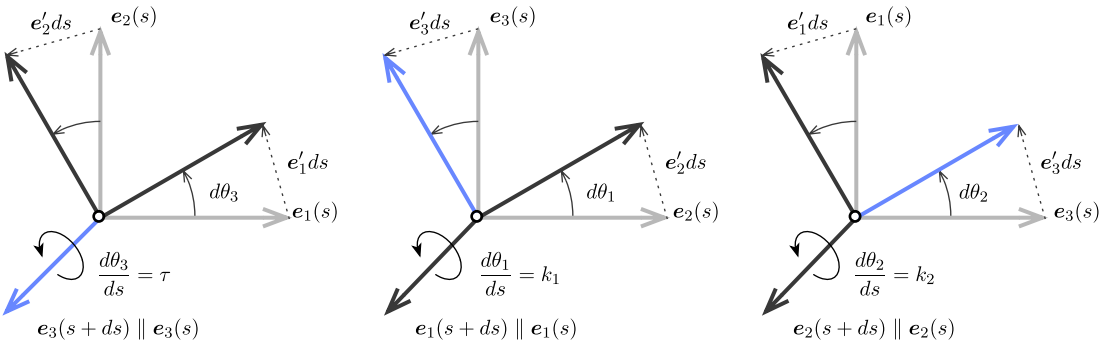

Figure 1.4 – Geometric interpretation of the angular velocity vector of a moving frame.

Governing equations

Computing the derivatives of the previous relationships leads to the following system of differential equations that the frame must satisfy for all $s \in [0, L]$:

$$\boldsymbol{e}_i'(s) \cdot \boldsymbol{e}_i(s) = 0 \tag{1.31a}$$
$$\boldsymbol{e}_i'(s) \cdot \boldsymbol{e}_j(s) = -\boldsymbol{e}_i(s) \cdot \boldsymbol{e}_j'(s) \quad , \quad i \neq j \tag{1.31b}$$

Thus, there exists 3 scalar functions (τ, k_1, k_2) such that $\{\boldsymbol{e}_3', \boldsymbol{e}_1', \boldsymbol{e}_2'\}$ can be expressed in the basis $\{\boldsymbol{e}_3, \boldsymbol{e}_1, \boldsymbol{e}_2\}$:

$$\boldsymbol{e}_3'(s) = k_2(s)\boldsymbol{e}_1(s) - k_1(s)\boldsymbol{e}_2(s) \tag{1.32a}$$
$$\boldsymbol{e}_1'(s) = -k_2(s)\boldsymbol{e}_3(s) + \tau(s)\boldsymbol{e}_2(s) \tag{1.32b}$$
$$\boldsymbol{e}_2'(s) = k_1(s)\boldsymbol{e}_3(s) - \tau(s)\boldsymbol{e}_1(s) \tag{1.32c}$$

It is common to rewrite this first-order linear system of differential equations as a matrix equation : [21,22]

$$\begin{bmatrix} \boldsymbol{e}_3'(s) \\ \boldsymbol{e}_1'(s) \\ \boldsymbol{e}_2'(s) \end{bmatrix} = \begin{bmatrix} 0 & k_2(s) & -k_1(s) \\ -k_2(s) & 0 & \tau(s) \\ k_1(s) & -\tau(s) & 0 \end{bmatrix} \begin{bmatrix} \boldsymbol{e}_3(s) \\ \boldsymbol{e}_1(s) \\ \boldsymbol{e}_2(s) \end{bmatrix} \tag{1.33}$$

Since the progression of any moving frame along γ is ruled by a first-order system of differential equations, a unique triplet $\{\tau, k_1, k_2\}$ leads to a set of moving frames equal to each other within a constant of integration.[23] Basically, with a given triplet $\{\tau, k_1, k_2\}$, one can propagate a given initial direct orthonormal trihedron (at $s = 0$ for instance) through the whole curve by integrating the system of differential equations. In general, a moving frame will be fully determined by τ, k_1 and k_2 together with the initial condition $\{\boldsymbol{e}_3(s=0), \boldsymbol{e}_1(s=0), \boldsymbol{e}_2(s=0)\}$.

[21] In the case of a space curve, where $\boldsymbol{e}_3$ is chosen to be the curve tangent unit vector and $\boldsymbol{e}_1$ is chosen to be the curve normal unit vector, this set of equations is known as the *Serret-Frenet formulas*.

[22] In the case of a space curve drawn on a surface, where $\boldsymbol{e}_3$ is chosen to be the curve tangent unit vector and $\boldsymbol{e}_1$ is chosen to be the surface normal unit vector, this set of equations is known as the *Darboux-Ribaucour formulas*.

[23] This assumption reminds the *Fundamental theorem of space curves* (section 1.4.3).

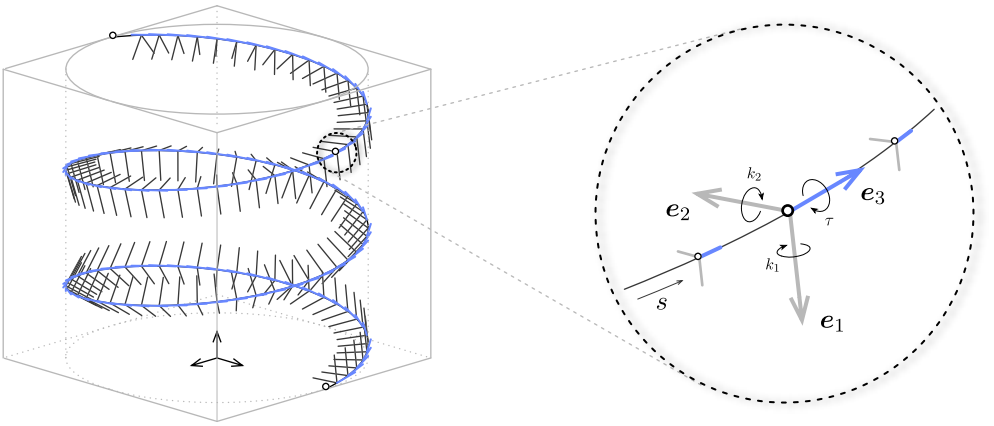

Figure 1.5 – Moving frame $F(s) = \{\boldsymbol{e}_3(s), \boldsymbol{e}_1(s), \boldsymbol{e}_2(s)\}$ on a circular helix. The frame is adapted as $\boldsymbol{e}_3(s) = \boldsymbol{t}(s)$.

Angular velocity

This system can be seen as the *equations of motion* of the frame moving along the curve γ at unit speed ($\|\gamma'\| = 1$). Indeed, introducing its *angular velocity vector* ($\boldsymbol{\Omega}$), the previous system is expressed as :

$$\boldsymbol{e}_i'(s) = \boldsymbol{\Omega}(s) \times \boldsymbol{e}_i(s) \quad \text{where} \quad \boldsymbol{\Omega}(s) = \begin{bmatrix} \tau(s) \\ k_1(s) \\ k_2(s) \end{bmatrix} \tag{1.34}$$

This result is straightforwardly deduced from equation (1.33). Note that the cross product reveals the skew-symmetric nature of the system, which could already be seen in equation (1.33). Geometrically, decomposing the infinitesimal rotation of the moving frame around its directors between arc length s and $s + ds$ (see figure 1.4) shows that the scalar functions τ, k_1 and k_2 effectively correspond to the angular speed of the frame moving along γ, respectively around $\boldsymbol{e}_3$, $\boldsymbol{e}_1$ and $\boldsymbol{e}_2$:

$$\frac{d\theta_3}{ds}(s) = \tau(s) \tag{1.35a}$$

$$\frac{d\theta_1}{ds}(s) = k_1(s) \tag{1.35b}$$

$$\frac{d\theta_2}{ds}(s) = k_2(s) \tag{1.35c}$$

1.5.2 Adapted moving frame

Let F be a moving frame as defined in the previous section. F is said to be *adapted* to γ if at each point $\gamma(s)$, $\boldsymbol{e}_3(s)$ is the unit tangent vector of γ (figure 1.5) :

$$\boldsymbol{e}_3(s) = \boldsymbol{t}(s) = \gamma'(s) \tag{1.36}$$

For an adapted frame, the components k_1 and k_2 of the angular velocity vector are related to the curvature of γ : [24]

$$\kappa(s) = \|\boldsymbol{e}_3'(s)\| = \|k_2(s)\boldsymbol{e}_1(s) + k_1(s)\boldsymbol{e}_2(s)\| = \sqrt{k_1(s)^2 + k_2(s)^2} \tag{1.37}$$

Moreover, recalling the definition of the curvature binormal vector ($\boldsymbol{\kappa b}$) from equation (1.21), it is easy to see that for an adapted moving frame the following relation holds :

$$\boldsymbol{\kappa b}(s) = k_1(s)\boldsymbol{e}_1(s) + k_2(s)\boldsymbol{e}_2(s) \tag{1.38}$$

Consequently, the angular velocity vector of an adapted moving frame can be written as :

$$\boldsymbol{\Omega}(s) = \boldsymbol{\kappa b}(s) + \tau(s)\boldsymbol{t}(s) \tag{1.39}$$

This last result is very interesting as it shows that any adapted moving frame will differ from each other only by their twisting speed, as $\boldsymbol{\Omega}_\perp = \boldsymbol{\kappa b}$ only depends on the curve.

1.5.3 Rotation-minimizing frame

Following [30, 29] we introduce the *rotation-miniminzing frame* notion. A frame $\{\boldsymbol{e}_3, \boldsymbol{e}_1, \boldsymbol{e}_2\}$ is said to be *rotation-miniminzing* regrading a given direction $\boldsymbol{d}$ if :

$$\boldsymbol{\Omega}(s) \cdot \boldsymbol{d}(s) = 0 \tag{1.40}$$

1.5.4 Parallel transport

The notion of *parallel transport* is somehow a generalization of the classical notion of collinearity in flat euclidean spaces (e.g. $\mathbb{R}^2$ or $\mathbb{R}^3$), to spaces that exhibit some non vanishing curvature (e.g. spheric or hyperbolic spaces).[25]

Relatively parallel fields

Following Bishop 1975 [23], we define what is a *(relatively) parallel field*. Let γ be a regular curve parametrized by arc length. Let $\boldsymbol{p}$ be a vector field along γ. The vector field $\boldsymbol{p}$ is said to be *parallel* if its derivative is purely

[24] This is why for an initially straight rod with an isotropic cross-section bending and torsion are uncoupled. Indeed, in that case the bending energy does not depend on the orientation of the cross-sections anymore as it depends only on the curvature of the rod : $\mathcal{E}_b = EI_1\kappa_1^2 + EI_2\kappa_2^2 = EI\kappa^2$.

[25] https://www.youtube.com/watch?v=p1tfZD2Bm0w

tangential, that is :

$$\boldsymbol{p}'(s) \times \boldsymbol{t}(s) = 0 \tag{1.41}$$

Consequently, for an adapted moving frame, the *normal fields* $\boldsymbol{e}_1$ and $\boldsymbol{e}_2$ are both *relatively parallels* if and only if the frame angular velocity is itself a normal field, that is : [26]

$$\boldsymbol{\Omega}(s) = \boldsymbol{\Omega}_{\perp}(s) = \kappa \boldsymbol{b}(s) \Leftrightarrow \boldsymbol{\Omega}(s) \cdot \boldsymbol{t}(s) = 0 \Leftrightarrow \tau(s) = 0 \tag{1.42}$$

In other words, a *relatively parallel normal field* : "turns, only whatever amount is necessary for it to remain normal, so it is as close to being parallel as possible without losing normality" [23].

Parallel transport of vectors along a curve

Reciprocally, it is possible to define the *parallel transport* of a vector along a curve γ as its propagation along γ at angular speed $\kappa \boldsymbol{b}$. An initial vector $\boldsymbol{p}_0 = \boldsymbol{p}(s_0)$ is parallel transported at arc length parameter s into the vector $\boldsymbol{p}(s)$ by integrating the following first-order differential equation along γ :

$$\boldsymbol{p}'(s) = \kappa \boldsymbol{b}(s) \times \boldsymbol{p}(s) \tag{1.43}$$

Consequently, the resulting vector field $\boldsymbol{p}$ is a parallel field. Note that a parallel field is not necessarily a normal field.

From the point of view of differential geometry, this means that the next vector $\boldsymbol{p}(s + ds)$ is obtained by rotating the previous one $\boldsymbol{p}(s)$ around the curve binormal $\boldsymbol{b}(s)$ by an infinitesimal angle $d\theta(s) = \kappa(s)ds$. Note that $\boldsymbol{b}(s)$ has the same direction as $\boldsymbol{t}(s) \times \boldsymbol{t}(s + ds)$.

Parallel transport of frames along a curve

Identically, the *parallel transport* of an adapted frame is defined as the parallel transport of its components along γ.

1.5.5 Frenet frame

The Frenet frame is a well-known particular adapted moving frame. It is defined as the map that attach to any given point of γ the corresponding Frenet trihedron $\{\boldsymbol{t}(s), \boldsymbol{n}(s), \boldsymbol{b}(s)\}$ where :

$$\boldsymbol{t}(s) = \gamma'(s) \tag{1.44a}$$

$$\boldsymbol{n}(s) = \frac{\boldsymbol{t}'(s)}{\kappa(s)} \tag{1.44b}$$

$$\boldsymbol{b}(s) = \boldsymbol{t}(s) \times \boldsymbol{n}(s) \tag{1.44c}$$

[26] A vector field $\boldsymbol{p}$ is said to be *normal* along a curve γ if : $\forall s \in [0, L]$, $\boldsymbol{p} \cdot \boldsymbol{t} = 0$.

Governing equations

The Frenet frame satisfies the *Frenet-Serret formulas* (see section 1.4.4), which govern the evolution of the frame along the curve γ :

$$\begin{bmatrix} \boldsymbol{t}'(s) \\ \boldsymbol{n}'(s) \\ \boldsymbol{b}'(s) \end{bmatrix} = \begin{bmatrix} 0 & \kappa(s) & 0 \\ -\kappa(s) & 0 & \tau_f(s) \\ 0 & -\tau_f(s) & 0 \end{bmatrix} \begin{bmatrix} \boldsymbol{t}(s) \\ \boldsymbol{n}(s) \\ \boldsymbol{b}(s) \end{bmatrix} \tag{1.45}$$

Remember the generic system of differential equations of an adapted moving frame attached to a curve, established in equation (1.33), where $\boldsymbol{e}_3(s) = \boldsymbol{t}(s)$, $k_1(s) = 0$, $k_2(s) = \kappa(s)$ and $\tau(s) = \tau_f(s)$.

Angular velocity

Consequently, the angular velocity vector ($\boldsymbol{\Omega_f}$) of the Frenet frame, also known as the *Darboux vector* in this particular case, is given by :

$$\boldsymbol{\Omega_f}(s) = \begin{bmatrix} \tau_f(s) \\ 0 \\ \kappa(s) \end{bmatrix} = \boldsymbol{\kappa b}(s) + \tau_f(s)\boldsymbol{t}(s) \tag{1.46}$$

Remark that the Frenet frame satisfies $\boldsymbol{\Omega_f}(s) \cdot \boldsymbol{n}(s) = 0$ and is thus a *rotation-miniminzing* frame regarding the normal vector ($\boldsymbol{n}$). The motion of this frame through the curve is known as *pitch-free*.

Note also that $\boldsymbol{t}'(s)$ and $\boldsymbol{b}'(s)$ are collinear to $\boldsymbol{n}(s)$. This means that the projection of $\boldsymbol{t}(s)$ and $\boldsymbol{b}(s)$ is conserved from one normal plane to another, that is $\boldsymbol{t}$ and $\boldsymbol{b}$ are parallel transported along the vector field $\boldsymbol{n}$.

Drawbacks and benefits

The Frenet frame is not continuously defined if γ is not $\mathcal{C}^2$. This is problematic for the study of slender beams as the centerline of a beam subject to concentrated external forces and moments or to material discontinuities will not be $\mathcal{C}^2$ but only picewise $\mathcal{C}^2$. In that case, the centerline tangent will be continuously defined everywhere but the curvature will be subject to discontinuities, that is $\boldsymbol{t}'$ will not be continuously defined.

Moreover, even if γ is $\mathcal{C}^2$, the Frenet frame is not defined where the curvature vanishes, which obviously is an admissible configuration for a beam centerline. This issue can be partially addressed by parallel transporting the normal vector along the straight regions of the curve. Thus, the extended frame will still satisfy the governing equations exposed in equation (1.45). However, if the osculating planes are not parallels on both sides of a region of null curvature, torsion will be subject to a discontinuity and so the Frenet frame (figure 1.3).[27] Again, if the region of null curvature is not a point, that is the region is not an inflexion point but a locus where the curve is locally a straight line, the change in torsion on both sides of the region can be accommodated by a continuous rotation from one end to the other.

One benefit of the Frenet frame is that, when transported along a *closed curve*, the frame at the end of the curve

[27] This is also highlighted in [26, 29].

will align back with the frame at the beginning of the curve, that is the frame will return to its initial value after a complete turn. During its trip, the frame will make a total twist of $\int_0^L \tau_f(s)ds = 0[2\pi]$ around the tangent vector.

A second benefit is that any adapted frame can be obtained by a rotation of the Frenet frame around the unit tangent vector [25, p.2].

1.5.6 Bishop frame

A *Bishop frame* denoted $\{\boldsymbol{t}, \boldsymbol{u}, \boldsymbol{v}\}$, also known as *zero-twisting* or *parallel-transported* frame, is an adapted moving frame that has no tangential angular velocity : [28]

$$\boldsymbol{\Omega} \cdot \boldsymbol{t} = \tau = \boldsymbol{u}' \cdot \boldsymbol{v} = -\boldsymbol{u} \cdot \boldsymbol{v}' = 0 \tag{1.47}$$

Because a Bishop frame is an adapted frame, it can be defined relatively to the Frenet frame by a rotation around the unit tangent vector. A Bishop frame is a frame that *cancels out* the rotational movement of the Frenet frame around the tangent vector. At arc length parameter s, the Frenet frame has continuously rotated around its tangent vector of a cumulative angle : $\int_0^s \tau_f(t)dt$. Thus, any Bishop frame will be obtained, within a constant rotation angle θ_0, through a rotation of the Frenet frame around the tangent vector by an angle :

$$\theta(s) = -\int_0^s \tau_f(t)dt + \theta_0(s) \tag{1.48}$$

Consequently, a Bishop frame can be expressed relatively to the Frenet frame as :

$$\begin{cases} \boldsymbol{u} = \cos\theta \boldsymbol{n} + \sin\theta \boldsymbol{b} \\ \boldsymbol{v} = -\sin\theta \boldsymbol{n} + \cos\theta \boldsymbol{b} \end{cases} \tag{1.49}$$

Governing equations

The Bishop frame satisfies the following system of differential equations, which governs the evolution of the frame along the curve γ :

$$\begin{bmatrix} \boldsymbol{t}'(s) \\ \boldsymbol{u}'(s) \\ \boldsymbol{v}'(s) \end{bmatrix} = \begin{bmatrix} 0 & \kappa(s)\sin\theta(s) & -\kappa(s)\cos\theta(s) \\ -\kappa(s)\sin\theta(s) & 0 & 0 \\ \kappa(s)\cos\theta(s) & 0 & 0 \end{bmatrix} \begin{bmatrix} \boldsymbol{t}(s) \\ \boldsymbol{u}(s) \\ \boldsymbol{v}(s) \end{bmatrix} \tag{1.50}$$

[28] Bishop frames were introduced as *relatively parallel adapted frames* in [23].

One can remember the generic differential equations of an adapted moving frame attached to a curve, where : [29]

$$k_1(s) = \kappa(s)\sin\theta(s) \quad , \quad k_2(s) = \kappa(s)\cos\theta(s) \quad , \quad \tau(s) = 0 \tag{1.51}$$

Angular velocity

Consequently, the angular velocity vector ($\boldsymbol{\Omega_b}$) of the Bishop frame is given by :

$$\boldsymbol{\Omega_b}(s) = \begin{bmatrix} 0 \\ \kappa(s)\sin\theta(s) \\ \kappa(s)\cos\theta(s) \end{bmatrix} = \boldsymbol{\kappa b}(s) \tag{1.52}$$

Remark that the Bishop frame satisfies $\boldsymbol{\Omega_b}(s)\cdot\boldsymbol{t}(s) = 0$ and is thus *rotation-miniminzing* regarding the tangent vector. The motion of this frame through the curve is known as *roll-free*.

Because the motion of this frame is described by an angular velocity vector that is nothing but the curvature binormal vector ($\boldsymbol{\Omega_b} = \boldsymbol{\kappa b}$), it can be interpreted in terms of *parallel transport* as defined in section 1.5.4. Thus, given an initial frame at arc length parameter $s = 0$, the Bishop frame at any arc length parameter (s) is obtained by parallel transporting the initial frame $\{\boldsymbol{t}(0), \boldsymbol{u}(0), \boldsymbol{v}(0)\}$ along the curve from 0 to s.

Drawbacks and benefits

One of the main benefits of the Bishop frame is that its generative method : "is immune to degeneracies in the curvature vector" [26]. Although we first expressed the construction of the Bishop frame relatively to the Frenet frame (which exists wherever γ is biregular), the existence of the Bishop frame, understood in terms of parallel transport, is guaranteed wherever the curvature binormal ($\boldsymbol{\kappa b} = \boldsymbol{t}\times\boldsymbol{t}'$) is defined. To be continuously defined over $[0, L]$, a Bishop frame only needs the curvature binormal vector to be piecewise continuously defined over $[0, L]$, which only requires that γ' is $\mathcal{C}^0$ and that γ'' is piecewise $\mathcal{C}^0$. Obviously, these weaker existence conditions are profitables to bypass the drawbacks of the Frenet frame regarding the modeling of slender beams listed in section 1.5.5.

Strictly speaking, a Bishop frame is not a reference frame as it is defined within an initial condition. However, we will see later that strains in a beam are modeled as a rate of change in the Bishop frame, and consequently the initial condition will disappear in the equations.

Unlike the Frenet frame, when transported along a *closed curve*, the Bishop frame at the end of the curve will not necessarily align back with the frame at the beginning of the curve.[30] Even if the frame returns to its initial value after a complete turn, it may returns in its position after several complete turns ($2k\pi$) around the curve

[29]

$$\begin{aligned} \tau &= \boldsymbol{u}'\cdot\boldsymbol{v} = (\boldsymbol{\Omega_f}\times\boldsymbol{u} + \theta'\boldsymbol{v})\cdot\boldsymbol{v} = \tau_f - \tau_f = 0 \\ k_1 &= -\boldsymbol{t}'\cdot\boldsymbol{v} = -\kappa\boldsymbol{n}\cdot\boldsymbol{v} = \kappa\sin\theta \\ k_2 &= \boldsymbol{t}'\cdot\boldsymbol{u} = \kappa\boldsymbol{n}\cdot\boldsymbol{u} = \kappa\cos\theta \end{aligned}$$

[30] "it is possible for closed curves to have parallel transport frames that do not match up after one full circuit of the curve" [27].

tangent. During its movement along the curve, the frame will make a total twist of $\int_0^L \tau_f(s)ds = \alpha[2\pi]$ around the tangent vector. This difference of angle is related to the concept of *holonomy*.

Remark also that Frenet and Bishop frames coincide for planar curves ($\tau_f = 0$), within a constant rotation around the unit tangent vector.

1.5.7 Comparison between Frenet and Bishop frames

Let γ be a *circular helix* of parameter a and k. In a cartesian coordinate system, it is defined as :

$$\boldsymbol{r}(t) = \big[a\cos t, a\sin t, kt\big] = a\cos t\,\boldsymbol{e}_x + a\sin t\,\boldsymbol{e}_y + kt\,\boldsymbol{e}_z \tag{1.53}$$

The speed of this parametrization, the curvature and the geometric torsion are uniform and given by :

$$v(t) = \sqrt{a^2+k^2} \tag{1.54a}$$
$$\kappa(t) = \frac{a}{a^2+k^2} \tag{1.54b}$$
$$\tau_f(t) = \frac{k}{a^2+k^2} \tag{1.54c}$$

The Frenet frame components are given by (with $\alpha = v\kappa$ and $\beta = v\tau_f$) :

$$\boldsymbol{t}(t) = \big[-\alpha\cos t, \alpha\sin t, \beta t\big] \tag{1.55a}$$
$$\boldsymbol{n}(t) = \big[-\cos t, -\sin t, 0\big] \tag{1.55b}$$
$$\boldsymbol{b}(t) = \big[\beta\sin t, -\beta\cos t, \alpha\big] \tag{1.55c}$$

And the Bishop frame components are given by :

$$\boldsymbol{u}(t) = \big[-\cos t\cos\beta t - \beta\sin t\sin\beta t, -\sin t\cos\beta t + \beta\cos t\sin\beta t, -\alpha\sin\beta t\big] \tag{1.56a}$$
$$\boldsymbol{v}(t) = \big[-\cos t\sin\beta t + \beta\sin t\cos\beta t, -\sin t\sin\beta t - \beta\cos t\cos\beta t, \alpha\cos\beta t\big] \tag{1.56b}$$

At $t = 0$ the two frames coincide. At $t > 0$ the Bishop frame is obtained from the Frenet frame by a rotation around $\boldsymbol{t}(t)$ of an angle $\theta(t) = -\tau_f \cdot (vt)$.

The angular velocities of the Frenet and Bishop frames are respectively given by :

$$\boldsymbol{\Omega}_f(t) = \big[\tau_f, 0, \kappa\big] \tag{1.57a}$$
$$\boldsymbol{\Omega}_b(t) = \big[0, \kappa\sin\theta, \kappa\cos\theta\big] \tag{1.57b}$$

The components of these angular velocities are plotted in figure 1.6 for a circular helix with parameter $a = 1.0$ and $k = 0.5$ while the parameter t varies from 0 to 2π. At $t = 2\pi$ the frame has made a full turn and its altitude has increased from 0 to π.

The components of the angular velocity of the Frenet frame are constant during the movement along the curve and the frame does not rotate around the normal vector as $\Omega_f^2 = 0$ (see figure 1.6a). The components of the angular velocity of the Bishop frame vary during the movement along the curve and the frame does not rotate

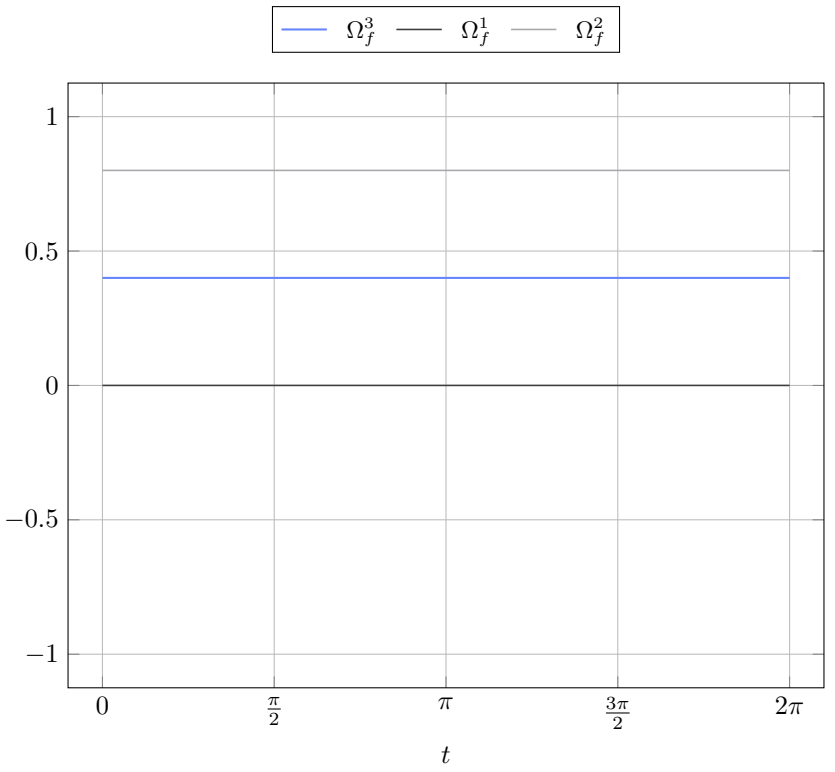

(a) Frenet frame

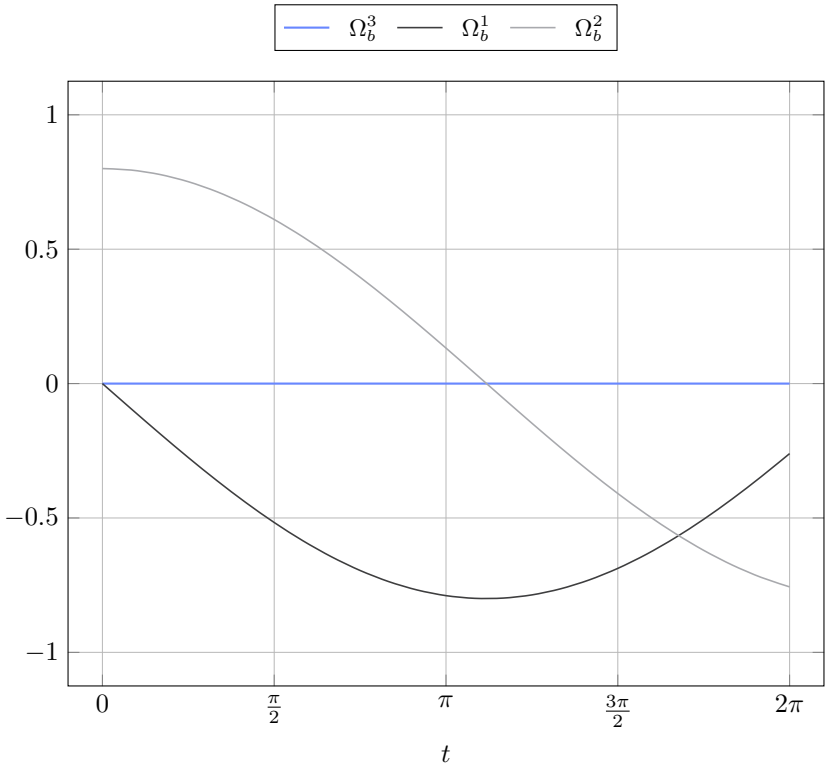

(b) Bishop frame

Figure 1.6 – Angular velocities of Frenet and Bishop frames for a circular helix ($a = 1.0$ and $k = 0.5$).

around the tangent vector as $\Omega_b^3 = 0$ (see figure 1.6b).

1.6 Discrete curves

The previous section has introduced the fundamental analytical tools to develop a solid understanding of the geometry of smooth space curves. These tools will be essentials for the construction of the beam model presented later in **??** and **??**. In this section we look for equivalent notions in the case of discrete space curves, as the developed model will be implemented in a numerical program to solve real mechanical problems through discrete element models (see **??**).

The study of these discrete equivalent notions belong to the recent field of *Discrete Differential Geometry* : "In some sense discrete differential geometry can be considered more fundamental than differential geometry since the later can be obtained form the former as a limit" [21, p.7]. In particular, we will see that they are several ways to define the discrete equivalents of the curvature and the unit tangent vector. Though these various ways are equivalent and match their smooth counterpart by passing to the limit, they exhibit different capabilities at the discrete level.

"There is no general theory or methodology in the literature, despite the ubiquitous use of discrete curves in mathematics and science. There are conflicting definitions of even basic concepts such as discrete curvature κ, discrete torsion τ, or discrete Frenet frame." [39, p.1].

1.6.1 Definition

Let Γ be a discrete (or polygonal) space curve. Γ is defined as an ordered sequence $\Gamma = (\boldsymbol{x}_0, \boldsymbol{x}_1, \dots, \boldsymbol{x}_n) \in \mathbb{R}^{3(n+1)}$ of $n+1$ pairwise disjoint *vertices* (see figure 1.7). Consecutive pairs of vertices define n straight segments $(\boldsymbol{e}_0, \boldsymbol{e}_1, \dots, \boldsymbol{e}_{n-1})$ called *edges*, pointing from one vertex to the next one : $\boldsymbol{e}_i = \boldsymbol{x}_{i+1} - \boldsymbol{x}_i$. The midpoint of $\boldsymbol{e}_i$ is a vertex denoted : $\boldsymbol{x}_{i+1/2} = \boldsymbol{x}_i + \frac{1}{2}\boldsymbol{e}_i$.

The length of $\boldsymbol{e}_i$ is denoted $l_i = \|\boldsymbol{e}_i\|$. The total length of Γ is denoted $L = \sum_{i=0}^{n-1} \|\boldsymbol{e}_i\|$. Additionally, we define the vertex-based mean length $\bar{l_i}$ at vertex $\boldsymbol{x}_i$:

$$\begin{cases} \bar{l_0} = l_0 & i = 0 \\ \bar{l_i} = \dfrac{1}{2}(l_{i-1} + l_i) & i \in [\![1, n-1]\!] \\ \bar{l_n} = l_{n-1} & i = n \end{cases} \tag{1.58}$$

Discrete unit tangent vector

Edge vectors lead to a natural definition of the *discrete unit tangent vector* along each edge : $\boldsymbol{u}_i = \boldsymbol{e}_i / l_i$. However, this definition makes no sense at vertices where all the curvature is condensed and measured by the turning angle (φ_i). This is often illustrated in terms of the Gauß map, a transformation in which edges will map to points and vertices will map to curves on the unit sphere.

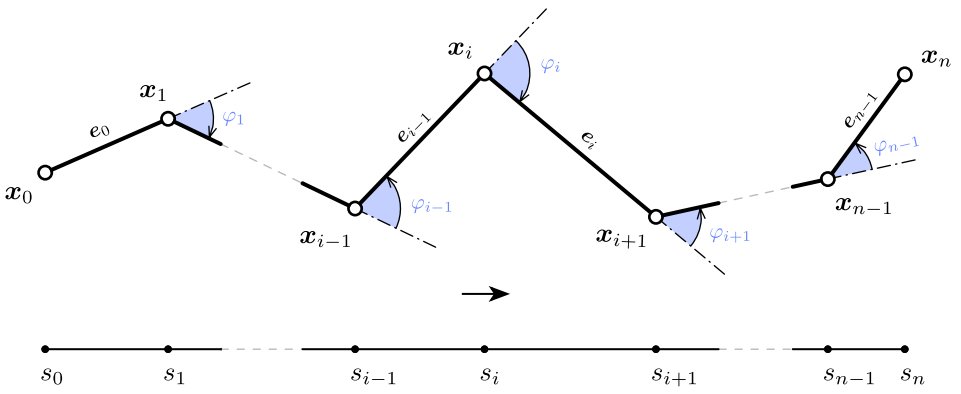

Figure 1.7 – Discrete curve representation and parametrization.

Discrete osculating plane

Consecutive pairs of edges lead to a natural definition of the *discrete osculating plane*, as the plane in which Γ locally lies on. This plane is well defined by its normal vector known as the *discrete unit binormal vector* ($\boldsymbol{b}_i = \frac{\boldsymbol{e}_{i-1} \times \boldsymbol{e}_i}{\|\boldsymbol{e}_{i-1} \times \boldsymbol{e}_i\|}$) only if $\boldsymbol{e}_{i-1}$ and $\boldsymbol{e}_i$ are non-collinear ; that is the curve is not locally a straight line, or equivalently the curvature does not vanish.

Discrete turning angle

The *turning angle* is defined as the oriented angle between to adjacent edges : $\varphi_i = \angle(\boldsymbol{e}_{i-1}, \boldsymbol{e}_i)$. It is defined only for all $i \in [\![1, n-1]\!]$. It corresponds to the angle of rotation, in the osculating plane, around the binormal vector ($\boldsymbol{b}_i$), to align $\boldsymbol{e}_{i-1}$ with $\boldsymbol{e}_i$. The sign of φ_i is taken in accordance to the right-hand rule regarding the orientation of $\boldsymbol{b}_i$. Thus, φ_i is necessarily bounded to $[0, \pi]$:

$$0 \leqslant \varphi_i \leqslant \pi \tag{1.59}$$

The next section will highlight the central role of the turning angle in the possible measurements of the discrete curvature.

Recall that for a planar curve, where φ denotes the angle between the tangent vector ($\boldsymbol{t} = \cos\varphi\, \boldsymbol{e}_x + \sin\varphi\, \boldsymbol{e}_y$) and the horizontal line of direction $\boldsymbol{e}_x$, the following relation holds : $\varphi(s_1) - \varphi(s_2) = \int_{s_1}^{s_2} \frac{d\varphi}{ds} ds = \int_{s_1}^{s_2} \kappa ds$.

1.6.2 Regularity

Let $\Gamma = (\boldsymbol{x}_0, \boldsymbol{x}_1, \ldots, \boldsymbol{x}_n)$ be a discrete curve of edges $\boldsymbol{e}_0, \boldsymbol{e}_1, \ldots, \boldsymbol{e}_{n-1}$. Γ is said to be :

- *regular* if no vertex kinks : $\boldsymbol{e}_{i-1} + \boldsymbol{e}_i \neq 0 \Leftrightarrow \varphi_i \neq \pi \mid \forall i \in [\![1, n-1]\!]$
- *biregular* if no vertex is flat : $\boldsymbol{e}_{i-1} - \boldsymbol{e}_i \neq 0 \Leftrightarrow \varphi_i \neq 0 \mid \forall i \in [\![1, n-1]\!]$

1.6.3 Parametrization

In the literature, discrete curves are usually considered as maps defined on $I = [\![0, n]\!] \in \mathbb{N}^{n+1}$. As a consequence, the discrete derivative of Γ is an edge-based quantity defined as :

$$\Gamma'_i = \frac{\Gamma(t_{i+1}) - \Gamma(t_i)}{t_{i+1} - t_i} = \boldsymbol{e}_i \quad , \quad \boldsymbol{x}_i = \Gamma(t_i) \quad , \quad t_i = i \tag{1.60}$$

Thus, as in the smooth case, a discrete curve is said to be parametrized by arc length if $\|\Gamma'\| = 1$, that is every edges are of unit length ($\|\boldsymbol{e}_i\| = 1$).[31] This constraint is sometimes relaxed to curves of constant edge length ($\|\boldsymbol{e}_i\| = c$) that are said to be parametrized *proportional* to arc length.

In the present work, to stick closer to the smooth case, we instead consider discrete curves as maps defined on $I = [t_0, t_1, \dots, t_n] \in \mathbb{R}^{n+1}$ where t denotes the discrete parametrization of Γ. As in the smooth case, the way to parametrized a curve is not unique.

Arc length parameter

By analogy with the smooth case, we define the curve arc length at vertices (see figure 1.7) as :

$$\begin{cases} s_0 = 0 & i = 0 \\ s_i = \displaystyle\sum_{k=1}^{i} \|\boldsymbol{e}_{k-1}\| & i \in [\![1, n-1]\!] \\ s_n = L & i = n \end{cases} \tag{1.61}$$

This definition naturally extends to the whole domain by piecewise linear interpolation. This is not different as considering the discrete curve as a continuous polygonal curve. Indeed, for any $s \in [s_i, s_{i+1}]$ there exists a normalized parameter $t = \frac{s - s_i}{s_{i+1} - s_i} \in [0, 1]$ so that :

$$s(t) = (1-t)s_i + ts_{i+1} = s_i + tl_i \tag{1.62a}$$

$$\boldsymbol{x}(t) = (1-t)\boldsymbol{x}_i + t\boldsymbol{x}_{i+1} = \boldsymbol{x}_i + t\boldsymbol{e}_i \tag{1.62b}$$

Note that this parametrization satisfies $\|\Gamma'\| = 1$ on $\bigcup_{i=1}^{n}]s_{i-1}, s_i[$ but Γ' remains undefined at vertices. This issue is the reason why defining the tangent vector at vertices can not be done unequivocally for discrete curves.

1.7 Discrete curvature

Vouga 2014 [22] defines and compares three different definitions of the discrete curvature that does not suppose that $\|\boldsymbol{e}_i\|$ is constant. By trying to mimic some properties of the curvature in the smooth case Carroll *et al.* 2014 [39] and Bobenko 2015 [40] also define and compare three different definitions of the discrete curvature from the osculating circle. One main drawback of all the said proposals is that the question of the curvature at start and end points is never treated. But this is of main importance when dealing with beams as the nature of the

[31] This assumption leads to the assertion that "A discrete curve is parameterized by arc length or it is not" [21, p.10].

boundary conditions can make the curvature to be null or not at its ends, depending if some moment has to be transferred or not. In this sens, the question of discrete curvature could not be treated separately with the question of the tangent vector.

1.7.1 Definition from osculating circles

Curvature is defined from the osculating circle, which is the best approximation of a curve by a circle.

Vertex-based osculating circle (circumscribed)

Let Γ be a discrete curve parametrized by arc length. The *vertex-based* (or circumscribed) osculating circle at vertex $\boldsymbol{x}_i$ is defined as the unique circle passing through the points $\boldsymbol{x}_{i-1}$, $\boldsymbol{x}_i$ and $\boldsymbol{x}_{i+1}$ (see figure 1.8a). This circle leads to the following definition of the curvature : [32]

$$\boldsymbol{\kappa b}_i = \frac{2\,\boldsymbol{e}_{i-1} \times \boldsymbol{e}_i}{\|\boldsymbol{e}_{i-1}\|\|\boldsymbol{e}_i\|\|\boldsymbol{e}_{i-1} + \boldsymbol{e}_i\|} \quad , \quad \kappa_i = \|\boldsymbol{\kappa b}_i\| = \frac{2\,\sin(\varphi_i)}{\|\boldsymbol{e}_{i-1} + \boldsymbol{e}_i\|} \tag{1.63}$$

This definition shows a good locality as the curvature is attached to the vertex $\boldsymbol{x}_i$, right in the place where it occurs on the discrete curve. In addition, this definition leads to a natural local spline interpolation by the circumscribed osculating circle itself. This interpolation has the advantage to pass exactly through three vertices, to lie on the osculating plane and to share the same curvature as Γ at $\boldsymbol{x}_i$. It also leads to a natural definition of the tangent vector at $\boldsymbol{x}_i$ (see section 1.8.1).

Moreover, while this definition is valid only on the current portion of Γ ($i \in [1, n-1]$), it is straightforwardly extended to its endings ($i = 0, n$), provided that a unit tangent vector $\boldsymbol{t}_0$ (respectively $\boldsymbol{t}_n$) is given at $\boldsymbol{x}_0$ (resp. $\boldsymbol{x}_n$), as the unique circle tangent to $\boldsymbol{t}_0$ (resp. $\boldsymbol{t}_n$) passing through $\boldsymbol{x}_0$ and $\boldsymbol{x}_1$ (resp. $\boldsymbol{x}_{n-1}$ and $\boldsymbol{x}_n$) :

$$\boldsymbol{\kappa b}_0 = \frac{2\,\boldsymbol{e}_0 \times \boldsymbol{t}_0}{\|\boldsymbol{e}_0\|^2} \quad , \quad \boldsymbol{\kappa b}_n = \frac{2\,\boldsymbol{t}_n \times \boldsymbol{e}_{n-1}}{\|\boldsymbol{e}_{n-1}\|^2} \tag{1.64}$$

This property will be very profitable in the discrete beam model developed later in the manuscript. It is examined more in details in section section 1.8 about the definition of the tangent vector.

However, there are some important drawbacks as the curvature is bounded to $[0, 2]$ (see figure 1.10). When the curve tends to kinks ($\varphi \mapsto \pi$), one would expect the curvature to diverge toward infinity, but instead it tends to a finite value equals to 0 ($l_{i-1} \neq l_i$) or 2 ($l_{i-1} = l_i$). This issue can be bypassed if the discretization is refined *enough*. A criterion is given in the next section (section 1.7.2).

[32] This curvature is also known as the *Menger curvature*.

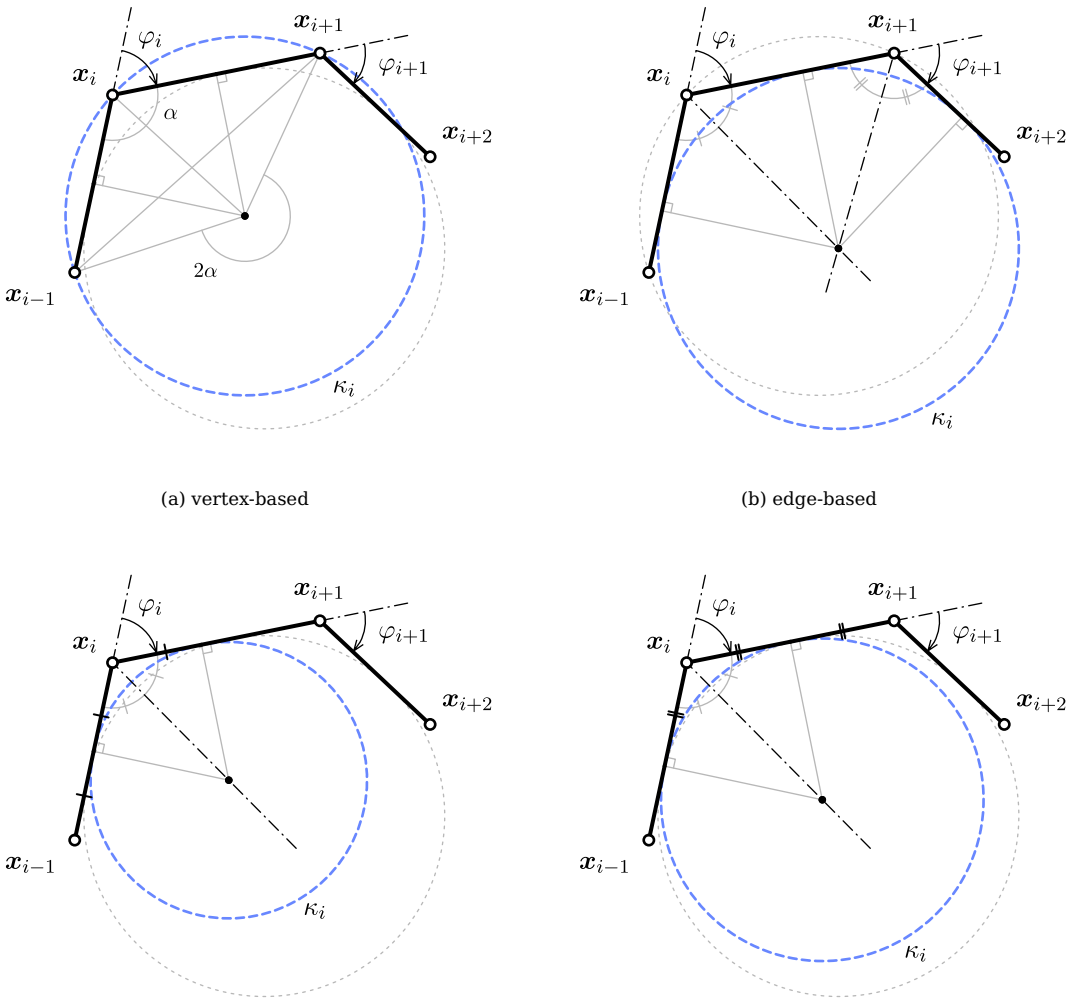

(a) vertex-based

(b) edge-based

(c) bitangent with $\|\boldsymbol{e}_{i-1}\|$

(d) bitangent with $\|\boldsymbol{e}_i\|$

Figure 1.8 – Several ways to define the osculating circle for discrete curves, leading to different notions of discrete curvature.

Curvature (κ_i)	Locality	$\varphi \mapsto 0$	$\varphi \mapsto \pi$	Ends	Dim	Fitting
$\kappa_1 = \frac{2\,\sin(\varphi_i)}{\|\boldsymbol{e}_{i-1}+\boldsymbol{e}_i\|}$	$\boldsymbol{x}_i$	0	$0, 2$	yes	space	clothoid
$\kappa_2 = \frac{\tan(\varphi_i/2)+\tan(\varphi_{i+1}/2)}{l_i}$	$\boldsymbol{e}_i$	0	∞	no	planar	circle
$\kappa_3 = \frac{2\,\tan(\varphi_i/2)}{\overline{l}_i}$	$\boldsymbol{x}_i$	0	∞	no	space	circles
$\kappa_4 = \frac{2\,\sin(\varphi_i/2)}{\overline{l}_i}$	$\boldsymbol{x}_i$	0	$0, 2$	no	space	clothoid
$\kappa_5 = \frac{\varphi_i}{\overline{l}_i}$	$\boldsymbol{x}_i$	0	$\pi/\overline{l}_i$	no	space	elastica

Table 1.1 – Review of several discrete curvature definitions mentioned in the literature.

Edge-based osculating circle (inscribed)

Let Γ be a discrete curve parametrized by arc length. The *edge-based* osculating circle at edge $\boldsymbol{e}_i$ is defined as the unique circle tangent to the edges $\boldsymbol{e}_{i-1}$, $\boldsymbol{e}_i$ and $\boldsymbol{e}_{i+1}$ (see figure 1.8b).

$$\kappa_i = \frac{\tan(\varphi_i/2) + \tan(\varphi_{i+1}/2)}{\|\boldsymbol{e}_i\|} \tag{1.65}$$

This definition shows an appropriate behavior : when the curve tends to kick the radius of curvature tends to zero ($\tan\varphi/2 \mapsto \infty$), and when the curve tends to be a straight line the curvature tends to 0 ($\tan\varphi/2 \mapsto 0$).

However, it needs Γ to be planar which is by far too restrictive regarding our goal (the modeling of 3D slender beams). Finally, this way of defining the curvature is not as local as one would expect as it is defined relatively to the edge $\boldsymbol{e}_i$ but not where the turning occurs, at vertices.

Bitangent osculating circle (inscribed)

Let Γ be a discrete curve parametrized by arc length. Following [22] we define the curvature regrading the mean length $\overline{l_i}$ attached to $\boldsymbol{x}_i$ as : [33]

$$\boldsymbol{\kappa b}_i = \frac{2}{\overline{l_i}}\left(\frac{\boldsymbol{e}_{i-1}\times\boldsymbol{e}_i}{\|\boldsymbol{e}_{i-1}\|\|\boldsymbol{e}_i\| + \boldsymbol{e}_{i-1}\cdot\boldsymbol{e}_i}\right) \quad , \quad \kappa_i = \|\boldsymbol{\kappa b}_i\| = \frac{2}{\overline{l_i}}\tan(\varphi_i/2) \tag{1.66}$$

This other definition combines the good locality of the vertex-based approach (see equation (1.63)) and the proper behavior at bounds of the edge-based approach (see equation (1.65)). Given two adjacent edges $\boldsymbol{e}_{i-1}$ and $\boldsymbol{e}_i$, there exists an infinite number of circles that are tangent to both edges (see figure 1.8c and figure 1.8d for two remarkable circles among them), which center points all lie on the $\varphi_i - \pi$ angle bisector line. The corresponding osculating circle, known as the *inscribed* circle, is constructed to touch both $\boldsymbol{e}_{i-1}$ and $\boldsymbol{e}_i$ at distance $\overline{l_i}/2$ from $\boldsymbol{x}_i$. In the case of a constant edge length discrete curve, this definition of the osculating circle merges to the circles proposed in figure 1.8c and figure 1.8d.

However, this definition still exhibits some drawbacks. Firstly, remark that there is an infinity of possible inscribed circles (defined as a circle that is bitangent to two connected edges). Indeed, this circle is unique only if the distance between the common vertex and the points of tangency are prescribed. Although it could seem natural to take the middle of the edges as points of tangency if they have the same length ($\|\boldsymbol{e}_i\| = \|\boldsymbol{e}_{i+1}\|$), there is no obvious choice at all for this parameter (compare figure 1.8c with figure 1.8d). Moreover, the lack of a natural interpolation spline which passes through the vertices and that is in correlation to the osculating circle is also detrimental in the context of our application.

Other definitions of osculating circles

In the literature, one can find other definitions for the discrete curvature that also correspond to the definition of an osculating circle. All these definitions are summarized in table 1.1. For further informations, the reader should refer to [39, 22, 40, 41].

[33] This definition is also presented in [40, 39] but in the more restrictive case of constant edge length discrete curves ($l_i = cst$).

In particular, Vouga [22] details which discrete curvature definition faithfully transposes which property of the smooth curvature. He remarks that there is no “free-lunch” as none of the proposed definitions satisfies every properties of the smooth curvature.

1.7.2 Benchmarking : sensitivity to non uniform discretization

In this section we compare the two main discrete curvature notions (circumscribed versus inscribed) regarding their sensibility to non uniform discretization.

This aspect is not treated in the actual literature, in which curves parametrized by arc length are usually treated as curves of constant edge length, though it is yet an important topic when it comes to the numerical modeling of true mechanical systems. Indeed, the presence of connexions between members will compromise the ability to enforce a constant discretization through all the elements of the structure. Additionally, vertices are obviously points of interest in a discrete model as they will be used to apply loads and enforce various constraints such as joints and support conditions. Finally, the accuracy of the discretized model is proportional to the sharpness of the discretization, whereas the computing time required to solve the model will grow as the sharpness increases. Consequently, one would distribute these points in the space as cleverly as possible and try to minimize their number as they increase the overall computation cost.

Introducing the coefficient $\alpha = \frac{\|\boldsymbol{e}_{i-1}\|}{\|\boldsymbol{e}_i\|}$, we rewrite the previous formulas for κ_1 and κ_3 as :

$$\begin{aligned} \kappa_1 &= \frac{2\,\sin(\varphi)}{\|\boldsymbol{e}_i\|(1+\alpha^2+2\alpha\,\cos(\varphi))^{1/2}} \\ \kappa_3 &= \frac{4\,\tan(\varphi/2)}{\|\boldsymbol{e}_i\|(1+\alpha)} \end{aligned} \tag{1.67}$$

These expressions lead to the following formula for the ratio κ_1/κ_3, which relies only on α and the turning angle φ between the edges $\boldsymbol{e}_{i-1}$ and $\boldsymbol{e}_i$:

$$\frac{\kappa_1}{\kappa_3}(\alpha) = \frac{\kappa_1}{\kappa_3}(1/\alpha) = \frac{(1+\alpha)\,cos^2(\varphi/2)}{((1-\alpha)^2+4\alpha\,cos^2(\varphi/2))^{1/2}} \tag{1.68}$$

Discrete curvatures are plotted in figure 1.10 for three values of α. The thickest line is for the case of uniform discretization ($\alpha = 1$), whereas the thin lines mark the boundary cases ($\alpha = 0.5, 2$). The ratio κ_1/κ_3 is plotted in blue and leads to only one thin line (remind equation (1.68)). The graph shows that κ_1 and κ_3 have a very close behavior for small turning angles. The variability regarding α is small when φ remains small and gets negligible as φ gets smaller.

Passing $\pi/4$ and increasing φ, κ_3 exhibits a good behavior : as the discrete curves tends to kink, κ_3 diverges towards the infinity as the smooth curvature would behave when the curve kinks. Conversely, the behavior of κ_1 is not appropriate as it converges to a fixed limit. This limit equals 2 when the edges have the same length and equals 0 when they have different lengths.

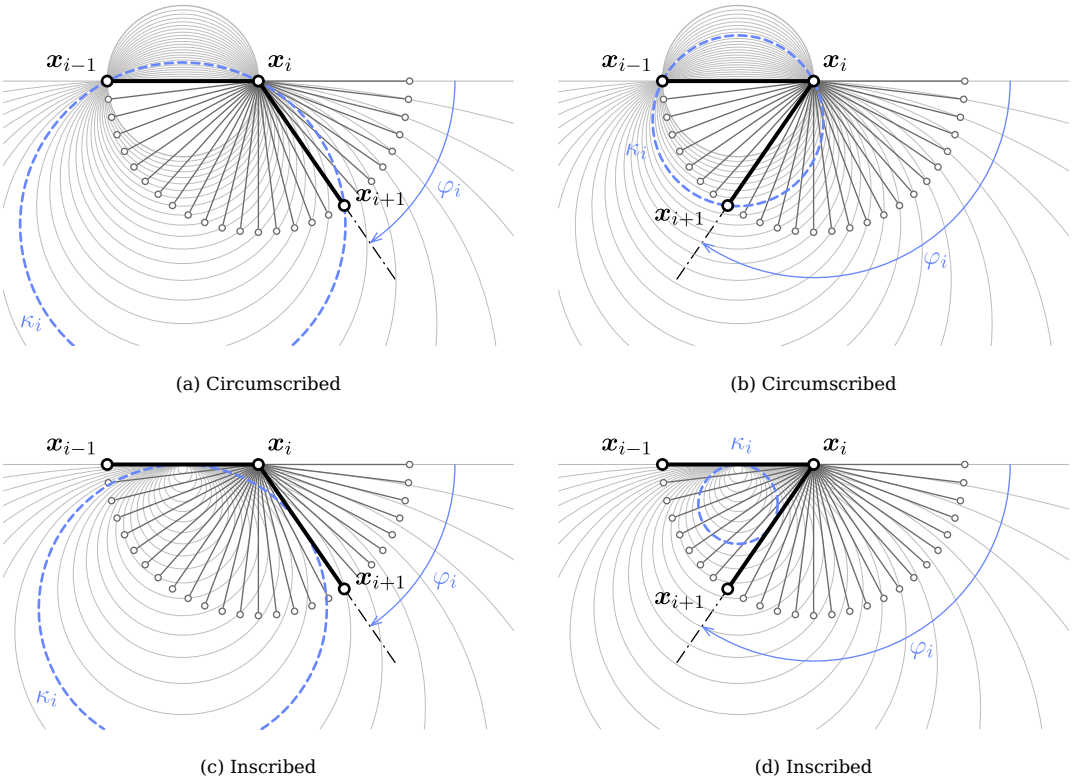

(a) Circumscribed

(b) Circumscribed

(c) Inscribed

(d) Inscribed

Figure 1.9 – Comparison of circumscribed and inscribed osculating circles for different values of the turning angle (φ).

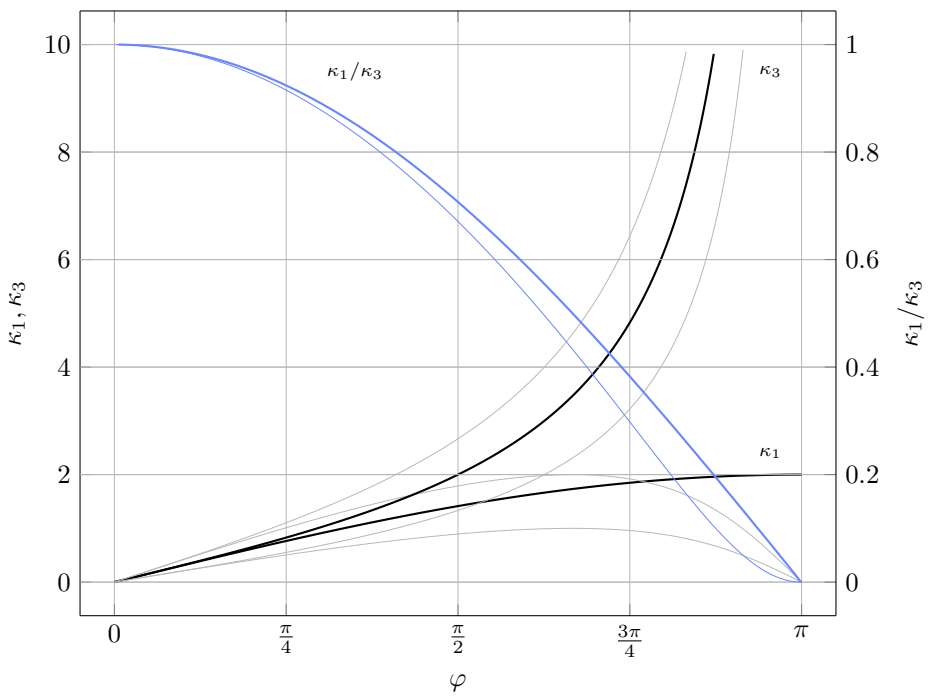

Figure 1.10 – Sensitivity of discrete curvatures to non uniform discretization ($\alpha \in [0.5, 2]$) over the whole domain of variation of the turning angle ($\varphi \in [0, \pi]$).

Conclusion

It appears that the discrete curvature related to the inscribed osculating circle exhibits a better behavior – that is a behavior closer to the smooth case – on the whole range of possible turning angles. This would be an advantage when modeling highly nonlinear beam configurations such as the ones encountered in hair simulations.

However, for the kind of structures we are studying here, those kind of configurations are not likely to arise. And if they do, the structure would be severely damaged and this situation is to be avoided by the designers. Moreover, the sharpness of the discretization could be increased to reduce the value of the turning angles and stay in the range $[0, \pi/4]$ where the circumscribed curvature gives accurate results.

1.7.3 Benchmarking : accuracy in bending energy representation

In this section we compare, for three remarkable types of curves (line, semicircle and elastica), the discrete bending energies $\mathcal{E}_1$ and $\mathcal{E}_3$ of the discrete curve, respectively based on definitions κ_1 and κ_3 (see table 1.1), to the bending energy $\mathcal{E}$ of the smooth curve. We study the convergence of these energies as the sharpness of the discretization increases. The smooth and discrete bending energies are defined as :

$$\mathcal{E} = \int_0^L \kappa^2 ds \tag{1.69a}$$

$$\mathcal{E}_i = \sum_i \overline{l}_i \kappa_i^2 \tag{1.69b}$$

Straight line

Let us consider any straight line. Its smooth curvature is null. So are the discrete curvatures κ_1 and κ_3 (see table 1.1). In this case, the discrete bending energies perfectly match the bending energy of the smooth curve :

$$\mathcal{E} = \mathcal{E}_1 = \mathcal{E}_3 = 0 \tag{1.70}$$

Semicircle

Let us consider a semicircle of curvature $\kappa = 1/r$ and length $L = \pi r$. This curve is discretized into n edges of equal length $|\boldsymbol{e}_n| = 2r\sin(\varphi/2)$ where $\varphi = \frac{\pi}{n}$ (see figure 1.11). The total length of the discrete curve is given by : $L_n = n|\boldsymbol{e}_n| = L\frac{\sin(\varphi/2)}{\varphi/2}$. In this simple case, the discrete bending energies can be expressed analytically :

$$\mathcal{E} = L\kappa^2 \tag{1.71a}$$

$$\mathcal{E}_1 = L_n\kappa_1^2 = \frac{\sin(\varphi/2)}{\varphi/2} \cdot \mathcal{E} \tag{1.71b}$$

$$\mathcal{E}_3 = L_n\kappa_3^2 = \frac{\sin(\varphi/2)}{(\varphi/2)\cos^2(\varphi/2)} \cdot \mathcal{E} \tag{1.71c}$$

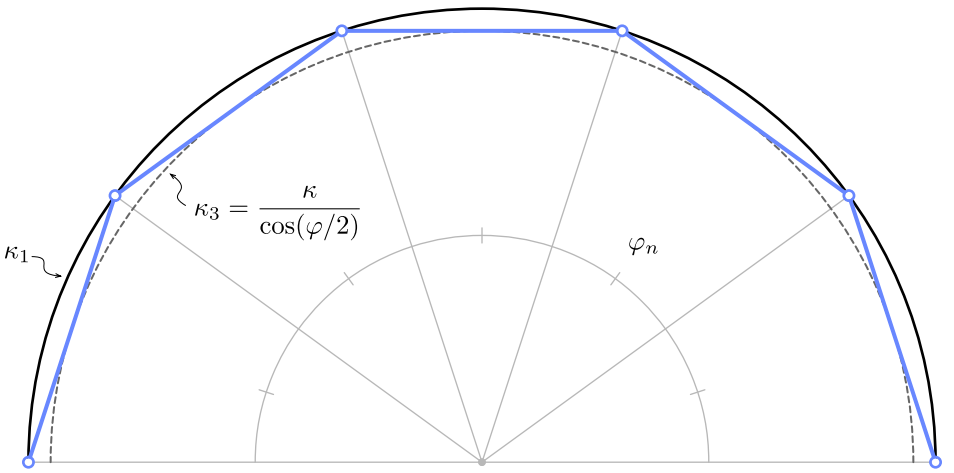

Figure 1.11 – Discretization of a semicircle and evaluation of its bending energy.

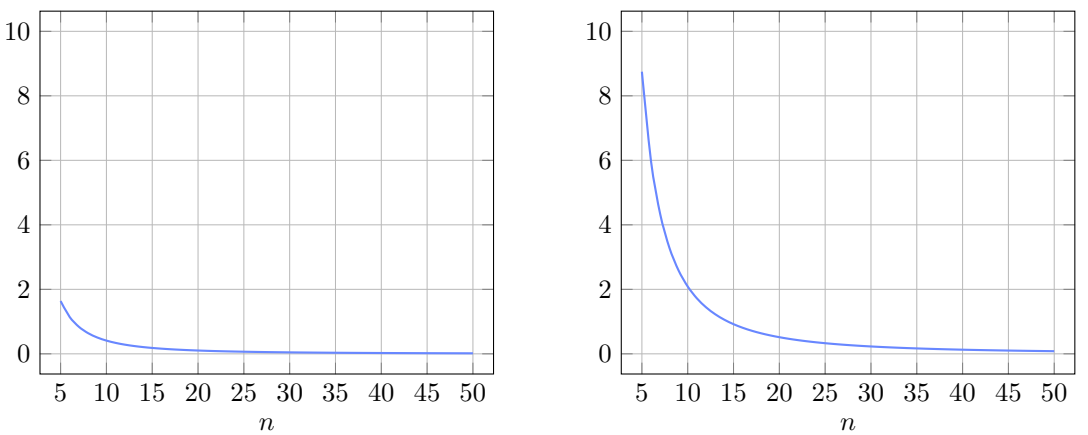

(a) $|1 - \frac{\mathcal{E}_1}{\mathcal{E}}(n)|$ in %

(b) $|1 - \frac{\mathcal{E}_3}{\mathcal{E}}(n)|$ in %

Figure 1.12 – Relative error in the estimation of the bending energy of a semicircle ($\mathcal{E}$) by the discrete energies $\mathcal{E}_1$ and $\mathcal{E}_3$, regarding the sharpness of the discretization.

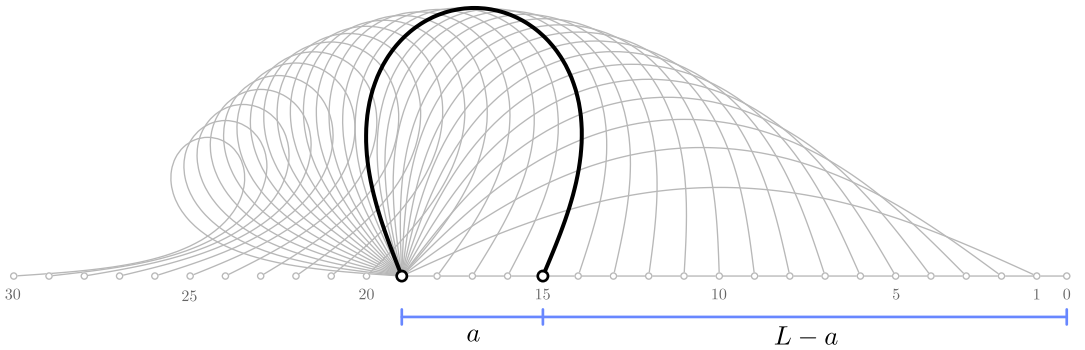

(a) sequence of elastica curves

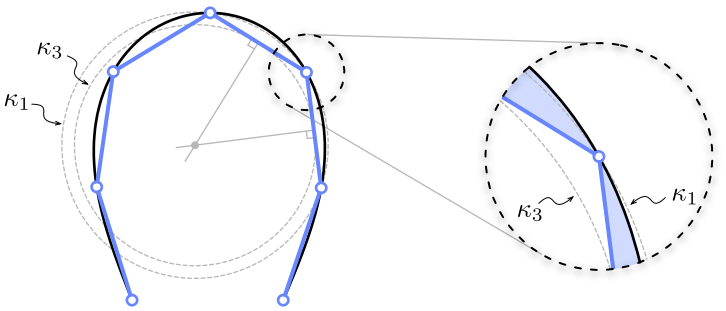

(b) zoom on the discretization

Figure 1.13 – Discretization of an elastica curve and evaluation of its bending energy.

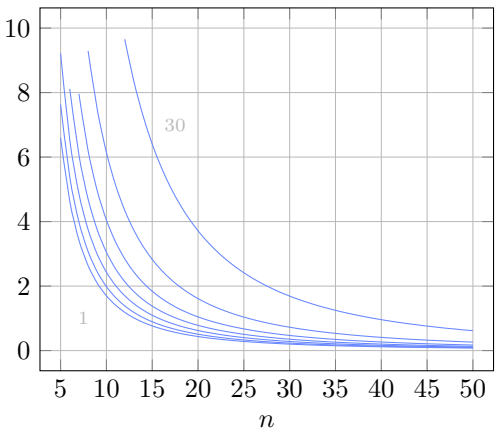

(a) $|1-\frac{\mathcal{E}_1}{\mathcal{E}}(n)|$ in %

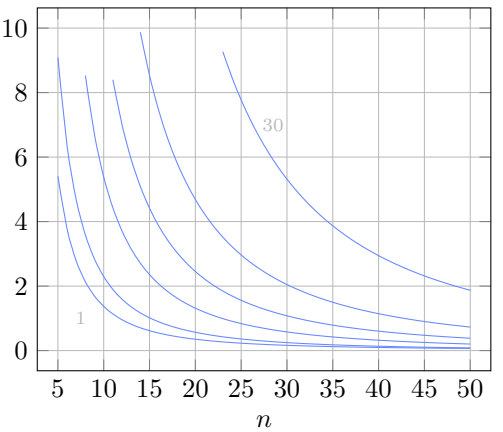

(b) $|1-\frac{\mathcal{E}_3}{\mathcal{E}}(n)|$ in %

Figure 1.14 – Relative error in the estimation of the bending energy of an elastica ($\mathcal{E}$) by the discrete energies $\mathcal{E}_1$ and $\mathcal{E}_3$, regarding the sharpness of the discretization. The curves (1,5,10,15,20,25,30) are chosen from figure 1.13a.

Note that κ_1 equals the curvature of the smooth curve. Consequently, the estimation error is only due to the estimation of the curve length ($L_n \neq L$). The ratios $\mathcal{E}_1/\mathcal{E}$ and $\mathcal{E}_3/\mathcal{E}$ are plotted in figure 1.12. Graphs show that $\mathcal{E}_1$ converges to the smooth case faster than $\mathcal{E}_3$.

Elastica

Let us consider a sequence of elastica curves of fixed length L and variable curvature κ (see figure 1.13a). This curves correspond to a buckled shape of a straight pinned-pinned beam that would have been forced to retract its span. These curves are discretized into n edges of equal length (see figure 1.13b). This time, there is no analytical expressions available for $\mathcal{E}$, $\mathcal{E}_1$ and $\mathcal{E}_3$. Results are obtained by numerical integration and plotted in figure 1.14. Again, graphs show that $\mathcal{E}_1$ converges to the smooth case faster than $\mathcal{E}_3$ for most of the curves excepted the ones with low overall curvature (1 to 5).

Conclusion

figures 1.12 and 1.14 show that for typical curves of mechanical interest – a semicircle is the shape of a rod with constant bending moment while the elastica is the shape of a buckled rod with no end moments – the circumscribed curvature gives a better approximation of the bending energy embedded in these curves. Hence, the circumscribed curvature seems to be a good candidate to maximize accuracy while minimizing the sampling of beam elements. This will lead to models with fewer nodes and will decrease the cost of the computation.

1.8 Discrete tangent vector

In this section we study how to define the discrete unit tangent vector relatively to a discrete curve. While a natural definition exists along the edges (see section 1.6.1), there is no obvious choice at vertices were the curve kinks.

The ability to define a unique tangent vector is very important to define the normal vector of a cross-section, to control beam endings, and to relate it to curvature. One would control the direction of the section (for a fixed/clamped support condition) or, conversly, one would control the moment and seek the corresponding tangent direction (for a pin boundary condition, we know there is no end moments so the curvature is null and we are looking for the tangent).

1.8.1 Circumscribed case

We consider the case where the curvature is defined according to the circumscribed osculating circle (see figure 1.15a).

Current portion

Let $\boldsymbol{x}_i$ be a vertex in the current portion of Γ. The circumscribed osculating circle gives a smooth approximation of Γ in the vicinity of $\boldsymbol{x}_i$ (see figure 1.15a). It leads to a natural definition of a unit tangent vector for five remarkable vertices as the tangent to the osculating circle at those points (resp. $\boldsymbol{x}_{i-1}$, $\boldsymbol{x}_{i-1/2}$, $\boldsymbol{x}_i$, $\boldsymbol{x}_{i+1/2}$, $\boldsymbol{x}_{i+1}$) :

$$\boldsymbol{t}_i^- = 2(\boldsymbol{t}_i \cdot \boldsymbol{u}_{i-1})\boldsymbol{u}_{i-1} - \boldsymbol{t}_i \tag{1.72a}$$

$$\boldsymbol{t}_{i-1/2} = \boldsymbol{u}_{i-1} \tag{1.72b}$$

$$\boldsymbol{t}_i = \frac{\|\boldsymbol{e}_i\|}{\|\boldsymbol{e}_{i-1} + \boldsymbol{e}_i\|}\boldsymbol{u}_{i-1} + \frac{\|\boldsymbol{e}_{i-1}\|}{\|\boldsymbol{e}_{i-1} + \boldsymbol{e}_i\|}\boldsymbol{u}_i \tag{1.72c}$$

$$\boldsymbol{t}_{i+1/2} = \boldsymbol{u}_i \tag{1.72d}$$

$$\boldsymbol{t}_i^+ = 2(\boldsymbol{t}_i \cdot \boldsymbol{u}_i)\boldsymbol{u}_i - \boldsymbol{t}_i \tag{1.72e}$$

Note that $\boldsymbol{t}_i^-$ (resp. $\boldsymbol{t}_i^+$) is obtained by a reflection of $-\boldsymbol{t}_i$ across the bisecting plane of $\boldsymbol{e}_{i-1}$ (resp. $\boldsymbol{e}_i$). A very important property is that the curvature binormal vector at $\boldsymbol{x}_i$ can be computed by three different ways :

$$\boldsymbol{\kappa b}_i = \frac{2\,\boldsymbol{e}_{i-1} \times \boldsymbol{e}_i}{\|\boldsymbol{e}_{i-1}\|\|\boldsymbol{e}_i\|\|\boldsymbol{e}_{i-1} + \boldsymbol{e}_i\|} = \begin{cases} \dfrac{2\,\boldsymbol{u}_{i-1} \times \boldsymbol{t}_i}{\|\boldsymbol{e}_{i-1}\|} \\ \dfrac{2\,\boldsymbol{t}_i \times \boldsymbol{u}_i}{\|\boldsymbol{e}_i\|} \end{cases} \tag{1.73}$$

The first expression is interpreted as the unique circle passing through three points ($\boldsymbol{x}_{i-1}$, $\boldsymbol{x}_i$, $\boldsymbol{x}_{i+1}$) as explained in section 1.7.1. Equivalently, there exist a unique circle defined by two points and a tangent vector. Precisely, the last two expressions in equation (1.73) can be interpreted as the curvature binormal vector of the unique circle passing through $\boldsymbol{x}_{i-1}$, $\boldsymbol{x}_i$ (resp. $\boldsymbol{x}_i$, $\boldsymbol{x}_{i+1}$) and tangent to $\boldsymbol{t}_i$ at $\boldsymbol{x}_i$.

Discontinuity of curvature

Let $\boldsymbol{t}_i^*$ be an arbitrary tangent vector at $\boldsymbol{x}_i$. Following equation (1.73) we define the *left-sided* (resp. *right-sided*) discrete curvatures at $\boldsymbol{x}_i$ in the circumscribed case as :

$$\boldsymbol{\kappa b}_i^-(\boldsymbol{t}_i^*) = \frac{2\,\boldsymbol{u}_{i-1} \times \boldsymbol{t}_i^*}{\|\boldsymbol{e}_{i-1}\|} \tag{1.74a}$$

$$\boldsymbol{\kappa b}_i^+(\boldsymbol{t}_i^*) = \frac{2\,\boldsymbol{t}_i^* \times \boldsymbol{u}_i}{\|\boldsymbol{e}_i\|} \tag{1.74b}$$

The corresponding osculating circle will be called the *left-sided* (resp. *right-sided*) circumscribed osculating circle. When $\boldsymbol{t}_i^* = \boldsymbol{t}_i$, the limits agree one to each other ($\boldsymbol{\kappa b}_i^- = \boldsymbol{\kappa b}_i^+ = \boldsymbol{\kappa b}_i$) and the osculating circles coincide. These definitions perfectly mimic the smooth case where, at a regular ($\|\gamma'\| \neq 0$) but not biregular ($\|\gamma''\| = 0$) point, the curvature is discontinuous while the tangent vector reminds smoothly defined.

In mechanics, this situation is likely to arise as discontinuities in material properties or concentrated applied moments will necessarily lead to discontinuities in curvature (recall that $M = EI\kappa$).

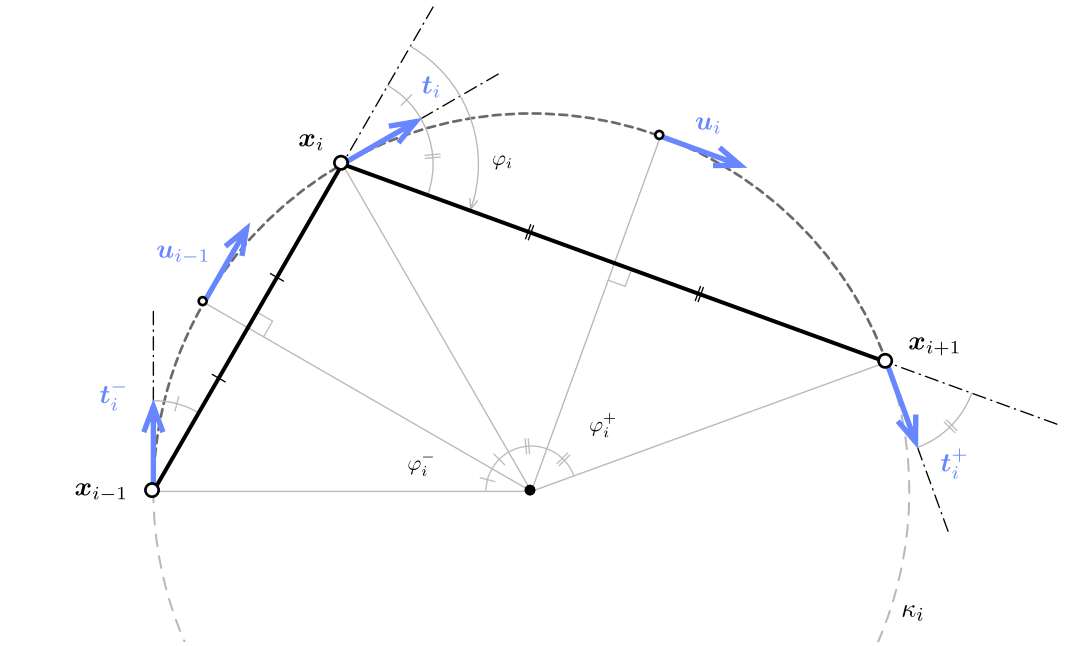

(a) current portion

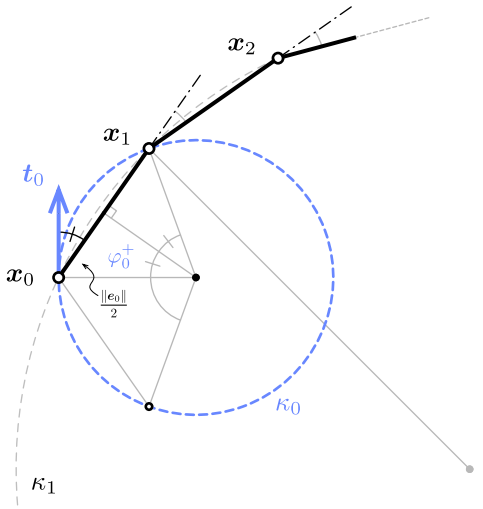

(b) start

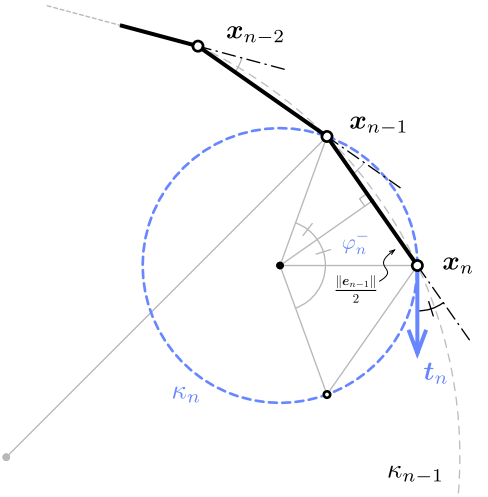

(c) end

Figure 1.15 – Definition of the tangent vector ($\boldsymbol{t}$) and related curvature binormal vector ($\boldsymbol{\kappa b}$) at vertices associated to the circumscribed curvature.

Curve endings

The definition of the left and right sided curvatures given for a vertex in the current portion of Γ are still valid for the end vertices $\boldsymbol{x}_0$ and $\boldsymbol{x}_n$. Provided that a unit tangent vector $\boldsymbol{t}_0^*$ (respectively $\boldsymbol{t}_n^*$) is given at $\boldsymbol{x}_0$ (resp. $\boldsymbol{x}_n$), the circumscribed osculating circle is defined as the unique circle passing through $\boldsymbol{x}_0$ and $\boldsymbol{x}_1$ (resp. $\boldsymbol{x}_{n-1}$ and $\boldsymbol{x}_n$) tangent to $\boldsymbol{t}_0^*$ (resp. $\boldsymbol{t}_n^*$) ; see figure 1.15b and figure 1.15c. It leads to the following curvature binormal vectors :

$$\boldsymbol{\kappa b}_0 = \boldsymbol{\kappa b}_0^+(\boldsymbol{t}_0^*) = \frac{2\,\boldsymbol{t}_0^* \times \boldsymbol{e}_0}{\|\boldsymbol{e}_0\|^2} \tag{1.75a}$$

$$\boldsymbol{\kappa b}_n = \boldsymbol{\kappa b}_n^-(\boldsymbol{t}_n^*) = \frac{2\,\boldsymbol{e}_{n-1} \times \boldsymbol{t}_n^*}{\|\boldsymbol{e}_{n-1}\|^2} \tag{1.75b}$$

Note that, contrary to the current portion, curvatures at endings are subjected to the definition of a unit tangent vector. This reflects the usual indetermination of boundary conditions. For a given beam whether the end is clamped and the tangent vector is known and one will seek the reacting moment due to the support ; whether the end is pinned and the reacting moment is null (so is the curvature) and one will seek the cross-section orientation.

1.8.2 Inscribed case

We now consider the case where the curvature is defined according to the inscribed osculating circle (see figure 1.16a). Remark that inscribed and circumscribed osculating circles are concentric when $l_{i-1} = l_i$.

Current portion

Let $\boldsymbol{x}_i$ be a vertex in the current portion of Γ. The inscribed osculating circle gives a smooth approximation of Γ in the vicinity of $\boldsymbol{x}_i$ (see figure 1.16a) ; though this approximation does not pass through the vertices. It is again possible to construct some unit tangent vectors based on this circle, but the analytic expressions are less compact than in the circumscribed case (resp. at $\boldsymbol{x}_{i-1}$, $\boldsymbol{x}_i$, $\boldsymbol{x}_{i+1}$) :

$$\boldsymbol{t}_i^- = \cos\left(\frac{\varphi_i}{2} + \varphi_i^-\right)\frac{\boldsymbol{u}_{i-1} + \boldsymbol{u}_i}{\|\boldsymbol{u}_{i-1} + \boldsymbol{u}_i\|} + \sin\left(\frac{\varphi_i}{2} + \varphi_i^-\right)\frac{\boldsymbol{u}_{i-1} - \boldsymbol{u}_i}{\|\boldsymbol{u}_{i-1} - \boldsymbol{u}_i\|} \tag{1.76a}$$

$$\boldsymbol{t}_i = \frac{\boldsymbol{u}_{i-1} + \boldsymbol{u}_i}{\|\boldsymbol{u}_{i-1} + \boldsymbol{u}_i\|} \tag{1.76b}$$

$$\boldsymbol{t}_i^+ = \cos\left(\frac{\varphi_i}{2} + \varphi_i^+\right)\frac{\boldsymbol{u}_{i-1} + \boldsymbol{u}_i}{\|\boldsymbol{u}_{i-1} + \boldsymbol{u}_i\|} - \sin\left(\frac{\varphi_i}{2} + \varphi_i^+\right)\frac{\boldsymbol{u}_{i-1} - \boldsymbol{u}_i}{\|\boldsymbol{u}_{i-1} - \boldsymbol{u}_i\|} \tag{1.76c}$$

In this form, the expressions of $\boldsymbol{t}_i^-$ and $\boldsymbol{t}_i^+$ exhibit lots of trigonometric computations. Consequently, they will be more costly to evaluate (numerically) than the ones given for the circumscribed case that exhibit only simple addition, product and division operations.

Though these points does not generally fall into mid-edge, the tangent vector can also be identified to $\boldsymbol{u}_{i-1}$ (resp.

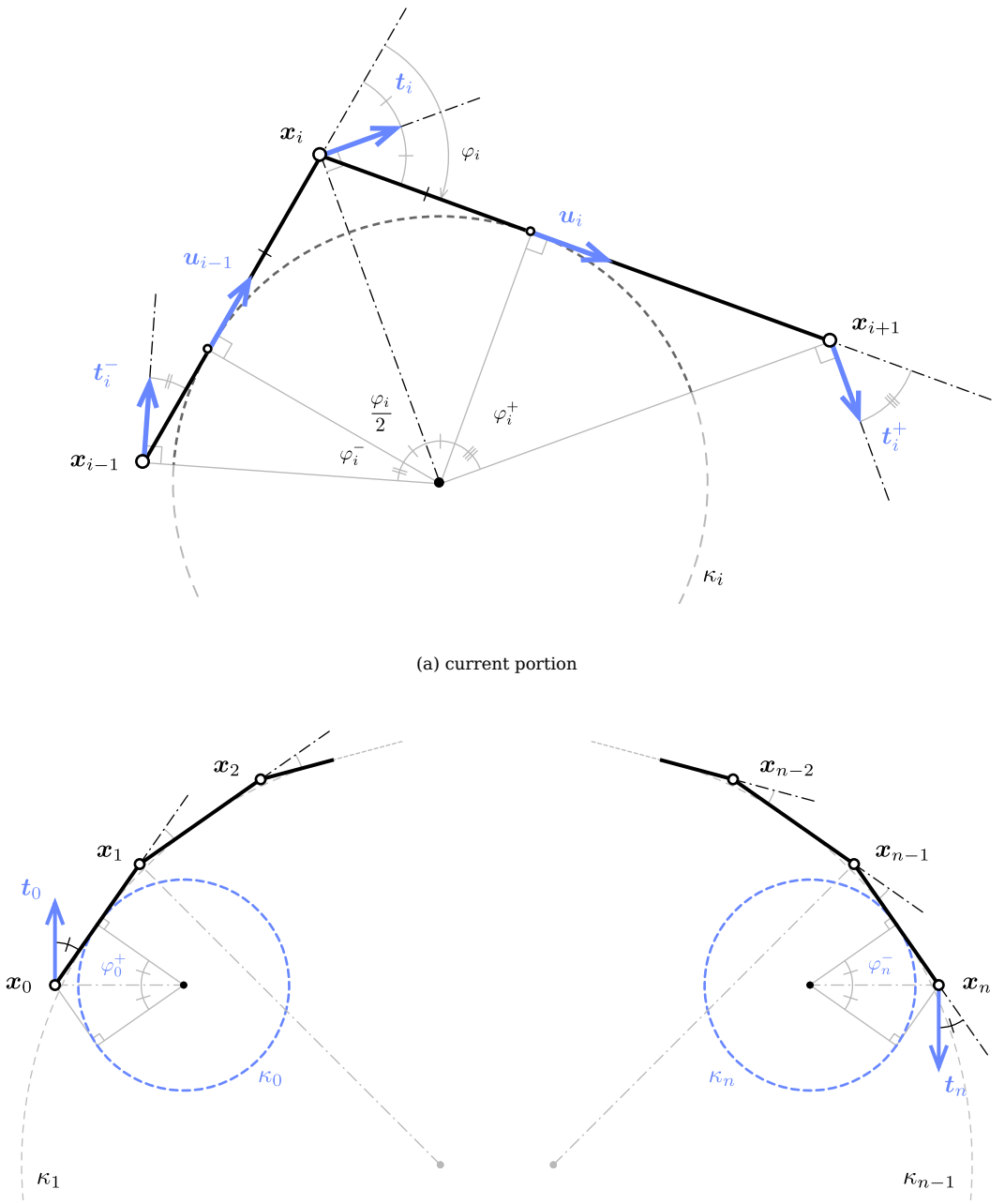

(a) current portion

(b) start

(c) end

Figure 1.16 – Definition of the tangent vector ($\boldsymbol{t}$) and related curvature binormal vector ($\boldsymbol{\kappa b}$) at vertices associated to the inscribed curvature.

$\boldsymbol{u}_i$) at point $\tilde{\boldsymbol{x}}_i^- = \boldsymbol{x}_i - \frac{1}{2}\overline{l}_i\boldsymbol{u}_{i-1}$ (resp. $\tilde{\boldsymbol{x}}_i^+ = \boldsymbol{x}_i + \frac{1}{2}\overline{l}_i\boldsymbol{u}_i$) :

$$\tilde{\boldsymbol{t}}_i^- = \boldsymbol{u}_{i-1} \tag{1.77a}$$

$$\tilde{\boldsymbol{t}}_i^+ = \boldsymbol{u}_i \tag{1.77b}$$

Similarly to the circumscribed case, one can remark that the curvature binormal vector at $\boldsymbol{x}_i$ can be computed in three different manners :

$$\boldsymbol{\kappa b}_i = \frac{2}{\overline{l}_i}\left(\frac{\boldsymbol{e}_{i-1}\times\boldsymbol{e}_i}{\|\boldsymbol{e}_{i-1}\|\|\boldsymbol{e}_i\| + \boldsymbol{e}_{i-1}\cdot\boldsymbol{e}_i}\right) = \begin{cases} \dfrac{2}{\overline{l}_i}\left(\dfrac{\boldsymbol{e}_{i-1}\times\boldsymbol{t}_i}{\boldsymbol{e}_{i-1}\cdot\boldsymbol{t}_i}\right) \\ \dfrac{2}{\overline{l}_i}\left(\dfrac{\boldsymbol{t}_i\times\boldsymbol{e}_i}{\boldsymbol{t}_i\cdot\boldsymbol{e}_i}\right) \end{cases} \tag{1.78}$$

The first expression is interpreted as the unique circle bitangent to $\boldsymbol{e}_{i-1}$ at $\tilde{\boldsymbol{x}}_i^-$ and $\boldsymbol{e}_i$ at $\tilde{\boldsymbol{x}}_i^+$, as explained in section 1.7.1. Equivalently, the last two expressions in equation (1.78) can be interpreted as the curvature binormal vector of the unique circle which center is on the line normal to $\boldsymbol{t}_i$ passing through $\boldsymbol{x}_i$, and that is tangent to $\boldsymbol{e}_{i-1}$ (resp. $\boldsymbol{e}_i$) at $\tilde{\boldsymbol{x}}_i^-$ (resp. $\tilde{\boldsymbol{x}}_i^+$).

Discontinuity of curvature

Let $\boldsymbol{t}_i^*$ be an arbitrary tangent vector at $\boldsymbol{x}_i$. Following equation (1.78) we define the *left-sided* (resp. *right-sided*) discrete curvature at $\boldsymbol{x}_i$ in the inscribed case as :

$$\boldsymbol{\kappa b}_i^-(\boldsymbol{t}_i^*) = \frac{2}{\overline{l}_i}\left(\frac{\boldsymbol{e}_{i-1}\times\boldsymbol{t}_i^*}{\boldsymbol{e}_{i-1}\cdot\boldsymbol{t}_i^*}\right) \tag{1.79a}$$

$$\boldsymbol{\kappa b}_i^+(\boldsymbol{t}_i^*) = \frac{2}{\overline{l}_i}\left(\frac{\boldsymbol{t}_i^*\times\boldsymbol{e}_i}{\boldsymbol{t}_i^*\cdot\boldsymbol{e}_i}\right) \tag{1.79b}$$

The corresponding osculating circles will be called the *left-sided* (resp. *right-sided*) inscribed osculating circle. When $\boldsymbol{t}_i^* = \boldsymbol{t}_i$, the limits agree one to each other ($\boldsymbol{\kappa b}_i^- = \boldsymbol{\kappa b}_i^+ = \boldsymbol{\kappa b}_i$) and the osculating circles coincide. These definitions perfectly mimic the smooth case where, at a regular ($\|\gamma'\| \neq 0$) but not biregular ($\|\gamma''\| = 0$) point, the curvature is discontinuous while the tangent vector reminds smoothly defined.

Curve endings

The definition of the left and right sided curvatures given for a vertex in the current portion of Γ are still valid for the end vertices $\boldsymbol{x}_0$ and $\boldsymbol{x}_n$. Provided that a unit tangent vector $\boldsymbol{t}_0^*$ (respectively $\boldsymbol{t}_n^*$) is given at $\boldsymbol{x}_0$ (resp. $\boldsymbol{x}_n$), the circumscribed osculating circle is defined as the unique circle passing through $\boldsymbol{x}_0$ and $\boldsymbol{x}_1$ (resp. $\boldsymbol{x}_{n-1}$ and $\boldsymbol{x}_n$)

tangent to $\boldsymbol{t}_0^*$ (resp. $\boldsymbol{t}_n^*$) ; see figure 1.16b and figure 1.16c. It leads to the following curvature binormal vectors :

$$\boldsymbol{\kappa b}_0 = \boldsymbol{\kappa b}_0^+(\boldsymbol{t}_0^*) = \frac{2}{\|\boldsymbol{e}_0\|}\left(\frac{\boldsymbol{t}_0^* \times \boldsymbol{e}_0}{\boldsymbol{t}_0^* \cdot \boldsymbol{e}_0}\right) \tag{1.80a}$$

$$\boldsymbol{\kappa b}_n = \boldsymbol{\kappa b}_n^-(\boldsymbol{t}_n^*) = \frac{2}{\|\boldsymbol{e}_{n-1}\|}\left(\frac{\boldsymbol{e}_{n-1} \times \boldsymbol{t}_n^*}{\boldsymbol{e}_{n-1} \cdot \boldsymbol{t}_n^*}\right) \tag{1.80b}$$

Note that, contrary to the current portion, curvatures at endings are subjected to the definition of a unit tangent vector. This reflects the usual indetermination of boundary conditions. For a given beam whether the end is clamped, the tangent vector is known and one will seek the reacting moment due to the support ; whether the end is pinned, the reacting moment is null (so is the curvature) and one will seek the cross-section orientation.

Conclusion

We have extended the comprehension of the discrete curvature to the extremities of the curve, for both the circumscribed and inscribed definitions of the discrete curvature. We have seen that these notions lead to a natural definition of the tangent at vertices in the current portion and at the extremities.

When the curvature is prescribed at a given vertex, equations (1.74a) and (1.74b) (circumscribed) or equations (1.79a) and (1.79a) (inscribed) need to be solved to determine the tangent vector. Remark that both systems are linear in $\boldsymbol{t}$.

1.9 Discrete parallel transport

Discrete parallel transport can be computed by analogy to the smooth case as the minimal rotation around t. However, this method becomes unstable when $\boldsymbol{t}_i$ an $\boldsymbol{t}_{i+1}$ get almost collinear because of the cross product (although the rotation angle tends to zero, the rotation axis becomes very sensitive to numerical instabilities).

Note that while these definitions of parallel transport are illustrated to transport vectors in space from one location $\{\boldsymbol{x}, \boldsymbol{t}\}(s)$ to another $\{\boldsymbol{x}, \boldsymbol{t}\}(s + ds)$, it is identically transposed to parallel transport in time from one location $\{\boldsymbol{x}, \boldsymbol{t}\}(t)$ to another $\{\boldsymbol{x}, \boldsymbol{t}\}(t + dt)$ as suggested in [42].

1.9.1 The rotation method

The rotation method is given by Bloomenthal 1990 [26]. First, the frame at $\boldsymbol{x}_i$ is simply translated at vertex $\boldsymbol{x}_{i+1}$. Then, the translated frame is rotated so that $\boldsymbol{t}_i$ aligns with $\boldsymbol{t}_{i+1}$. The rotation axis is chosen to be $\boldsymbol{b} = \boldsymbol{t}_i \times \boldsymbol{t}_{i+1}$ and the angle of rotation is denoted α (see figure 1.17a). This is analogous to the smooth case.

1.9.2 The double reflexion method

The double reflection method is given by Wang *et al.* 2008 [29]. It is supposed to be of order $o(h^4)$ whereas the rotation method is only $o(h^2)$, where $h = \sup_{i \in [\![0,n]\!]} \|\boldsymbol{e}_i\|$ is the sharpness of the discretization. Though their

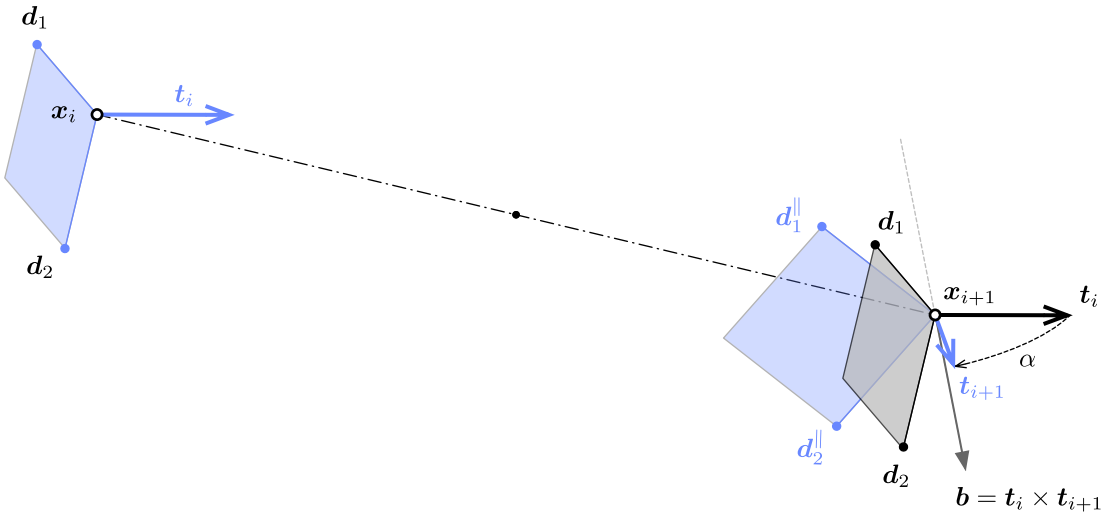

(a) rotation method

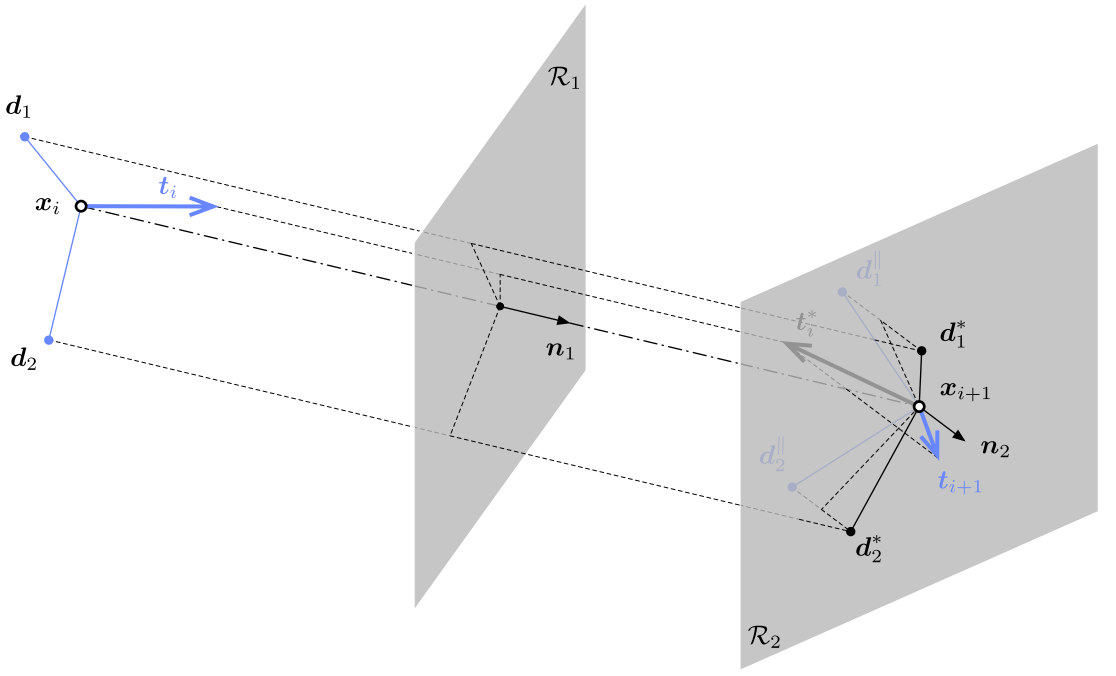

(b) double reflection method

Figure 1.17 – Two methods to parallel transport a frame from $\{\boldsymbol{x}_i, \boldsymbol{t}_i\}$ to $\{\boldsymbol{x}_{i+1}, \boldsymbol{t}_{i+1}\}$.

computation cost is quite similar, the double reflection method is not subject to instability when $\boldsymbol{t}_i$ and $\boldsymbol{t}_{i+1}$ tend to be collinear, which is an obvious advantage.

We denote $\mathcal{R}_{\boldsymbol{x}}^{\boldsymbol{n}}$ the reflection across the plane passing through the point $\boldsymbol{x}$ and normal to the unit vector $\boldsymbol{n} = \boldsymbol{e}_i/\|\boldsymbol{e}_o\|$. Thus, $\boldsymbol{v}$ is maped through $\mathcal{R}$ into $\boldsymbol{v}^* = \boldsymbol{v} - 2(\boldsymbol{v}\cdot\boldsymbol{n})\boldsymbol{n}$.

Let $\mathcal{R}_1 = \mathcal{R}_{\boldsymbol{x}_{i+1/2}}^{\boldsymbol{n}_1}$ be the reflection across the bisecting plane of $\boldsymbol{e}_i$ ($\boldsymbol{n}_1 = \boldsymbol{u}_i$). Let $\boldsymbol{t}_i^* = \mathcal{R}_1(\boldsymbol{t}_i)$ be the image of $\boldsymbol{t}_i$ by $\mathcal{R}_1$. Let $\mathcal{R}_2 = \mathcal{R}_{\boldsymbol{x}_{i+1}}^{\boldsymbol{n}_2}$ be the reflection across the bisecting plane of the points $\boldsymbol{x}_{i+1} + \boldsymbol{t}_i^*$ and $\boldsymbol{x}_{i+1} + \boldsymbol{t}_{i+1}$. Thus, $\boldsymbol{n}_2 = \frac{\boldsymbol{t}_{i+1} - \boldsymbol{t}_i^*}{\|\boldsymbol{t}_{i+1} - \boldsymbol{t}_i^*\|}$ (see figure 1.17b).

Parallel transport is defined as the *double reflection* through $\mathcal{R}_1$ and $\mathcal{R}_2$:

$$\mathcal{P}_{\{\boldsymbol{x}_i,\,\boldsymbol{t}_i\}}^{\{\boldsymbol{x}_{i+1},\,\boldsymbol{t}_{i+1}\}} = \mathcal{P}_i^{i+1} = \mathcal{R}_2 \circ \mathcal{R}_1 \tag{1.81}$$

Let $\mathcal{F}_i = \{\boldsymbol{t}_i, \boldsymbol{d}_1, \boldsymbol{d}_2\}$ be an orthonormal frame at $\boldsymbol{x}_i$. Let $\mathcal{F}_i^* = \mathcal{R}_1(\mathcal{F}_i) = \{\boldsymbol{t}_i^*, \boldsymbol{d}_1^*, \boldsymbol{d}_2^*\}$ be the image of $\mathcal{F}_i$ by $\mathcal{R}_1$. Then :

$$\boldsymbol{t}_i^* = \boldsymbol{t}_i - 2(\boldsymbol{t}_i\cdot\boldsymbol{n}_1)\boldsymbol{n}_1 \tag{1.82a}$$
$$\boldsymbol{d}_1^* = \boldsymbol{d}_1 - 2(\boldsymbol{d}_1\cdot\boldsymbol{n}_1)\boldsymbol{n}_1 \tag{1.82b}$$
$$\boldsymbol{d}_2^* = \boldsymbol{d}_1^* \times \boldsymbol{t}_i^* \tag{1.82c}$$

Let $\mathcal{F}_i^{\parallel} = \mathcal{R}_2(\mathcal{F}_i^*) = \{\boldsymbol{t}_{i+1}, \boldsymbol{d}_1^{\parallel}, \boldsymbol{d}_2^{\parallel}\}$ be the image of $\mathcal{F}_i^*$ by $\mathcal{R}_2$. Then the parallel transported vectors are given by :

$$\boldsymbol{d}_1^{\parallel} = \boldsymbol{d}_1^* - 2(\boldsymbol{d}_1^*\cdot\boldsymbol{n}_2)\boldsymbol{n}_2 \tag{1.83a}$$
$$\boldsymbol{d}_2^{\parallel} = \boldsymbol{t}_{i+1} \times \boldsymbol{d}_1^{\parallel} \tag{1.83b}$$

The double reflection is equivalent to a rotation around the line $\mathcal{D}$ defined as the intersection of the two reflection planes, of direction $\boldsymbol{b} = \boldsymbol{n}_1 \times \boldsymbol{n}_2$, by an angle $\alpha = 2\angle(\boldsymbol{n}_1, \boldsymbol{n}_2) = 2\arcsin(\|\boldsymbol{b}\|)$.

Remark that for both the circumscribed (see figure 1.15a) and inscribed (see figure 1.16a) osculating circles :

$$\boldsymbol{t}_i = \mathcal{R}_{\boldsymbol{x}_{i-1/2}}^{\boldsymbol{u}_{i-1}} \circ \mathcal{R}_{\boldsymbol{x}_i}^{\boldsymbol{t}_i}(\boldsymbol{t}_i^-) \tag{1.84a}$$
$$\boldsymbol{t}_i = \mathcal{R}_{\boldsymbol{x}_i}^{\boldsymbol{t}_i} \circ \mathcal{R}_{\boldsymbol{x}_{i+1/2}}^{\boldsymbol{u}_i}(\boldsymbol{t}_i^+) \tag{1.84b}$$

1.10 Conclusion

This chapter has established all the geometrical tools required for our future discrete beam model. Our analysis shows that for the type of structures we want to model the discrete curvature defined according to the circumscribed osculating circle is the most suitable as :

- it provides an unequivocal definition of the discrete curvature in the current portion and at the extremities of the curve ;
- it exhibits the fastest convergence when regarding the evaluation of the bending energy of typical curves ;

- it leads to a natural local spline interpolation passing through the curve’s vertices ;
- it leads to a natural definition of the tangent vector at vertices and at midspan of edges ;
- it enables the modeling of curvature discontinuities.

1.11 References

[1] F. Otto, *IL13 Multihalle Mannheim*, B. Burkhardt, M. Chaitos, J. Langner, W. Langner and G. Lubberger, Eds., ser. Institut für leichte Flächentragwerke (IL). Stuttgart, 1978.

[2] E. Happold and I. Liddell, "Timber lattice roof for the Mannheim bundesgartenschau", *The Structural Engineer*, vol. 53, no. 3, pp. 99–135, 1975.

[3] M. McQuaid, F. Otto and S. Ban, "Engineering and Architecture: building the Japan pavilion", in *Shigeru Ban*, Phaidon Press, 2006, pp. 8–11.

[4] R. Harris and O. Kelly, "The structural engineering of the Downland gridshell", in *Space Structures 5*, vol. 1, 2002, pp. 161–172.

[5] R. Harris, S. Haskins and J. Roynon, "The Savill Garden gridshell: design and construction", *The Structural Engineer*, vol. 86, no. 17, pp. 27–34, 2008.

[6] C. Douthe, O. Baverel and J.-F. Caron, "Form-finding of a grid shell in composite materials", *Journal of the International Association for Shell and Spatial Structures*, vol. 47, no. 1, pp. 53–62, 2006.

[7] C. Douthe, J.-F. Caron and O. Baverel, "Gridshell structures in glass fibre reinforced polymers", *Construction and Building Materials*, vol. 24, no. 9, pp. 1580–1589, 2010.

[8] O. Baverel, J.-F. Caron, F. Tayeb and L. du Peloux, "Gridshells in composite materials: construction of a 300m^2 forum for the Solidays' festival in Paris", *Structural Engineering International*, vol. 22, no. 3, pp. 408–414, 2012.

[9] L. du Peloux, F. Tayeb, O. Baverel and J.-F. Caron, "Construction of a large composite gridshell tructure: a lightweight structure made with pultruded glass fibre reinforced polymer tubes", *Structural Engineering International*, vol. 26, no. 2, pp. 160–167, 2016.

[10] B. D'Amico, A. Kermani and H. Zhang, "Form finding and structural analysis of actively bent timber grid shells", *Engineering Structures*, vol. 81, pp. 195–207, 2014.

[11] D. Naicu, R. Harris and C. Williams, "Timber gridshells: design methods and their application to a temporary pavilion", in *World Conference on Timber Engineering*, Quebec City, Canada, 2014.

[12] B. D'Amico, A. Kermani, H. Zhang, A. Pugnale, S. Colabella and S. Pone, "Timber gridshells: numerical simulation, design and construction of a full scale structure", *Structures*, vol. 3, pp. 227–235, 2015.

[13] J. Haddal Mork, S. Dyvik Hillersøy, B. Manum, A. Rønnquit and N. Labonnote, "Introducing the segment lath - A simplified modular timber gridshell built in Trondheim Norway", in *World Conference on Timber Engineering*, Vienna, Austria, 2016.

[14] R. Mesnil, "Structural explorations of fabrication-aware design spaces for non-standard architecture", PhD thesis, Université Paris-Est, 2017.

[15] F. Tayeb, B. Lefevre, O. Baverel, J.-F. Caron and L. du Peloux, "Design and realisation of composite gridshell structures", *Journal of the International Association for Shell and Spatial Structures*, vol. 56, no. 1, pp. 49–59, 2015.

[16] M. Bergou, M. Wardetzky, S. Robinson, B. Audoly and E. Grinspun, "Discrete elastic rods", *ACM Transactions on Graphics*, vol. 27, no. 3, 63:1–63:12, 2008.

[17] L. du Peloux, F. Tayeb, B. Lefevre, O. Baverel and J.-F. Caron, "Formulation of a 4-DoF torsion/bending element for the formfinding of elastic gridshells", in *Proceedings of the IASS Annual Symposium*, Amsterdam, Netherlands, 2015.

[18] B. Lefevre, F. Tayeb, L. du Peloux and J.-F. Caron, “A 4-degree-of-freedom Kirchhoff beam model for the modeling of bending–torsion couplings in active-bending structures”, *International Journal of Space Structures*, vol. 32, no. 2, pp. 69–83, 2017.

[19] G. F. A. L’Hospital, *Analyse des infiniment petits, pour l’intelligence des lignes courbes*. A Paris, de l’Imprimerie royale, 1696.

[20] J. Delcourt, “Analyse et géométrie, histoire des courbes gauches de Clairaut à Darboux”, *Archive for History of Exact Sciences*, vol. 65, no. 3, pp. 229–293, 2011.

[21] T. Hoffmann, “Discrete differential geometry of curves and Surfaces”, in *Math-for-Industry Lecture Note Series*, vol. 18, 2009.

[22] E. Vouga, “Plane curves”, in *Lectures in Discrete Differential Geometry*, Austin, USA, 2014, ch. 1.

[23] R. Bishop, “There is more than one way to frame a curve”, *The American Mathematical Monthly*, vol. 82, no. 3, pp. 246–251, 1975.

[24] F. Klok, “Two moving coordinate frames for sweeping along a 3D trajectory”, *Computer Aided Geometric Design*, vol. 3, no. 3, pp. 217–229, 1986.

[25] H. Guggenheimer, “Computing frames along a trajectory”, *Computer Aided Geometric Design*, vol. 6, no. 1, pp. 77–78, 1989.

[26] J. Bloomenthal, “Calculation of reference frames along a space curve”, in *Graphics Gems*, A. S. Glassner, Ed., vol. 1, San Diego, USA: Academic Press Professional, Inc., 1990, pp. 567–571.

[27] A. J. Hanson and H. Ma, “Parallel transport approach to curve framing”, Indiana University, Bloomington, USA, Tech. Rep., 1995.

[28] T. Poston, S. Fang and W. Lawton, “Computing and approximating sweeping surfaces based on rotation minimizing frames”, in *Proceedings of the 4th International Conference on CAD/CG*, Wuhan, China, 1995.

[29] W. Wang, B. Jüttler, D. Zheng and Y. Liu, “Computation of rotation minimizing frames”, *ACM Transactions on Graphics*, vol. 27, no. 1, 2:1–2:18, 2008.

[30] R. T. Farouki, C. Giannelli, M. L. Sampoli and A. Sestini, “Rotation-minimizing osculating frames”, *Computer Aided Geometric Design*, vol. 31, no. 1, pp. 27–42, 2014.

[31] F. Frenet, “Sur les courbes à double courbure”, *Journal de Mathématiques Pures et Appliquées*, vol. 17, no. 1, pp. 437–447, 1852.

[32] J. Delcourt, “Analyse et géométrie : les courbes gauches de Clairaut à Serret”, PhD thesis, Université Paris-VI, 2007.

[33] J. Bernoulli, “Quo continentur Anekdota”, in *Opera omnia, tam antea sparsim edita, quam hactenus inedita*, 4, Marci-Michaelis Bousquet, Lausannae & Genevae, 1742.

[34] H. Pitot, “Sur la quadrature de la moitié d’une courbe, qui est la compagne de la cycloïde”, *Histoire de l’Académie Royale des Sciences*, vol. 1, pp. 65–67, 1724.

[35] J. L. Coolidge, *A history of geometrical methods*, ser. Dover Books on Mathematics. Oxford: Oxford, Clarendon press, 2013.

[36] G. Monge, *Application de l’analyse à la géométrie, à l’usage de l’Ecole impériale polytechnique*, 4th ed. Paris: Ve Bernard, 1809.

[37] L. Euler, “De motu turbinatorio, chordarum musicarum”, in *Novi Commentarii Academiae Scientiarum Imperialis Petropolitanae*, vol. 19, Petropoli, 1775, pp. 340–370.

[38] A. Gray, E. Abbena and S. Salamon, *Modern differential geometry of curves and surfaces with Mathematica*, 3rd ed. Chapman & Hall/CRC, 2006.

[39] D. Carroll, E. Hankins, E. Kose and I. Sterling, “A survey of the differential geometry of discrete curves”, *The Mathematical Intelligencer*, vol. 36, no. 4, pp. 28–35, 2014.

[40] A. Bobenko, *Discrete differential geometry*, 2nd ed. 2015.

[41] P. Romon, *Courbes discrètes planes*, ser. Références sciences. Ellipses, 2013, ch. 1.

[42] M. Bergou, B. Audoly, E. Vouga, M. Wardetzky and E. Grinspun, “Discrete viscous threads”, *ACM Transactions on Graphics*, vol. 29, no. 4, 116:1–116:10, 2010.

Appendix Part III

A Review of built elastic gridshells

N	Year	Nickname	Type	City	Country	Ref.
1	1962	Experimental structure	Workshop	Berkeley	USA	[43]
2	1962	Exhibition pavilion	Pavilion	Essen	Germany	[43]
3	1967	German Pavilion	Pavilion	Montreal	Canada	[43]
4	1973	Seibu	Experiment	Tokyo	Japan	[1]
5	1974	Basket shell	Experiment	Amehabad	India	[43]
6	1974	Experimental structure	Experiment	London	England	[43]
7	1975	Mannheim Multihalle	Building	Mannheim	Germany	[43]
8	1973	Ferrocement gridshell	Building	Ahmedabad	India	[1]
9	1976	AA Bamboo Latice Shell	Workshop	London	England	[1]
10	1976	Test structure of a gridshell	Experiment	Stuttgart	Germany	[43]
11	1977	Small Pavilion	Workshop	Mexico City	Mexico	[1]
12	1977	Small Greenhouse	Workshop	Zitacuaro	Mexico	[1]
13	1977	Experimental structure	Workshop	Mexico City	Mexico	[1]
14	1977	Experimental structure	Workshop	Mexico City	Mexico	[1]
15	1995	Westminster Lodge	Building	Dorset	England	[44]
16	1998	Earth Center	Building	Doncaster	England	
17	2000	Japan Pavilion	Pavilion	Hannover	Germany	[3]
18	2002	Downland	Building	Downland	England	[45]
19	2002	Life Science Centre Trust	Building	Pishwanton	England	
20	2003	Woodland Center	Building	Filmwell	England	
21	2006	Savill	Building	Savill	England	[5]
22	2007	Chiddingstone Orangery	Roofing	Kent	England	
23	2007	ENPC	Experiment	Noisy-Champs	France	[6]
24	2011	Solidays	Pavilion	Paris	France	[8]
25	2012	Toledo	Workshop	Naples	Italy	[10]
26	2013	Créteil	Building	Créteil	France	[9]
27	2013	ZA	Workshop	Cluj	Romania	
28	2014	F2	Workshop	San Antonio	USA	
29	2014	Toledo 2.0	Workshop	Naples	Italy	[12]
30	2015	Booby	Experiment	Noisy-Champs	France	[46]
31	2016	JPO	Pavilion	Toulouse	France	
32	2016	FAV	Pavilion	Montpellier	France	
33	2016	CLC	Workshop	Noisy-Champs	France	
34	2016	Trondheim	Workshop	Trondheim	Norway	[13]

Table A.1 – Project review - general informations.

N	Material	Layer	Pitch	Surface	Span	Section
			m	m^2	m	mm
1	steel	single	0.82	52	7.8	double Ø21.7
2	hemelock pine	single	0.48	198	16.8	60x40
3	hemelock pine	single	0.50	365	17.5	42x35 - 42x28
4	aluminium	single	0.50	72	8.5	20x20x2
5	bamboo	single	0.48	225	15.0	Ø25.4
6	yellow pine	single	0.45	82	6.0	14x19
7	hemelock pine	double	0.50	7400	60.0	50x50
8	steel	single	0.50	80	8.0	Ø19x1.2
9	bamboo	single	0.7	63	7.0	Ø25.4
10	hemelock pine	single	0.50	38	6.7	15x15
11	pine	single	0.50	62	6.0	16x24
12	wood	double	0.4	81	9.0	20x22
13	aluminium	single	0.50	58	7.3	double Ø8.0
14	steel	single		17	4.0	double Ø5.0
15	roundwood thinnings	double				Ø100.0
16	oak	single	0.4	36	6.0	32x15
17	cardboard	single	1.0	2500	35.0	Ø120x22
18	oak	double	1.0 - 0.5	710	16.0	50x35
19	larch	single	0.6	80	10.0	35x25
20	chestnut	single	0.6	300	12.0	75x25
21	larch	double	1.0	2000	24.0	80x50
22	sweet chestnut	double	1.0	50	5.0	40x30
23	GFRP	single	1.0	170	13.0	Ø41.7x3.5
24	GFRP	single	1.0	280	15.0	Ø41.7x3.5
25	fir	double	0.50	75	6.5	
26	GFRP	single	1.0	350	17.5	Ø41.7x3.5
27	larch	double	0.7	234	13.0	70x20
28	wood	double		144	12.0	
29	larch	double	0.50	100	10.0	50x20
30	GFRP	single	0.25	10	3.4	Ø10
31	pine	double	0.6	50	7.0	48x12
32	pine	double	0.6	50	7.0	48x12
33	pine	double	0.6	50	7.0	48x12
34	spruce	double	0.50	100	10.0	48x23

Table A.2 – Project review - key numbers.

A.1 References

[1] F. Otto, *IL13 Multihalle Mannheim*, B. Burkhardt, M. Chaitos, J. Langner, W. Langner and G. Lubberger, Eds., ser. Institut für leichte Flächentragwerke (IL). Stuttgart, 1978.

[3] M. McQuaid, F. Otto and S. Ban, "Engineering and Architecture: building the Japan pavilion", in *Shigeru Ban*, Phaidon Press, 2006, pp. 8–11.

[5] R. Harris, S. Haskins and J. Roynon, "The Savill Garden gridshell: design and construction", *The Structural Engineer*, vol. 86, no. 17, pp. 27–34, 2008.

[6] C. Douthe, O. Baverel and J.-F. Caron, "Form-finding of a grid shell in composite materials", *Journal of the International Association for Shell and Spatial Structures*, vol. 47, no. 1, pp. 53–62, 2006.

[8] O. Baverel, J.-F. Caron, F. Tayeb and L. du Peloux, "Gridshells in composite materials: construction of a 300m^2 forum for the Solidays' festival in Paris", *Structural Engineering International*, vol. 22, no. 3, pp. 408–414, 2012.

[9] L. du Peloux, F. Tayeb, O. Baverel and J.-F. Caron, "Construction of a large composite gridshell tructure: a lightweight structure made with pultruded glass fibre reinforced polymer tubes", *Structural Engineering International*, vol. 26, no. 2, pp. 160–167, 2016.

[10] B. D'Amico, A. Kermani and H. Zhang, "Form finding and structural analysis of actively bent timber grid shells", *Engineering Structures*, vol. 81, pp. 195–207, 2014.

[12] B. D'Amico, A. Kermani, H. Zhang, A. Pugnale, S. Colabella and S. Pone, "Timber gridshells: numerical simulation, design and construction of a full scale structure", *Structures*, vol. 3, pp. 227–235, 2015.

[13] J. Haddal Mork, S. Dyvik Hillersøy, B. Manum, A. Rønnquit and N. Labonnote, "Introducing the segment lath - A simplified modular timber gridshell built in Trondheim Norway", in *World Conference on Timber Engineering*, Vienna, Austria, 2016.

[43] F. Otto, *IL10 Grid Shells*, B. Burkhardt, J. Hennicke and E. Schauer, Eds., ser. Institut für leichte Flächentragwerke (IL). Stuttgart, 1974.

[44] R. Burton, M. Dickson and R. Harris, "The use of roundwood thinnings in buildings: a case study", *Building Research and Information*, vol. 26, no. 2, pp. 76–93, 1998.

[45] R. Harris, J. Romer, O. Kelly and S. Johnson, "Design and construction of the Downland gridshell", *Building Research and Information*, vol. 31, no. 6, pp. 427–454, 2003.

[46] P. Cuvilliers, C. Douthe, L. du Peloux and R. Le Roy, "Hybrid structural skin: prototype of a GFRP elastic gridshell braced by a fibre-reinforced conrete envelope", *Journal of the International Association for Shell and Spatial Structures*, vol. 58, no. 1, pp. 65–78, 2017.

B Parabolic interpolation

B.1 Introduction

In this appendix, we give the required formulas to conduct a parabolic interpolation of a scalar or vector-valued function over an interval.

We look for a polynomial interpolation of order 2 of a continuous scalar or vector-valued function $\boldsymbol{V} : t \mapsto \boldsymbol{V}(t)$ over the interval $[t_0, t_2]$; supposing that the value of the function is known for three distinct parameters $t_0 < t_1 < t_2$:

$$\boldsymbol{V}(t_0) = \boldsymbol{V}_0 \tag{B.1a}$$
$$\boldsymbol{V}(t_1) = \boldsymbol{V}_1 \tag{B.1b}$$
$$\boldsymbol{V}(t_2) = \boldsymbol{V}_2 \tag{B.1c}$$

This interpolation method is employed several times in this thesis, for instance to evaluate the position of a kinetic energy peak during the dynamic relaxation process. It is also employed for evaluating the bending moment and the curvature of a discrete rod at mid-edge, knowing its values at vertices.

Note that this interpolation method is valid if the basis in which $\boldsymbol{V}$ is decomposed does not depend on the parameter t. Otherwise, the classical transportation term should be considered ($\boldsymbol{\omega} \times \boldsymbol{V}$).

B.2 Lagrange interpolating polynomial

The Lagrange interpolation of order two is given by the following polynomial :

$$\boldsymbol{V}(t) = \boldsymbol{V}_0 \frac{(t-t_1)(t-t_2)}{(t_0-t_1)(t_0-t_2)} + \boldsymbol{V}_1 \frac{(t-t_0)(t-t_2)}{(t_1-t_0)(t_1-t_2)} + \boldsymbol{V}_2 \frac{(t-t_0)(t-t_1)}{(t_2-t_0)(t_2-t_1)} \tag{B.2}$$

B.3 Reparametrization

Lets introduce the distances l_0 and l_1 in the parametric space :

$$l_0 = t_1 - t_0 \tag{B.3a}$$
$$l_1 = t_2 - t_1 \tag{B.3b}$$

Lets introduce the change of variable $u = t - t_1$. The polynomial in equation (B.2) can be rewritten in the form :

$$\boldsymbol{V}(u) = \boldsymbol{V}_0 \frac{u(u-l_1)}{l_0(l_0+l_1)} - \boldsymbol{V}_1 \frac{(u+l_0)(u-l_1)}{l_0 l_1} + \boldsymbol{V}_2 \frac{u(u+l_0)}{l_1(l_0+l_1)} \tag{B.4}$$

where :

$$u_0 = -l_0 \tag{B.5a}$$
$$u_1 = 0 \tag{B.5b}$$
$$u_2 = l_1 \tag{B.5c}$$

The derivative of this polynomial is also required to determine the extremum value of $\boldsymbol{V}$. Differentiating equation (B.4) gives :

$$\boldsymbol{V}'(u) = \boldsymbol{V}_0 \frac{2u-l_1}{l_0(l_0+l_1)} - \boldsymbol{V}_1 \frac{2u+(l_0-l_1)}{l_0 l_1} + \boldsymbol{V}_2 \frac{2u+l_0}{l_1(l_0+l_1)} \tag{B.6}$$

This expression can be factorized to give the more compact form :

$$\boldsymbol{V}'(u) = \left(\frac{\boldsymbol{V}_1 - \boldsymbol{V}_0}{l_0}\right) \frac{l_1 - 2u}{l_0+l_1} + \left(\frac{\boldsymbol{V}_2 - \boldsymbol{V}_1}{l_1}\right) \frac{l_0 + 2u}{l_0+l_1} \tag{B.7}$$

B.4 Characteristic values

Using equation (B.4) the interpolated values of $\boldsymbol{V}$ at mid distance between t_0 and t_1 ($u = -l_0/2$), and at mid distance between t_1 and t_2 ($u = +l_1/2$) are given by :

$$\boldsymbol{V}_{01} = \boldsymbol{V}_0 \frac{l_0+2l_1}{4(l_0+l_1)} + \boldsymbol{V}_1 \frac{l_0+2l_1}{4l_1} - \boldsymbol{V}_2 \frac{{l_0}^2}{4l_1(l_0+l_1)} \tag{B.8a}$$
$$\boldsymbol{V}_{12} = -\boldsymbol{V}_0 \frac{{l_1}^2}{4l_0(l_0+l_1)} + \boldsymbol{V}_1 \frac{2l_0+l_1}{4l_0} + \boldsymbol{V}_2 \frac{2l_0+l_1}{4(l_0+l_1)} \tag{B.8b}$$

Using equation (B.7) the interpolated values of $\boldsymbol{V}'$ at mid distance between t_0 and t_1 ($u = -l_0/2$), and at mid distance between t_1 and t_2 ($u = +l_1/2$) are given by :

$$\boldsymbol{V}'_{01} = \frac{\boldsymbol{V}_1 - \boldsymbol{V}_0}{l_0} \tag{B.9a}$$

$$\boldsymbol{V}'_{12} = \frac{\boldsymbol{V}_2 - \boldsymbol{V}_1}{l_1} \tag{B.9b}$$

Remark that this is an interesting result as at these parameters the evaluation of $\boldsymbol{V}'$ boils down to a finite difference scheme.

Using equation (B.7) and introducing $\alpha = \frac{l_0}{l_0+l_1}$ the interpolated values of $\boldsymbol{V}'$ at t_0, t_1 and t_2 are given by :

$$\boldsymbol{V}'_0 = (1+\alpha)\boldsymbol{V}'_{01} - \alpha\boldsymbol{V}'_{12} \tag{B.10a}$$

$$\boldsymbol{V}'_1 = (1-\alpha)\boldsymbol{V}'_{01} + \alpha\boldsymbol{V}'_{12} \tag{B.10b}$$

$$\boldsymbol{V}'_2 = (\alpha-1)\boldsymbol{V}'_{01} + (2-\alpha)\boldsymbol{V}'_{12} \tag{B.10c}$$

Lets rewrite equations (B.8a) and (B.8b) with the help of α :

$$\boldsymbol{V}_{01} = \frac{1}{4}\left((2-\alpha)\boldsymbol{V}_0 + \frac{2-\alpha}{1-\alpha}\boldsymbol{V}_1 - \frac{\alpha^2}{1-\alpha}\boldsymbol{V}_2\right) \tag{B.11a}$$

$$\boldsymbol{V}_{01} = \frac{1}{4}\left(-\frac{(1-\alpha)^2}{\alpha}\boldsymbol{V}_0 + \frac{1+\alpha}{\alpha}\boldsymbol{V}_1 + (1+\alpha)\boldsymbol{V}_2\right) \tag{B.11b}$$

B.5 Extremum value

The extremum value of the parabola is obtained for $\boldsymbol{V}'(u^*) = 0$. It's a minimum if $\boldsymbol{V}'_{12} > \boldsymbol{V}'_{01}$ and it's a maximum if $\boldsymbol{V}'_{12} > \boldsymbol{V}'_{01}$:

$$u^* = \frac{l_1\boldsymbol{V}'_{01} + l_0\boldsymbol{V}'_{12}}{2(\boldsymbol{V}'_{01} - \boldsymbol{V}'_{12})} \tag{B.12}$$

Remark that if $\boldsymbol{V}'_{12} = \boldsymbol{V}'_{01}$ it does not make sens to compute u^* as in this case the parabola degenerates into a line. The value of the function at this parameter is given by :

$$\boldsymbol{V}(u^*) = \boldsymbol{V}_1 + \frac{(l_1\boldsymbol{V}'_{01} + l_0\boldsymbol{V}'_{12})^2}{4(l_0+l_1)(\boldsymbol{V}'_{01} - \boldsymbol{V}'_{12})} \tag{B.13}$$

The parabola in equation (B.4) now writes :

$$\boldsymbol{V}(u) = -\frac{\boldsymbol{V}'_{01} - \boldsymbol{V}'_{12}}{l_0+l_1}(u-u^*)^2 + \boldsymbol{V}(u^*) \tag{B.14}$$

The extremum is located in $[t_0, t_2]$ if the sign of $\boldsymbol{V}'$ changes on this interval. This condition is satisfied whenever $\boldsymbol{V}'_{01} \cdot \boldsymbol{V}'_{12} < 0$.

Finally, in the special case of a uniform discretization where $l_0 = l_1 = l$, equations (B.12) and (B.13) become :

$$u^* = \frac{l}{2}\left(\frac{\boldsymbol{V}_0 - \boldsymbol{V}_2}{\boldsymbol{V}_0 - 2\boldsymbol{V}_1 + \boldsymbol{V}_2}\right) \tag{B.15a}$$

$$\boldsymbol{V}(u^*) = \boldsymbol{V}_1 - \frac{u^*}{4l}(\boldsymbol{V}_2 - \boldsymbol{V}_0) \tag{B.15b}$$

Bibliography

[1] F. Otto, *IL13 Multihalle Mannheim*, B. Burkhardt, M. Chaitos, J. Langner, W. Langner and G. Lubberger, Eds., ser. Institut für leichte Flächentragwerke (IL). Stuttgart, 1978.

[2] E. Happold and I. Liddell, "Timber lattice roof for the Mannheim bundesgartenschau", *The Structural Engineer*, vol. 53, no. 3, pp. 99–135, 1975.

[3] M. McQuaid, F. Otto and S. Ban, "Engineering and Architecture: building the Japan pavilion", in *Shigeru Ban*, Phaidon Press, 2006, pp. 8–11.

[4] R. Harris and O. Kelly, "The structural engineering of the Downland gridshell", in *Space Structures 5*, vol. 1, 2002, pp. 161–172.

[5] R. Harris, S. Haskins and J. Roynon, "The Savill Garden gridshell: design and construction", *The Structural Engineer*, vol. 86, no. 17, pp. 27–34, 2008.

[6] C. Douthe, O. Baverel and J.-F. Caron, "Form-finding of a grid shell in composite materials", *Journal of the International Association for Shell and Spatial Structures*, vol. 47, no. 1, pp. 53–62, 2006.

[7] C. Douthe, J.-F. Caron and O. Baverel, "Gridshell structures in glass fibre reinforced polymers", *Construction and Building Materials*, vol. 24, no. 9, pp. 1580–1589, 2010.

[8] O. Baverel, J.-F. Caron, F. Tayeb and L. du Peloux, "Gridshells in composite materials: construction of a 300m^2 forum for the Solidays' festival in Paris", *Structural Engineering International*, vol. 22, no. 3, pp. 408–414, 2012.

[9] L. du Peloux, F. Tayeb, O. Baverel and J.-F. Caron, "Construction of a large composite gridshell tructure: a lightweight structure made with pultruded glass fibre reinforced polymer tubes", *Structural Engineering International*, vol. 26, no. 2, pp. 160–167, 2016.

[10] B. D'Amico, A. Kermani and H. Zhang, "Form finding and structural analysis of actively bent timber grid shells", *Engineering Structures*, vol. 81, pp. 195–207, 2014.

[11] D. Naicu, R. Harris and C. Williams, "Timber gridshells: design methods and their application to a temporary pavilion", in *World Conference on Timber Engineering*, Quebec City, Canada, 2014.

[12] B. D'Amico, A. Kermani, H. Zhang, A. Pugnale, S. Colabella and S. Pone, "Timber gridshells: numerical simulation, design and construction of a full scale structure", *Structures*, vol. 3, pp. 227–235, 2015.

[13] J. Haddal Mork, S. Dyvik Hillersøy, B. Manum, A. Rønnquit and N. Labonnote, “Introducing the segment lath - A simplified modular timber gridshell built in Trondheim Norway”, in *World Conference on Timber Engineering*, Vienna, Austria, 2016.

[14] R. Mesnil, “Structural explorations of fabrication-aware design spaces for non-standard architecture”, PhD thesis, Université Paris-Est, 2017.

[15] F. Tayeb, B. Lefevre, O. Baverel, J.-F. Caron and L. du Peloux, “Design and realisation of composite gridshell structures”, *Journal of the International Association for Shell and Spatial Structures*, vol. 56, no. 1, pp. 49–59, 2015.

[16] M. Bergou, M. Wardetzky, S. Robinson, B. Audoly and E. Grinspun, “Discrete elastic rods”, *ACM Transactions on Graphics*, vol. 27, no. 3, 63:1–63:12, 2008.

[17] L. du Peloux, F. Tayeb, B. Lefevre, O. Baverel and J.-F. Caron, “Formulation of a 4-DoF torsion/bending element for the formfinding of elastic gridshells”, in *Proceedings of the IASS Annual Symposium*, Amsterdam, Netherlands, 2015.

[18] B. Lefevre, F. Tayeb, L. du Peloux and J.-F. Caron, “A 4-degree-of-freedom Kirchhoff beam model for the modeling of bending–torsion couplings in active-bending structures”, *International Journal of Space Structures*, vol. 32, no. 2, pp. 69–83, 2017.

[19] G. F. A. L’Hospital, *Analyse des infiniment petits, pour l’intelligence des lignes courbes*. A Paris, de l’Imprimerie royale, 1696.

[20] J. Delcourt, “Analyse et géométrie, histoire des courbes gauches de Clairaut à Darboux”, *Archive for History of Exact Sciences*, vol. 65, no. 3, pp. 229–293, 2011.

[21] T. Hoffmann, “Discrete differential geometry of curves and Surfaces”, in *Math-for-Industry Lecture Note Series*, vol. 18, 2009.

[22] E. Vouga, “Plane curves”, in *Lectures in Discrete Differential Geometry*, Austin, USA, 2014, ch. 1.

[23] R. Bishop, “There is more than one way to frame a curve”, *The American Mathematical Monthly*, vol. 82, no. 3, pp. 246–251, 1975.

[24] F. Klok, “Two moving coordinate frames for sweeping along a 3D trajectory”, *Computer Aided Geometric Design*, vol. 3, no. 3, pp. 217–229, 1986.

[25] H. Guggenheimer, “Computing frames along a trajectory”, *Computer Aided Geometric Design*, vol. 6, no. 1, pp. 77–78, 1989.

[26] J. Bloomenthal, “Calculation of reference frames along a space curve”, in *Graphics Gems*, A. S. Glassner, Ed., vol. 1, San Diego, USA: Academic Press Professional, Inc., 1990, pp. 567–571.

[27] A. J. Hanson and H. Ma, “Parallel transport approach to curve framing”, Indiana University, Bloomington, USA, Tech. Rep., 1995.

[28] T. Poston, S. Fang and W. Lawton, “Computing and approximating sweeping surfaces based on rotation minimizing frames”, in *Proceedings of the 4th International Conference on CAD/CG*, Wuhan, China, 1995.

[29] W. Wang, B. Jüttler, D. Zheng and Y. Liu, “Computation of rotation minimizing frames”, *ACM Transactions on Graphics*, vol. 27, no. 1, 2:1–2:18, 2008.

[30] R. T. Farouki, C. Giannelli, M. L. Sampoli and A. Sestini, “Rotation-minimizing osculating frames”, *Computer Aided Geometric Design*, vol. 31, no. 1, pp. 27–42, 2014.

[31] F. Frenet, “Sur les courbes à double courbure”, *Journal de Mathématiques Pures et Appliquées*, vol. 17, no. 1, pp. 437–447, 1852.

[32] J. Delcourt, “Analyse et géométrie : les courbes gauches de Clairaut à Serret”, PhD thesis, Université Paris-VI, 2007.

[33] J. Bernoulli, “Quo continentur Anekdota”, in *Opera omnia, tam antea sparsim edita, quam hactenus inedita*, 4, Marci-Michaelis Bousquet, Lausannae & Genevae, 1742.

[34] H. Pitot, “Sur la quadrature de la moitié d’une courbe, qui est la compagne de la cycloïde”, *Histoire de l’Académie Royale des Sciences*, vol. 1, pp. 65–67, 1724.

[35] J. L. Coolidge, *A history of geometrical methods*, ser. Dover Books on Mathematics. Oxford: Oxford, Clarendon press, 2013.

[36] G. Monge, *Application de l’analyse à la géométrie, à l’usage de l’Ecole impériale polytechnique*, 4th ed. Paris: Ve Bernard, 1809.

[37] L. Euler, “De motu turbinatorio, chordarum musicarum”, in *Novi Commentarii Academiae Scientiarum Imperialis Petropolitanae*, vol. 19, Petropoli, 1775, pp. 340–370.

[38] A. Gray, E. Abbena and S. Salamon, *Modern differential geometry of curves and surfaces with Mathematica*, 3rd ed. Chapman & Hall/CRC, 2006.

[39] D. Carroll, E. Hankins, E. Kose and I. Sterling, “A survey of the differential geometry of discrete curves”, *The Mathematical Intelligencer*, vol. 36, no. 4, pp. 28–35, 2014.

[40] A. Bobenko, *Discrete differential geometry*, 2nd ed. 2015.

[41] P. Romon, *Courbes discrètes planes*, ser. Références sciences. Ellipses, 2013, ch. 1.

[42] M. Bergou, B. Audoly, E. Vouga, M. Wardetzky and E. Grinspun, “Discrete viscous threads”, *ACM Transactions on Graphics*, vol. 29, no. 4, 116:1–116:10, 2010.

[43] F. Otto, *IL10 Grid Shells*, B. Burkhardt, J. Hennicke and E. Schauer, Eds., ser. Institut für leichte Flächentragwerke (IL). Stuttgart, 1974.

[44] R. Burton, M. Dickson and R. Harris, “The use of roundwood thinnings in buildings: a case study”, *Building Research and Information*, vol. 26, no. 2, pp. 76–93, 1998.

[45] R. Harris, J. Romer, O. Kelly and S. Johnson, “Design and construction of the Downland gridshell”, *Building Research and Information*, vol. 31, no. 6, pp. 427–454, 2003.

[46] P. Cuvilliers, C. Douthe, L. du Peloux and R. Le Roy, “Hybrid structural skin: prototype of a GFRP elastic gridshell braced by a fibre-reinforced conrete envelope”, *Journal of the International Association for Shell and Spatial Structures*, vol. 58, no. 1, pp. 65–78, 2017.

Publications from the author

2017 P. Cuvilliers, C. Douthe, L. du Peloux and R. Le Roy, “Hybrid structural skin: prototype of a GFRP elastic gridshell braced by a fibre-reinforced conrete envelope”, *Journal of the International Association for Shell and Spatial Structures*, vol. 58, no. 1, pp. 65–78, 2017.

B. Lefevre, F. Tayeb, L. du Peloux and J.-F. Caron, “A 4-degree-of-freedom Kirchhoff beam model for the modeling of bending–torsion couplings in active-bending structures”, *International Journal of Space Structures*, vol. 32, no. 2, pp. 69–83, 2017.

2016 L. du Peloux, F. Tayeb, O. Baverel and J.-F. Caron, “Construction of a large composite gridshell tructure: a lightweight structure made with pultruded glass fibre reinforced polymer tubes”, *Structural Engineering International*, vol. 26, no. 2, pp. 160–167, 2016.

2015 L. du Peloux, F. Tayeb, B. Lefevre, O. Baverel and J.-F. Caron, “Formulation of a 4-DoF torsion/bending element for the formfinding of elastic gridshells”, in *Proceedings of the IASS Annual Symposium*, Amsterdam, Netherlands, 2015.

F. Tayeb, B. Lefevre, O. Baverel, J.-F. Caron and L. du Peloux, “Design and realisation of composite gridshell structures”, *Journal of the International Association for Shell and Spatial Structures*, vol. 56, no. 1, pp. 49–59, 2015.

2013 L. du Peloux, F. Tayeb, O. Baverel and J.-F. Caron, “Faith can also move composite gridshells”, in *Proceedings of the IASS Annual Symposium*, Worclaw, Poland, 2013, pp. 1–7.

F. Tayeb, J.-F. Caron, O. Baverel and L. du Peloux, “Stability and robustness of a 300m^2 composite gridshell structure”, *Construction and Building Materials*, vol. 49, pp. 926–938, 2013.

2012 O. Baverel, J.-F. Caron, F. Tayeb and L. du Peloux, “Gridshells in composite materials: construction of a 300m^2 forum for the Solidays’ festival in Paris”, *Structural Engineering International*, vol. 22, no. 3, pp. 408–414, 2012.

2011 L. du Peloux, O. Baverel, J.-F. Caron and F. Tayeb, “From shape to shell: a design tool to materialize freeform shapes using gridshell structures”, in *Design Modeling Symposium*, Berlin, Deutschland, 2011.